STRESSED AND SHEARING RESISTANCE IN SOIL BENEATH A RIGID WHEEL

Mosaid M. Al-Hussaini, et al

Army Engineer Waterways Experiment Station
Vicksburg, Mississippi

September 1974

Unclassified
SECURITY CLASSIFICATION OF THIS PAGE (When Data Entered)

AD/A-000 609

REPORT DOCUMENTATION PAGE

READ INSTRUCTIONS BEFORE COMPLETING FORM

1. REPORT NUMBER: Technical Report S-74-7	2. GOVT ACCESSION NO.
3. RECIPIENT'S CATALOG NUMBER	
4. TITLE (and Subtitle): STRESSES AND SHEARING RESISTANCE IN SOIL BENEATH A RIGID WHEEL	5. TYPE OF REPORT & PERIOD COVERED: Final report
6. PERFORMING ORG. REPORT NUMBER	
7. AUTHOR(s): Mosaid M. Al-Hussaini; Paul A. Gilbert	8. CONTRACT OR GRANT NUMBER(s)
9. PERFORMING ORGANIZATION NAME AND ADDRESS: U. S. Army Engineer Waterways Experiment Station, Soils and Pavements Laboratory, P. O. Box 631, Vicksburg, Mississippi 39180	10. PROGRAM ELEMENT, PROJECT, TASK AREA & WORK UNIT NUMBERS: Project No. 4A061102B52E, Task 01, Work Unit 013
11. CONTROLLING OFFICE NAME AND ADDRESS: Office, Chief of Engineers, U. S. Army, Washington, D. C. 20314	12. REPORT DATE: September 1974
	13. NUMBER OF PAGES: ~~116~~ 118
14. MONITORING AGENCY NAME & ADDRESS (if different from Controlling Office)	15. SECURITY CLASS. (of this report): Unclassified
	15a. DECLASSIFICATION/DOWNGRADING SCHEDULE

16. DISTRIBUTION STATEMENT (of this Report)

Approved for public release; distribution unlimited.

17. DISTRIBUTION STATEMENT (of the abstract entered in Block 20, if different from Report)

18. SUPPLEMENTARY NOTES

19. KEY WORDS (Continue on reverse side if necessary and identify by block number)

Computer applications
Rigid wheels
Shear properties
Soil stresses
Soil-wheel interaction
Vehicle mobility
Wheels

20. ABSTRACT (Continue on reverse side if necessary and identify by block number)

The problem of vehicle mobility is a complex one in that a rigorous analytical treatment of the mechanics involved between vehicle characteristics, such as geometry, size, and driving forces, and the properties and responses of soil that supports a moving vehicle has not been developed. In general, immobilization problems occur as a result of the loss of or excessive demand for traction created by a combination of sinkage, slope, forces applied, obstacles, and environmental conditions. Immobilization problems associated

(Continued)

20. ABSTRACT (Continued)

with poor traction due to weak soils or slippery surfaces are not limited to rigid or pneumatic-tired wheels, but also affect powered track wheels with grousers. Two approaches have been followed in attempting to solve the soil-wheel interaction problem: an analytical approach based on the elastic solution of a plane strain problem, and an experimental approach based on the relationship between the shear and normal stresses that may occur within the vicinity of or at the interface of the soil and the wheel of a moving vehicle. The analytical solution is based on the assumption that the stresses within the soil are the results of the tangential and radial stresses created by a wheel partially embedded in soil with an impending rotation. The Airy stress function was used in representing the stresses within the soil in terms of analytic functions. The Schwarz-Christoffel equation was used to transform the geometry and the boundary condition of the region beneath the wheel and to match them with the stress functions. The Cauchy integral equation was applied on the transformed boundary conditions to obtain the shear and normal stress at any point within the region of the soil-wheel system. A computer program for reducing the results and obtaining numerical values of the stresses at any point within the vicinity of the wheel was also written. It is believed that the analytical solution developed will permit the evaluation of stresses within the soil beneath a wheel that result from various combinations of radial and tangential stresses. The experimental investigation was designed to investigate the shear stresses and traction forces that may exist between a model rigid wheel or tire wheel and the supporting soil. CH material (Vicksburg buckshot clay) was compacted and tested in an annular torsion shear machine. Four types of specimens were tested in this study: the first series of tests consisted of shearing homogeneous soil specimens; in the second series, the soil was sheared against smooth rubber; in the third series, the soil was sheared against polished stainless steel; and in the fourth series, a nonhomogeneous soil specimen, with upper and lower halves having different water contents, was sheared. The initial normal stresses used in the test program were 5, 15, and 30 psi, and all specimens were sheared under constant-volume conditions at rates of shear deformations of 0.002, 0.2, and 2.0 in./min. Test results showed that nonhomogeneous soil specimens with upper and lower halves having water contents of 26 and 16 percent, respectively, were stronger than homogenous soil specimens with a uniform water content of 26 percent and that the strengths of both types of soil specimens were higher than those at the interface of smooth rubber or polished stainless steel and soil. Test results showed that the strength of nonhomogeneous soil specimens was higher than that of homogeneous soil specimens with uniform water content, and the strengths of both types of soil specimens were higher than those at the interface of smooth rubber or polished stainless steel on soil. The results also showed that the shear resistance developed between soil and rubber is much higher than that developed between soil and polished steel. The shear stress at failure for all test series showed an increase with increasing initial normal stress and increasing rate of shear deformation. The shear stresses at the interfaces of smooth rubber and soil and also of polished steel and soil dropped sharply when the plane of contact was covered with a film of water. The peak shear stress obtained from each test series was plotted as a function of the corresponding normal stress in order to facilitate its use in analytical solutions.

PREFACE

The study reported herein was conducted at the U. S. Army Engineer Waterways Experiment Station (WES) under the sponsorship of the Office, Chief of Engineers, Directorate of Military Engineering, Project No. 4A061102B52E, "Research in Military Engineering and Construction," Task 01, "Environmental Characterization System Research," Work Unit 013, "Field Determination of Shear Strength Parameters and Traction in Near-Surface Soils," Work Unit Accession No. DA of 8156.

The analytical and experimental studies described in this report were performed during the period September 1970 to June 1971 by Dr. M. M. Al-Hussaini, Project Engineer, and Mr. P. A. Gilbert, both of the Embankment and Foundation Branch, Soils and Pavements Laboratory (S&PL). This report was prepared by Dr. Al-Hussaini, assisted by Mr. Gilbert, under the immediate supervision of Mr. J. R. Compton, Chief, Embankment and Foundation Branch, and the general supervision of Mr. J. P. Sale, Chief, and Mr. S. J. Johnson, Special Assistant, S&PL. Useful suggestions and comments by Dr. G. Y. Baladi, S&PL, are appreciated.

Directors of WES during the course of the investigation and preparation and publication of this report were BG E. D. Peixotto, CE, and COL G. H. Hilt, CE. Technical Director was Mr. F. R. Brown.

CONTENTS

CONTENTS

CONVERSION FACTORS, U. S. CUSTOMARY TO METRIC (SI)
UNITS OF MEASUREMENT

U. S. customary units of measurement used in this report can be converted to metric (SI) units as follows:

Multiply	By	To Obtain
inches	0.0254	meters
square inches	0.00064516	square meters
pounds (mass)	0.4535924	kilograms
pounds (force)	4.448222	newtons
pounds (force) per square inch	6894.757	pascals
pounds (mass) per cubic foot	16.01846	kilograms per cubic meter
inches per minute	0.0254	meters per minute
Fahrenheit degrees	5/9	Celsius degrees or Kelvins*

* To obtain Celsius (C) temperature readings from Fahrenheit (F) readings, use the following formula: $C = (5/9)(F - 32)$. To obtain Kelvin (K) readings, use: $K = (5/9)(F - 32) + 273.15$.

STRESSES AND SHEARING RESISTANCE IN SOIL BENEATH A RIGID WHEEL

PART I: INTRODUCTION

Background

1. The prediction of the stress distribution beneath a wheel is important in soil-wheel interaction studies since the magnitudes of radial and tangential forces generated by the vehicle are the governing factors in the stability of the supporting soil, which the ultimate mobilization of a vehicle depends upon. Two approaches are known to be used in prediction of stresses beneath wheels or tracks of military vehicles:

a. The analytical approach in which the soil is idealized and assumed to have elastic[1] or plastic properties.[2]

b. The experimental approach in which pressure or stress cells are used to measure the vertical component of stress at the contact area of the wheel[3,4] or beneath the soil surface.[1]

Analytical approach

2. The analytical analysis of stress distribution within the soil beneath a military vehicle is mainly based on Boussinesq's theory,[5] which is derived to evaluate the stress distribution beneath a concentrated load acting vertically on the horizontal plane of a semi-infinite, elastic, homogeneous material. According to Boussinesq's theory, the vertical stress σ_y at any point within the medium can be expressed as:

$$\sigma_y = \frac{3}{2\pi y^2} \frac{P}{\left[1 + \left(\frac{r}{y}\right)^2\right]^{5/2}} \qquad (1)$$

where

P = intensity of the applied load

r = radial distance from the load

y = depth of the point below the surface as shown in fig. 1a

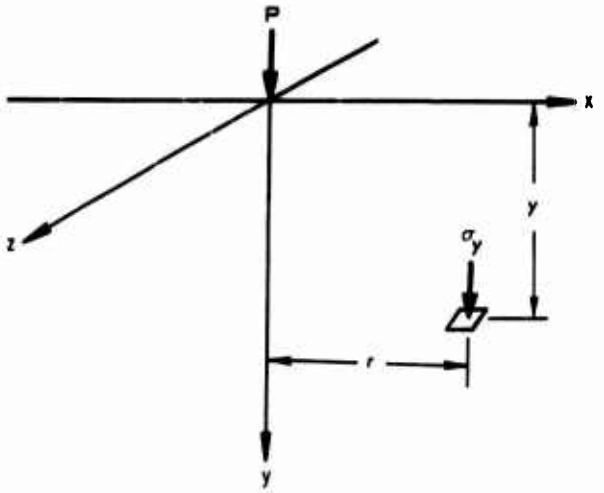

a. CONCENTRATED FORCE ACTING ON A SEMI-INFINITE MASS

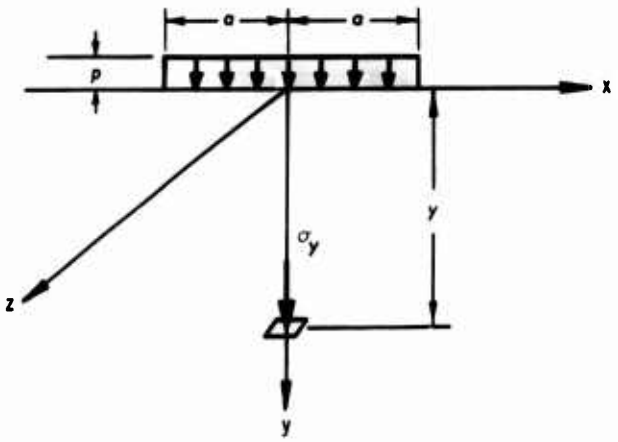

b. VERTICAL STRESS ACTING ON A CIRCULAR AREA

Fig. 1. Graphical representation of vertical stress in semi-infinite mass

Equation 1 has been integrated by Egorov[6] to obtain the stress and displacement beneath a uniformly loaded circular area. The special case of vertical stress σ_y beneath the center line of the loaded area can be expressed as follows:

$$\sigma_y = P\left\{1 - \frac{1}{\left[\left(\frac{a}{y}\right)^2 + 1\right]^{3/2}}\right\} \qquad (2)$$

where

a = radius of the loaded area as shown in fig. 1b

3. The most attractive aspect of equations 1 and 2 is that the vertical stress at any point is only a function of the shape and the intensity of the applied load and also the distance of the point from the surface but not of the elastic properties of the medium. However, the Boussinesq and Egorov equations were derived for specific conditions, and unless their basic assumptions are fully satisfied, their random application in mobility problems may lead to erroneous results. Pertinent points that must be kept in mind before applying equation 1 or 2 in evaluation of stress distribution beneath a wheel are:

a. The projection of the contact area between the wheel and the soil is neither a point nor a circle but rather an ellipse.

b. The theories were derived for a semi-infinite medium with a horizontal plane surface, and they do not take into consideration the geometry at the soil surface created by the moving wheel.

c. The theories do not account for the shear stresses on the contact area between the wheel and soil, which are responsible for the traction resistance of a moving vehicle.

d. The applied stresses are usually in the radial and tangential direction of the wheel-soil contact area and are not perpendicular to the horizontal surface of soil.

Experimental approach

4. Because of the limited application of the Boussinesq and Egorov theories in mobility study, more emphasis was placed on experimental stress analysis. Indeed, many experimental devices, such as the U. S. Army Engineer Waterways Experiment Station (WES) pressure cell,[7]

have been used in measuring vertical stresses, at the surface and within the soil mass, induced by a stationary or moving vehicle. Pressure cells used are either operated by fluid, such as mercury, or are electronic strain gages; they vary in shape, size, and accuracy, and they differ even in the way they are placed in soil to obtain better resolution.[4] The description and the advantages of each type of pressure cell are beyond the scope of this report. However, regardless of the type pressure cell used, there is always physical limitation inherent in this branch of study that makes pressure cell readings highly inconsistent. According to Knight,[8] inconsistency in the measured data can be attributed to any one or a combination of several factors, such as variable path of vehicle due to guide-channel movement in the soft soil, pressure cell movement during the response period, stress concentration or dispersion due to variable soil conditions above and adjacent to the cell, or improper seating of the pressure cell. Other such factors are the size of the cell compared to the maximum size of soil particles and the sensitivity of pressure cell reading to lateral and shear stresses that cannot be measured by the existing pressure cells. Thus it appears that in addition to the enormous cost and time involved in experimental stress analysis using pressure cells, it is almost impossible to obtain a precise measurement with the presently available instrumentation.

Purpose

5. From the above discussion, it can be stated that current analytical and experimental techniques are inadequate to provide data input for the design of improved military vehicles from the standpoint of their ability to travel across natural terrain. Such an objective cannot be achieved unless the stress distribution at the surface and within the soil as it is deformed by the moving wheel is thoroughly understood. This objective represents in part the purpose of this report.

6. The primary purposes of this investigation were:

a. To present a new theoretical approach for determining the magnitudes and the orientations of normal and shear stresses beneath a circular depression when acted upon by uniform radial and tangential stresses.

b. To generalize the solution to include the evaluation of normal and shear stresses under any combination of radial and tangential stresses.

c. To use the analytical solution in solving practical problems of mobility studies, such as towed and power wheels, and to provide theoretical reasons to explain their observed performance variation.

d. To stimulate interest in the development of a more closed-form solution based on broadly accepted stress-strain relations that can be used more systematically and logically in terrain-vehicle mechanics as well as applied soil mechanics.

e. To investigate the physical properties of typical soil and to estimate the relationships between the normal and shear stresses that can be expected at the interface between the soil and a wheel of a moving vehicle.

f. To study the influence of different factors, such as water content, rate of shear deformation, density, surface wetness, and initial stress levels, on the relationship between the shear and normal stresses that occur with the soil-wheel system.

Scope

7. Theoretical solutions were developed in this study to investigate the distribution of normal and shear stresses within a semi-infinite mass, the upper boundary of which consisted of a segment of circular arc connected with two straight lines extended to infinity, in an effort to generate a reasonable analytical solution to the wheel-soil interaction problem. The circular arc, which simulates the area of contact between the moving wheel (i.e., rigid wheel or pneumatic tire with inflation pressure close to average contact pressure), is acted upon by a uniform radial or tangential or a combination of both stresses. Results of normal and shear stresses within the framework of the proposed wheel-soil system are presented as influence tables; thus, their usage will not be restricted to specific cases. Available analytical and experimental data provided by WES and other investigators were also

correlated with the new solutions whenever possible.

8. The experimental study was limited to CH material, compacted at water contents of 26 and 30 percent, which correspond to dry densities of 95 and 92 pcf,* respectively. Because laboratory tests were intended to simulate soil-wheel field conditions as closely as possible, it was decided to shear the soil specimens under constant volume for large shear deformations and at rates of strain higher than those commonly used in soil testing. The WES 1947 annular shear apparatus was chosen for the test program after equipping it with a constant-volume loading system and automatic recording system. The experimental study was limited to shearing of (a) homogeneous soil specimens, (b) soil against tire rubber, (c) soil against steel, and (d) soil specimens inhomogeneous with respect to water. The initial normal stresses imposed on soil specimens at the beginning of shear were limited to 5, 15, and 30 psi, which are comparable to those normally encountered under moving vehicles. The rates of shear deformation adopted in the test program were 0.002, 0.200, and 2.00 in./min.

---

* A table of factors for converting U. S. customary units of measurement to metric (SI) units is presented on page 5.

PART II: STRESS DISTRIBUTION BENEATH A UNIFORMLY LOADED CIRCULAR SEGMENT IN A SEMI-INFINITE MASS

9. WES was assigned the task of conducting experimental tests simulating the movement of wheels on soft soil in an attempt to find some meaningful way to improve design of military vehicles for mobility in rugged terrain. This task was an extension of trafficability of soil studies that have been taking place at WES for many years. As a result of the experimental study, an effort was made to explore and determine the interdependent stress relationship that exists between the wheel and the supporting soil.

Statement of the Problem

10. In this study, attention was focused toward the determination of stress within the soil mass from the knowledge of contact stresses beneath the moving wheel. The first step consisted of a study of uniform radial and tangential contact stresses that will be expanded later on to include any form or combination of contact stresses desired. Allowance will be made to extend the solution for the determination of a strain field within the soil-wheel system in order to provide better understanding of the soil deformation pattern beneath the wheel, such as sinkage, bulldozing, etc., on a more rational and more exact basis.

Assumptions

11. As an introduction to the analytical solution, the following assumptions were made:

a. The contact surface between the soil and the wheel has a circular curvature.

b. The soil beneath the wheel is a modified semi-infinite mass.

c. The soil is weightless and isotropic.

d. The contact stresses between the wheel and soil are uniform radial and tangential stresses.

e. A state of plane strain conditions exists within the framework of the wheel-soil system.

12. The assumptions stated above are justified as follows.

The deformation of a rigid wheel or pneumatic tire with medium to high inflation pressure is not appreciable compared to the deformation of soft soil. As a result, the deformed shape of soil tends to take the shape of the wheel, which justifies the first assumption. The second assumption is justified because stresses are significant only within the vicinity of the wheel and diminish very rapidly with increasing distance from the surface. The soil region is called a modified semi-infinite mass because of the presence of circular depression (see fig. 2) in the half-space. The assumption of weightless material is justified simply because stress due to wheel load is concentrated at regions close to the surface, whereas effect of stress due to the weight of soil is immaterial. However, the effect of the weight of material becomes more significant at great depth.

13. The assumption that the contact radial stress is assumed to be uniform is based on actual WES test data[3,4] that show that the vertical stresses along the central portion of the contact area in the direction of motion are fairly constant and proportional to the inflation pressure. Since the normal contact pressure is constant and the coefficient of friction between a given soil and wheel is constant, then the resulting shear stress has to be uniform. Thus, the assumption of uniform tangential stress is also justified.

14. In defense of the last assumption, it could be said that vertical and horizontal components are at their maximum in the direction of the applied stress, i.e., in a plane parallel to the vehicle motion. However, the deformation in planes transverse to vehicle motion, even at the surface, is almost negligible compared to that in planes in the direction of motion. Thus, the existence of plane strain conditions within the soil-wheel system is not far from reality.

Theoretical considerations

15. In the previous section, it was shown that the wheel-soil interaction problem can be closely approximated as plane strain cases. Thus, equations for plane strain theory of elasticity are applicable. However, before an analytical solution to plane strain problems can be obtained, the conditions of equilibrium, boundary, and compatibility

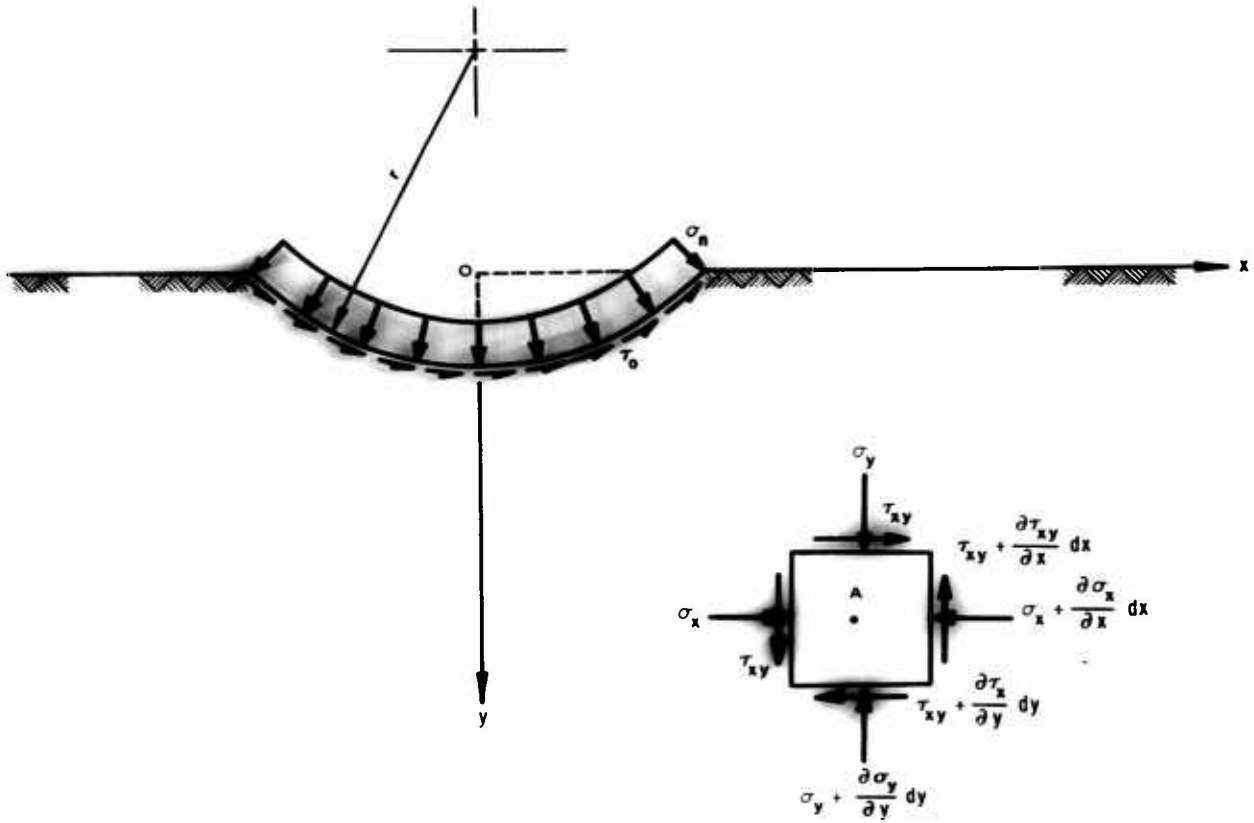

Fig. 2. State of stress at a point within the soil mass

must be satisfied.[9] These three conditions constitute the necessary and sufficient conditions to satisfy the solution of an elasticity problem.

16. Equilibrium conditions. Consider a soil element, at point A beneath a wheel (see fig. 2), to be under plane strain conditions. This element (see fig. 3a) is considered to be so small that loading is essentially uniform and representable in the first approximation by a single load in the center of the plane of application. Since the material is considered to be weightless, the equilibrium condition can be obtained by summing forces in the x and y directions, resulting in the following:

$$\frac{\partial \sigma_x}{\partial x} + \frac{\partial \tau_{xy}}{\partial y} = 0 \tag{3a}$$

$$\frac{\partial \sigma_y}{\partial y} + \frac{\partial \tau_{xy}}{\partial y} = 0 \tag{3b}$$

where

σ_x and σ_y = normal stresses in the x and y directions, respectively

τ_{xy} = shear stress

17. Boundary conditions. The stress components vary throughout the soil mass, and equilibrium conditions must be satisfied at any point within the soil mass, including the boundary. In this respect, the boundary stresses are considered to be a continuation of the internal stress distribution. Assuming BC is any small element that coincides with the boundary, then the boundary conditions from fig. 3b are:

$$\sigma_x \cos(n,x) + \tau_{xy} \cos(n,y) = \bar{X} \tag{4a}$$

$$\sigma_y \cos(n,y) + \tau_{xy} \cos(n,x) = \bar{Y} \tag{4b}$$

where

$\bar{X}$ and $\bar{Y}$ = components of surface forces per unit area in the x and y directions, respectively, and

$\cos(n,x)$ and $\cos(n,y)$ = the direction cosines

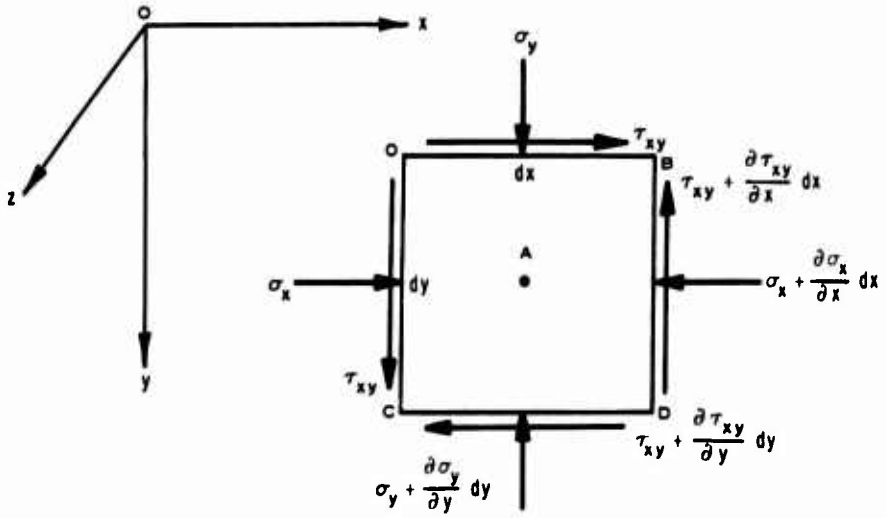

a. AN ELEMENT WITHIN THE MASS

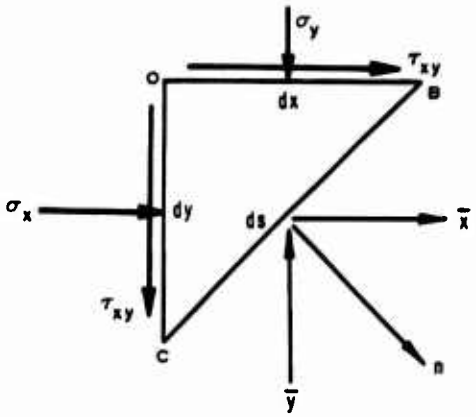

b. AN ELEMENT ON THE BOUNDARY

Fig. 3. Graphical representation of equilibrium and boundary conditions

Geometrically, the direction cosines can be represented in terms of dx , dy , and ds , as:

$$\cos(n,x) = \frac{dy}{ds} \tag{5a}$$

$$\cos(n,y) = -\frac{dx}{ds} \tag{5b}$$

18. Compatibility condition. A compatibility condition exists if the strain components at any point A due to the applied loads fit their neighboring points perfectly in a manner that satisfies strain condition. The compatibility equation in terms of stress components for plane strain case can be written as

$$\left(\frac{\partial^2}{\partial x^2} + \frac{\partial^2}{\partial y^2}\right)(\sigma_x + \sigma_y) = \nabla^2(\sigma_x + \sigma_y) = 0 \tag{6}$$

where

∇^2 = Laplacian operator

19. Stress function. As stated previously, the equilibrium and compatibility equations represent necessary and sufficient conditions to solve for the stress components σ_x , σ_y , and τ_{xy} . In order to solve the differential equations 3 and 6, a new function $U(x,y)$* may be introduced such as:

$$\sigma_x = \frac{\partial^2 U(x,y)}{\partial y^2} \tag{7a}$$

$$\sigma_y = \frac{\partial^2 U(x,y)}{\partial x^2} \tag{7b}$$

$$\tau_{xy} = -\frac{\partial^2 U(x,y)}{\partial x \partial y} \tag{7c}$$

---

* This function $U(x,y)$, which is called stress function or Airy's stress function, was first introduced in 1862 by G. B. Airy.[9]

Adding equations 7a and 7b yields:

$$\sigma_x + \sigma_y = \frac{\partial^2 U(x,y)}{\partial y^2} + \frac{\partial^2 U(x,y)}{\partial x^2} = \nabla^2 U(x,y) \tag{8}$$

20. If the stress components σ_x, σ_y, and τ_{xy} are single-valued with a continuous first and second derivative throughout the region occupied by the soil, then the function $U(x,y)$ must have a single value and continuous third- and fourth-order derivatives throughout the soil beneath the wheel.

21. It is apparent that the equations of equilibrium are identically satisfied by simply substituting equations 7a, 7b, and 7c into equations 3a and 3b. However, a true and unique solution to the problem can be obtained only when compatibility is also satisfied. This condition is accomplished by substituting equations 7a, 7b, and 7c into equation 6 as follows:

$$\frac{\partial^4 U(x,y)}{\partial x^4} + 2\,\frac{\partial^4 U(x,y)}{\partial x^2 \partial y^2} + \frac{\partial^4 U(x,y)}{\partial y^4} = 0 \tag{9}$$

Thus, the problem of solving differential equations 1, 2, and 7 is reduced to the solution of one biharmonic equation that satisfies both the equilibrium and compatibility conditions. The solution of equation 11 (given later) that satisfies the boundary condition in a simply connected region* is a correct solution.

Complex Representation of the Weightless Plane Strain Problem

22. It has been shown that the evaluation of the stresses σ_x, σ_y, and τ_{xy} within a simple connected region lies in the solution of a biharmonic differential equation such as equation 11 (given below). The solution of a biharmonic equation is very tedious and involved without introducing some means to simplify the problem. One method of

---

* A region R is called simply connected if any simple closed curve that lies in R can be shrunk to a point without leaving the region.

simplifying the problem is to transform the biharmonic equation to a harmonic one* using some analytic function.** Such a procedure is similar to that developed by Muskhelishvili[11] and the notations used are those adopted by Baladi.[12]

Representation of stress function
in terms of harmonic complex function

23. Assuming the existence of a given function $P(x,y)$ equivalent to $\nabla^2 U(x,y)$, equations 8 and 9 can be written as:

$$\sigma_x + \sigma_y = \nabla^2 U(x,y) = P(x,y) \tag{10}$$

$$\nabla^4 U(x,y) = \nabla^2 P(x,y) = 0 \tag{11}$$

Thus, the function $P(x,y)$ is a harmonic function and will have a conjugate harmonic function $Q(x,y)$. Consequently, $P(x,y) + iQ(x,y)$ is the analytic function of $z = x + iy$ and can be written as:

$$W(z) = P(x,y) + iQ(x,y) \tag{12}$$

The integration of this function with respect to z yields another analytic function. Let that function be defined as $4\phi(z)$. Consequently

$$\phi(z) = p(x,y) + iq(x,y) = \frac{1}{4}\int w(z)\, dz \tag{13}$$

where

$p(x,y)$ and $q(x,y)$ = real and imaginary parts, respectively, of $\phi(z)$

Thus, the function $w(z)$ can be obtained by differentiating equation 13

$$\phi'(z) = \frac{\partial p(x,y)}{\partial x} + i\,\frac{\partial q(x,y)}{\partial y} = \frac{1}{4}\, w(z) = \frac{1}{4}\left[P(x,y) + iQ(x,y)\right] \tag{14}$$

---

* Harmonic function is the one that satisfies Laplace's equation.[10]

** Analytic function in a region is a function whose derivative exists at all points within the region.

24. Equating the real parts of the second and last members of equation 14 in conjunction with the Cauchy-Riemann* condition yields

$$\frac{\partial p(x,y)}{\partial x} = \frac{\partial q(x,y)}{\partial y} = \frac{1}{4} P(x,y) = \frac{1}{4} \nabla^2 U(x,y) \tag{15}$$

or

$$\nabla^2 U(x,y) - 2 \frac{\partial p(x,y)}{\partial x} - 2 \frac{\partial q(x,y)}{\partial y} = 0 \tag{16}$$

which is equivalent to

$$\nabla^2 \left[U(x,y) - xp(x,y) - yq(x,y) \right] = 0 \tag{17}$$

25. Equation 17 represents a harmonic function equal to $p_1(x,y)$. Consequently, the stress function $U(x,y)$ is equal to

$$U(x,y) = xp(x,y) + yq(x,y) + p_1(x,y) \tag{18}$$

Equation 18 clearly demonstrates that any stress function can be formulated by use of the appropriate conjugate harmonic functions $p(x,y)$, $q(x,y)$, and a harmonic function $p_1(x,y)$. However, the functions $p(x,y)$ and $q(x,y)$ were used for a mathematical expediency but not necessarily for the solution. This necessitates the introduction of another harmonic function $q_1(x,y)$ conjugate to $p_1(x,y)$, and both functions form the real and imaginary parts, respectively, of a function of the complex variable $\chi(z)$ where $z = x + iy$, such that

$$\chi(z) = p_1(x,y) + iq_1(x,y) \tag{19}$$

Thus, the stress function $U(x,y)$ can be expressed as follows:

$$U(x,y) = xp(x,y) + yq(x,y) + \mathrm{Re}\chi(z) \tag{20}$$

---

* The Cauchy-Riemann equations that satisfy the analytic function $\phi(z)$ are $\partial p(x,y)/\partial x = \partial q(x,y)/\partial y$ and $\partial p(x,y)/\partial y = -[\partial q(x,y)/\partial x]$.

where

Re = real part of a complex function

The above equation can be rewritten as:

$$U(x,y) = Re\left[(x - iy)p(x,y) + i(x - iy)q(x,y)\right] + Re\chi(z) \qquad (21)$$

However, $x - iy$ is conjugate of z, which may be denoted by $\overline{z}$. Thus

$$U(x,y) = Re\left\{\overline{z}\left[p(x,y) + iq(x,y)\right] + \chi(z)\right\} \qquad (22)$$

Recall that $p(x,y) + iq(x,y) = \phi(z)$. Consequently

$$U(x,y) = Re\left[\overline{z}\phi(z) + \chi(z)\right] \qquad (23)$$

26. Through use of the property of complex variable,[10] equation 23 can be transferred to the following form:

$$2U(x,y) = \overline{z}\phi(z) + z\overline{\phi(z)} + \chi(z) + \overline{\chi(z)} \qquad (24)$$

Taking the partial derivative of equation 24 with respect to y, multiplying it by i, and then adding to the product the partial derivative with respect to x yields:

$$\frac{\partial U(x,y)}{\partial x} + i\,\frac{\partial U(x,y)}{\partial y} = \phi(z) + z\overline{\phi'(z)} + \overline{\chi'(z)} \qquad (25)$$

However, taking the second portion of equation 24 with respect to x and y and then adding the results yields:

$$\nabla^2 U(x,y) = \left[\phi'(z) + \overline{\phi'(z)}\right] = 4Re\left[\phi'(z)\right] \qquad (26)$$

Comparing equation 26 with equation 10, then

$$\nabla^2 U(x,y) = \sigma_x + \sigma_y = 4Re\left[\phi'(z)\right] \qquad (27)$$

Boundary stress in
terms of complex functions

27. So far, the sum of stresses $\sigma_x + \sigma_y$ has been expressed in terms of complex potential; thus, the next logical step is to represent the state of stress at a point in terms of complex functions. It has been shown in equation 7 that

$$\sigma_x = \frac{\partial^2 U(x,y)}{\partial y^2} \qquad (7a \text{ bis})$$

$$\sigma_y = \frac{\partial^2 U(x,y)}{\partial x^2} \qquad (7b \text{ bis})$$

$$\tau_{xy} = - \frac{\partial^2 U(x,y)}{\partial x \partial y} \qquad (7c \text{ bis})$$

Also, geometrical relationships presented in fig. 3b indicate that

$$\cos (n,x) = \cos (s,y) = \frac{dy}{ds} \qquad (28a)$$

$$\cos (n,y) = -\cos (s,x) = - \frac{dx}{ds} \qquad (28b)$$

28. In addition, the boundary conditions presented previously in equation 4 are:

$$\overline{X} = \sigma_x \cos (n,x) + \tau_{xy} \cos (n,y) \qquad (4a \text{ bis})$$

$$\overline{Y} = \sigma_y \cos (n,y) + \tau_{xy} \cos (n,x) \qquad (4b \text{ bis})$$

Substituting equations 7 and 28 into equation 4 yields:

$$\overline{X} = \frac{\partial^2 U(x,y)}{\partial y^2} \frac{dy}{ds} + \frac{\partial^2 U(x,y)}{\partial x \partial y} \frac{dx}{ds} = \frac{d}{ds} \left[\frac{\partial U(x,y)}{\partial y} \right] \qquad (29a)$$

$$\overline{Y} = - \frac{\partial^2 U(x,y)}{\partial x^2} \frac{dx}{ds} - \frac{\partial^2 U(x,y)}{\partial x \partial y} \frac{dy}{ds} = - \frac{d}{ds} \left[\frac{\partial U(x,y)}{\partial x} \right] \qquad (29b)$$

Equations 29a and 29b can be combined into one equation by multiplying the second equation by i and adding the first one. Then

$$\overline{X} + i\overline{Y} = \frac{d}{ds}\left[\frac{\partial U(x,y)}{\partial y} - i\,\frac{\partial U(x,y)}{\partial x}\right] \tag{30}$$

or, for convenience, this equation can be written as

$$\overline{X} + i\overline{Y} = -i\,\frac{d}{ds}\left[\frac{U(x,y)}{\partial x} + i\,\frac{U(x,y)}{\partial y}\right] \tag{31}$$

Comparing the above equation with equation 25, it can be written that

$$\overline{X} + i\overline{Y} = -i\,\frac{d}{ds}\left[\phi(z) + z\overline{\phi'(z)} + \overline{\chi'(z)}\right] \tag{32}$$

29. The value of ds in equation 32 corresponds to both dx and dy as indicated previously in fig. 3b. If ds traverses along the y axis, then

$$ds = dy = -i\,dz$$

Also

$$\overline{X} = \sigma_x$$

and

$$\overline{Y} = \tau_{xy}$$

Substituting these values into equation 32 and taking the derivative with respect to z yields the following equation:

$$\sigma_x + i\tau_{xy} = \phi'(z) + \overline{\phi'(z)} - z\overline{\phi''(z)} - \overline{\chi''(z)} \tag{33}$$

If, on the other hand, ds traverses only along the x axis, then:

$$ds = dx = dz$$

Also

$$\overline{X} = -\tau_{xy}$$

and

$$\overline{Y} = -\sigma_y$$

Substituting into equation 32 and taking the derivative with respect to z yields:

$$\sigma_y - i\tau_{xy} = \phi'(z) + \overline{\phi'(z)} + z\overline{\phi''(z)} + \overline{\chi''(z)} \tag{34}$$

30. Simpler forms can be obtained by adding and subtracting equations 33 and 34:

$$\sigma_x + \sigma_y = 2\left[\phi'(z) + \overline{\phi'(z)}\right] = 4\mathrm{Re}\left[\phi'(z)\right] \tag{35}$$

and

$$\sigma_y - \sigma_x - 2i\tau_{xy} = 2\left[z\overline{\phi''(z)} + \overline{\chi''(z)}\right] \tag{36}$$

Changing i to -i on both sides of equation 36 yields the alternative form

$$\sigma_y - \sigma_x + 2i\tau_{xy} = 2\left[\overline{z}\phi''(z) + \chi''(z)\right] \tag{37}$$

For convenience, let $\phi'(z) = \Phi(z)$ and $\chi''(z) = \psi(z)$; thus, equations 35 and 37 can be presented in the following form:

$$\sigma_x + \sigma_y = 2\left[\Phi(z) + \overline{\Phi(z)}\right] = 4\mathrm{Re}\left[\Phi(z)\right] \tag{38a}$$

$$\sigma_y - \sigma_x + 2i\tau_{xy} = 2\left[\overline{z}\Phi'(z) + \psi(z)\right] \tag{38b}$$

Equation 38 can be used to determine the stress components in terms of complex potentials $\Phi(z)$ and $\psi(z)$. Thus, if definite functions for $\Phi(z)$ and $\psi(z)$ are chosen, the state of stress from equation 38 can be obtained.

Introduction to Conformal Mapping

31. In previous parts of this report, it has been shown that the state of stress at a point in a region can be defined by two analytic functions with continuous first and second derivatives. Thus, the solution of any particular problem lies in obtaining analytic functions that satisfy the stresses at any point within the region, including the boundaries. However, most practical problems, including the one under consideration, do not have a simple geometric boundary. Therefore, the solution to the problem is to transform the region under consideration with its complicated boundary to another one with a smooth boundary, such that each point in the original region corresponds to only one point in the new region. Once the solution has been established in the new region, it can be carried back by the inverse transformation to the region of the original problem. A transformation that possesses the property of preserving angles of intersection and the approximate image of small shapes is said to be conformal[13] and the technique used is called conformal mapping.

Schwarz-Christoffel transformation

32. According to Riemann's mapping theory,[10] an analytic function exists that will map any pair of simply connected regions* conformally onto each other. To clarify this statement, let C_1 in fig. 4a be a simple closed curve in the z plane ($z = x + iy$) forming the boundary of a region R_1. Let C_2 in fig. 4b be another simple closed curve in the t plane ($t = r + is$) forming the boundary of a region R_2. Then there exists a function $t = f(z)$ analytic in R_1 that maps each point in the interior of C_1 onto the interior of C_2. However, the determination of a transformation function that maps conformally a complicated region onto one with simple geometry is not readily available and may require a series of auxiliary functions between the original region and the region in which the stresses at any point can be defined in

---

* If a simple closed curve lying in a region can be shrunk to a point without leaving the region, then that region is called simply connected.

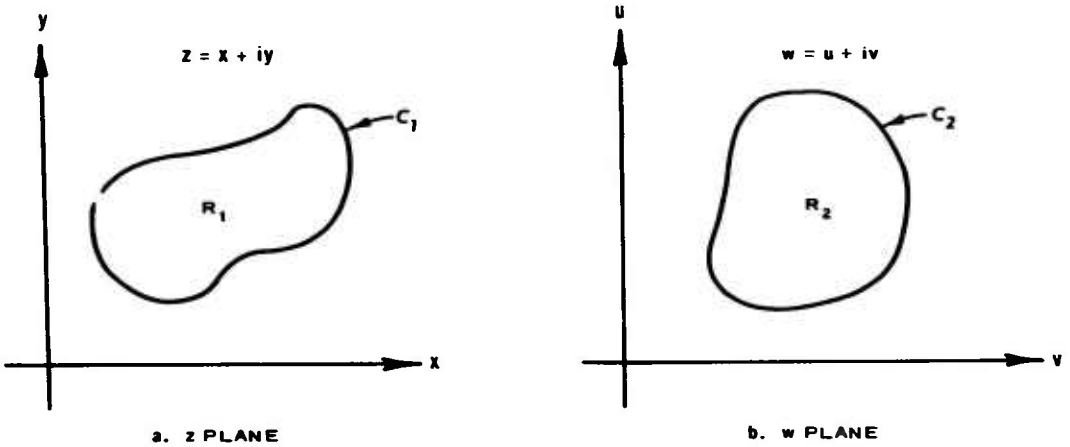

Fig. 4. Graphical representation of z and w planes

terms of analytic functions. The transformation functions used in this study were obtained from Kober's Dictionary of Conformal Representations.[14]

33. One method of special interest to this study is the transformation of a region inside a polygon, whose sides never cross one another, in any plane onto another polygon or on the upper half of another plane. To illustrate this, let w_1 , w_2 , ... w_n shown in fig. 5a be the vertices of a polygon in the w plane ($w = u + iv$) that correspond to interior radian angles, α_1 , α_2 , ... α_n . Also let r_1 , r_2 , ... r_n ($r_1 < r_2 \ldots < r_n$) be the points on the real axis of the t plane ($t = r + is$) that correspond to the vertices w_1 , w_2 , ... w_n of the polygon, respectively (see fig. 4b).

34. A transformation that maps the interior of the polygon of the w plane onto the upper half of the t plane and the boundary of the polygon on the real axis of the t plane is given by

$$w = M \int_{t_1}^{t_2} \frac{dt}{(t - r_1)^{1-\alpha_1/\pi}(t - r_2)^{1-\alpha_2/\pi} \ldots (t - r_n)^{1-\alpha_n/\pi}} + N \qquad (39)$$

where

M and N = complex constants that control the size and position of the polygon

Equation 39 is called the Schwarz-Christoffel transformation.

35. The above transformation is in effect mapping a polygon of the w plane onto a similar polygon in the t plane in such a way that the open sides of the polygon extend to $r = \pm\infty$ of the real axis of the t plane. It may also be said that the region bounded by the opening of the w plane and a semicircle with infinite radius that occupies the entire upper half of the t plane comprise the interior of another polygon in the t plane. Therefore, the Schwarz-Christoffel transformation maps conformally the region bounded by the polygon w_1 , w_2 , ... w_n onto the interior of the polygon r_1 , r_2 , ... r_n and the semicircle with infinite radius that covers the entire upper half of the t plane.

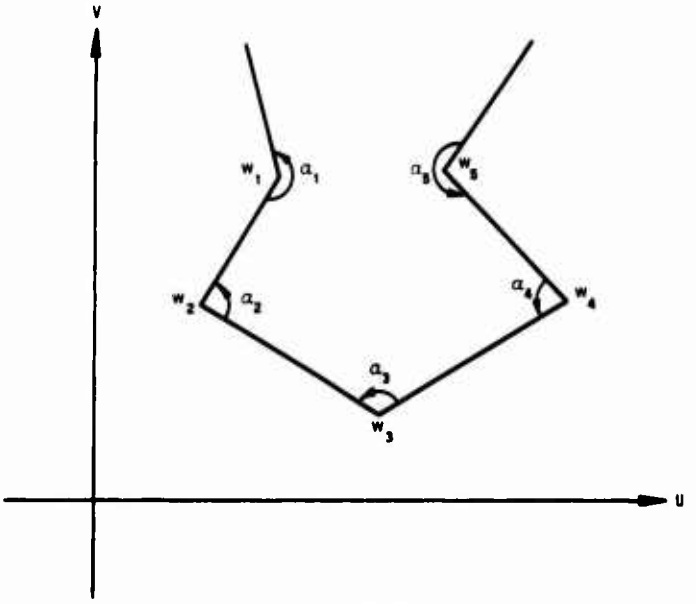

a. w PLANE

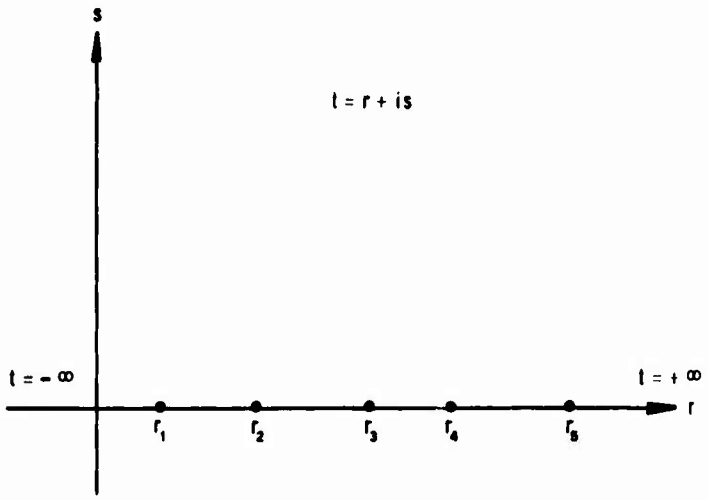

b. t PLANE

Fig. 5. Graphical representation of Schwarz-Christoffel transformation

Transformation of Cartesian coordinates to curvilinear coordinates

36. If the boundary of a region is described by a set of orthogonal curves, a case that is encountered in many practical problems and also in using Schwarz-Christoffel transformation, then it is more convenient to use curvilinear coordinates rather than Cartesian coordinates. The geometrical transformation between the Cartesian and curvilinear coordinates may be described as follows: let c in fig. 6 be a vector originating at some point $z = f(t)$, where $t = r + is$. Also, let c_x and c_y be the projection of c on the x and y axes and c_r and c_s be its projection on the r and s axes, respectively. According to Muskhelishvili,[11] the transformation equation can be expressed as:

$$c_r + ic_s = (c_x + ic_y)e^{-i\theta} \tag{40}$$

where

θ = angle between c_x and c_r measured counterclockwise

In the above equation, $e^{-i\theta}$ is the only unknown that needs to be determined.

37. To determine $e^{i\theta}$, let the point z be given a displacement dz in the direction of r. The corresponding point in the t plane will exhibit a displacement $dr > 0$ in the direction of r. Since

$$z = f(r + is) = f(t) \tag{41}$$

then

$$dz = f'(t)\, ds \tag{42}$$

By definition

$$dz = |dz|\, e^{i\theta} = f'(t)e^{i\theta}\, ds \tag{43}$$

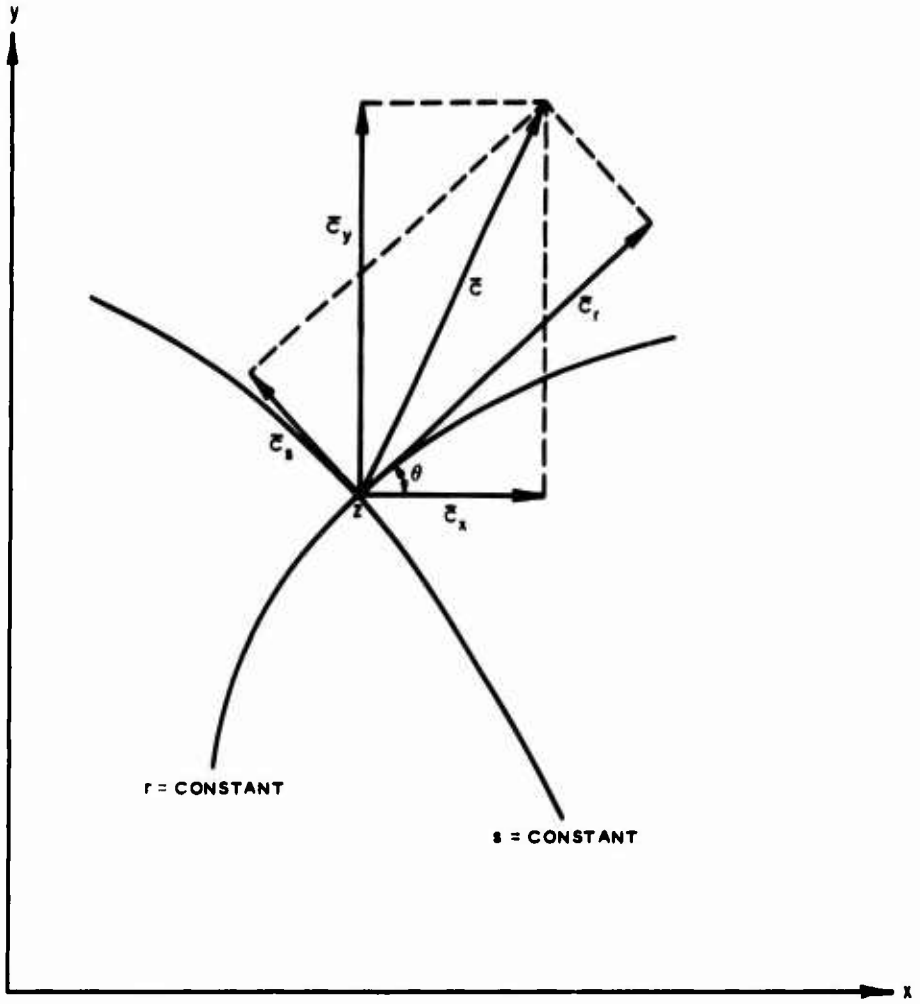

Fig. 6. Transformation of Cartesian coordinates to curvilinear coordinates

Equations 42 and 43 can be combined to obtain

$$f'(t)\,ds = |f'(t)|\,e^{i\theta}\,|ds| \tag{44}$$

or

$$e^{i\theta} = \frac{f'(t)\,ds}{|f'(t)|\,|ds|} = \frac{f'(t)}{|f'(t)|} \tag{45}$$

Therefore

$$e^{-i\theta} = \frac{\overline{f'(t)}}{|f'(t)|} \tag{46}$$

Dividing equation 45 by equation 46 yields

$$e^{2i\theta} = \frac{f'(t)}{\overline{f'(t)}} \tag{47}$$

Finally, the transformation from Cartesian to curvilinear coordinates can be completed by substituting equation 46 into equation 43 to obtain

$$c_r + ic_s = \frac{\overline{f(t)}}{|f'(t)|}\,(c_x + c_y) \tag{48}$$

Representation of stress components in curvilinear coordinates

38. It has been shown in equation 38 that the Cartesian components of stress can be presented in terms of complex potentials $\phi(z)$ and $\psi(z)$. If it is necessary to use curvilinear coordinates, then the complex potential can be expressed as a function of t, and z can also be expressed in terms of t by using equation 41. Ultimately, it is possible to express the Cartesian stress components σ_x, σ_y, τ_{xy} at a point in the z plane in terms of σ_r, σ_s, τ_{rs} corresponding to the same point in the t plane. In order to do that, let the stresses σ_r, σ_s, τ_{rs} be the normal and shear stresses acting on an element, as shown in fig. 7, in the t plane. According to Timoshenko,[9] the relationship between σ_x, σ_y, τ_{xy} and σ_r, σ_s, τ_{rs} can be expressed as follows:

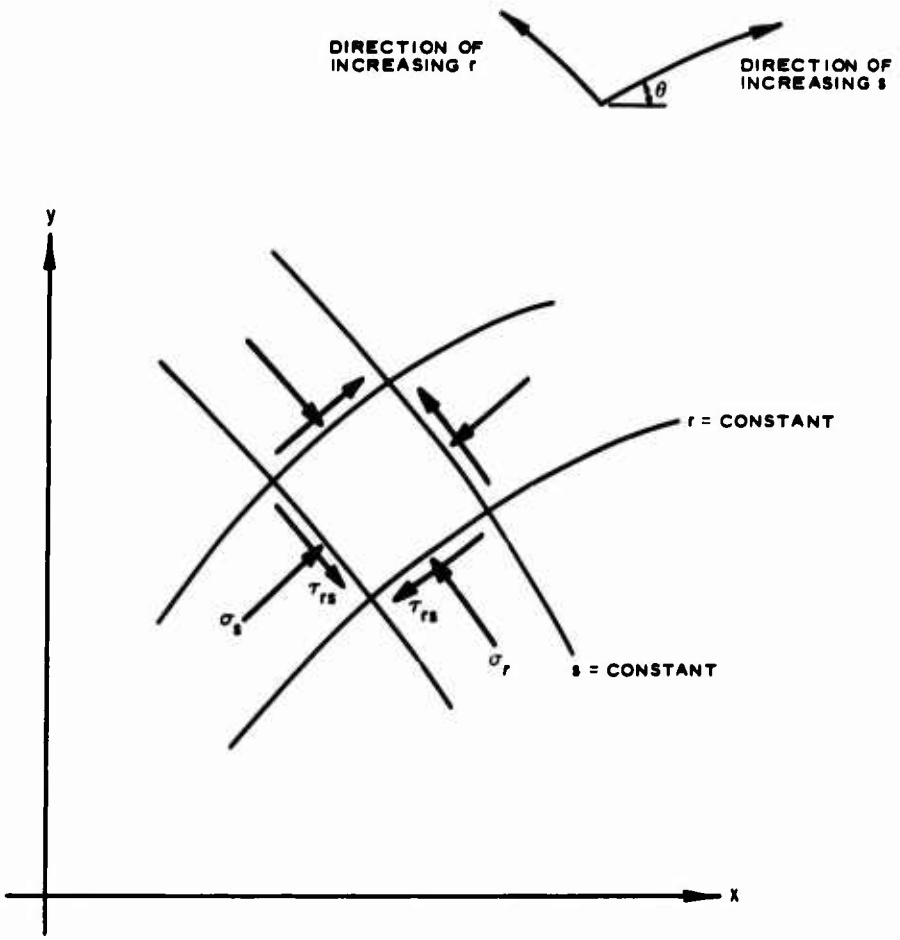

Fig. 7. Curvilinear stress components acting on an element

$$\sigma_r + \sigma_s = \sigma_x + \sigma_y \tag{49a}$$

$$\sigma_s - \sigma_r + 2i\tau_{rs} = (\sigma_y - \sigma_x + 2i\tau_{xy})e^{2i\theta} \tag{49b}$$

39. Recognizing equations 38a and 38b, thus it is also possible to express σ_r, σ_s, and τ_{rs} in terms of complex potential. Then

$$\sigma_r + \sigma_s = 2\left[\phi(z) + \overline{\phi(z)}\right] = 4\mathrm{Re}\left[\phi(z)\right] \tag{50a}$$

$$\sigma_s - \sigma_r + 2i\tau_{rs} = 2\left[\bar{z}\phi'(z) + \psi(z)\right]e^{2i\theta} \tag{50b}$$

Of course, $\phi(z)$ and $\psi(z)$ are complex potentials in the z plane; therefore, the next logical step is to find their equivalent in the t plane.

Complex representation
of stresses in t plane

40. Equation 41 indicates that $z = f(t)$; therefore, the functions $\phi(z)$ and $\psi(z)$ can be written in terms of t as follows:

$$\phi(z) = \phi\left[f(t)\right] = \phi(t) \tag{51a}$$

and

$$\psi(z) = \psi\left[f(t)\right] = \psi(t) \tag{51b}$$

Therefore

$$\phi'(z)f'(t) = \phi'(t) \quad \text{or} \quad \phi'(z) = \frac{\phi'(t)}{f'(t)} \tag{52a}$$

and

$$\psi'(z)f'(t) = \psi'(t) \quad \text{or} \quad \psi'(z) = \frac{\psi'(t)}{f'(t)} \tag{52b}$$

Substituting equations 47, 51, and 52 in equation 50 leads to

$$\sigma_r + \sigma_s = 2\left[\phi(t) + \overline{\phi(t)}\right] = 4\mathrm{Re}\left[\phi(t)\right] \tag{53a}$$

$$\sigma_s - \sigma_r + 2i\tau_{rs} = 2\left[\overline{f(t)}\,\frac{\phi'(t)}{f'(t)} + \psi(t)\right]\frac{f'(t)}{\overline{f'(t)}} \tag{53b}$$

For convenience, equation 53b can be written as

$$\sigma_s - \sigma_r + 2i\tau_{rs} = 2\left[\overline{f(t)}\,\frac{\phi'(t)}{\overline{f'(t)}} + \frac{f'(t)}{\overline{f'(t)}}\,\psi(t)\right] \tag{53c}$$

Thus, if $\phi(t)$, $\psi(t)$, and $f(t)$ are known, the stresses σ_r, σ_s, and τ_{rs} can be defined, which in turn allows the determination of σ_x, σ_y, and τ_{xy}.

PART III: ANALYTICAL SOLUTION OF THE PROBLEM

41. The boundary of the problem under consideration (fig. 1) consists of a portion of a circular arc connected with two straight lines along the x axis extending to infinity. The circular arc simulates the area of contact between the wheel (i.e., rigid wheel or pneumatic tire with inflation pressure equal to or higher than the average contact pressure) and the soft soil of infinite depth. The circular arc is acted upon by a uniform radial stress N and a uniform tangential stress T, where N and T could be any combination of normal and shear stresses developed on the contact area between the moving wheel and the soil. In short, the wheel-soil interaction problem is reduced to the evaluation of stresses within a semi-infinite region bounded by a circular arc and two straight lines extended to infinity.

Geometric Transformation

42. Since the boundary of the region along the x axis consists of a circular arc and two straight lines, the boundary is piecewise, i.e., the derivative at the point of contact between the arc and the straight lines does not exist. Therefore, the solution lies in transforming the region with its piecewise boundary to a semi-infinite region with smooth boundaries so every point in the actual region will correspond to one and only one point in the new region. This will be accomplished by the following transformation.

Transformation of half plane with circular segment removed onto infinite strip

43. Since direct transformation from the region under consideration onto the half-space is not readily available, an intermediate transformation using an auxiliary plane will be used. In fig. 8, let the region R_1, in the z plane, with points c, d, and e having their abscissas at $x = +1$, $x = 0$, and $x = -1$, respectively, be on the region R_2 which forms an infinite strip of width K in the upper

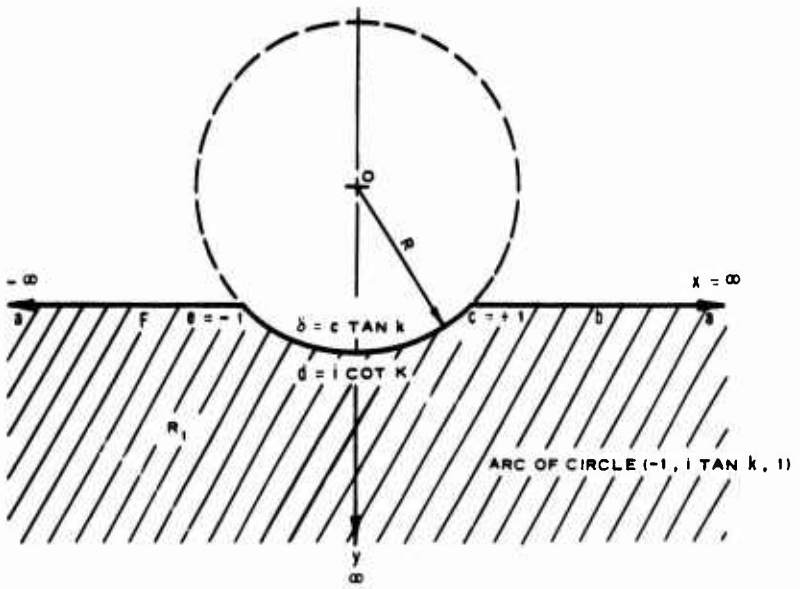

a. z PLANE

$$z = \tanh w = \frac{e^{2w} - 1}{e^{2w} + 1}$$

$$w = \tanh^{-1} z = \frac{1}{2} \ln \frac{1 + z}{1 - z}$$

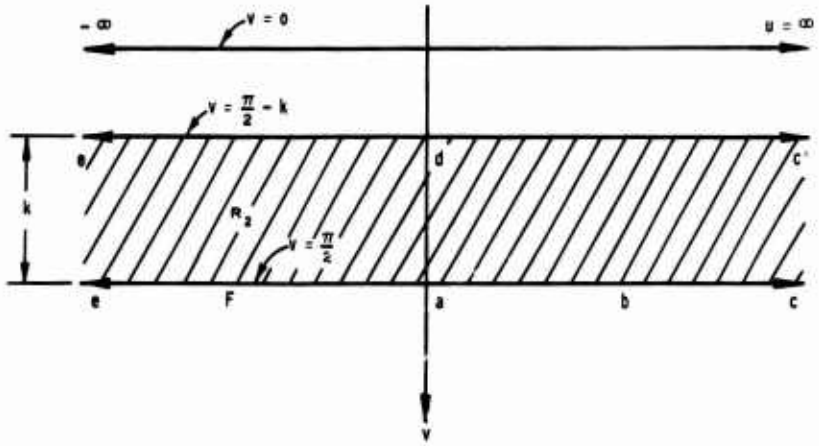

b. w PLANE

Fig. 8. Transformation of half plane with circular segment removed on infinite strip

half of the w plane. The value of K is directly related to the depth of sinkage δ by the following equation

$$\delta = \cot K = R - \sqrt{R^2 - 1} \tag{54}$$

The relations between δ, K, and the radius of the wheel R are presented in fig. 9.

44. The mapping function necessary to transform the region R_1, point by point, onto region R_2 can be expressed as

$$z = \tanh w = \frac{e^{2w} - 1}{e^{2w} + 1} \tag{55}$$

or

$$w = \tanh^{-1} z = \frac{1}{2} \ln \frac{1 + z}{1 - z} \tag{56}$$

Verification of the
transformation function

45. Equation 55 can be easily verified by resolving z and w to their real and imaginary parts, which after some trigonometric manipulation can be written as

$$x + iy = \frac{\tanh u}{\cos^2 v + \tanh^2 u \sin^2 v} + i \frac{\cot v \operatorname{sech}^2 u}{\cot^2 v + \tanh^2 u} \tag{57}$$

Therefore, by substituting the values of u and v at any known point in the w plane, the corresponding values of x and y on the z plane can be obtained. For example, at point c, $u = \infty$ and $y = \pi/2$; thus, the corresponding values of x and y can be obtained by directly substituting the values of u and v in equation 57. Thus

$$x + iy = \frac{\tanh (\infty)}{\cos^2 \left(\frac{\pi}{2}\right) + \tan^2 (\infty) \sin^2 \left(\frac{\pi}{2}\right)} + i \frac{\cot \left(\frac{\pi}{2}\right) \operatorname{sech}^2 (\infty)}{\cot^2 \left(\frac{\pi}{2}\right) + \tanh^2 (\infty)} \tag{58}$$

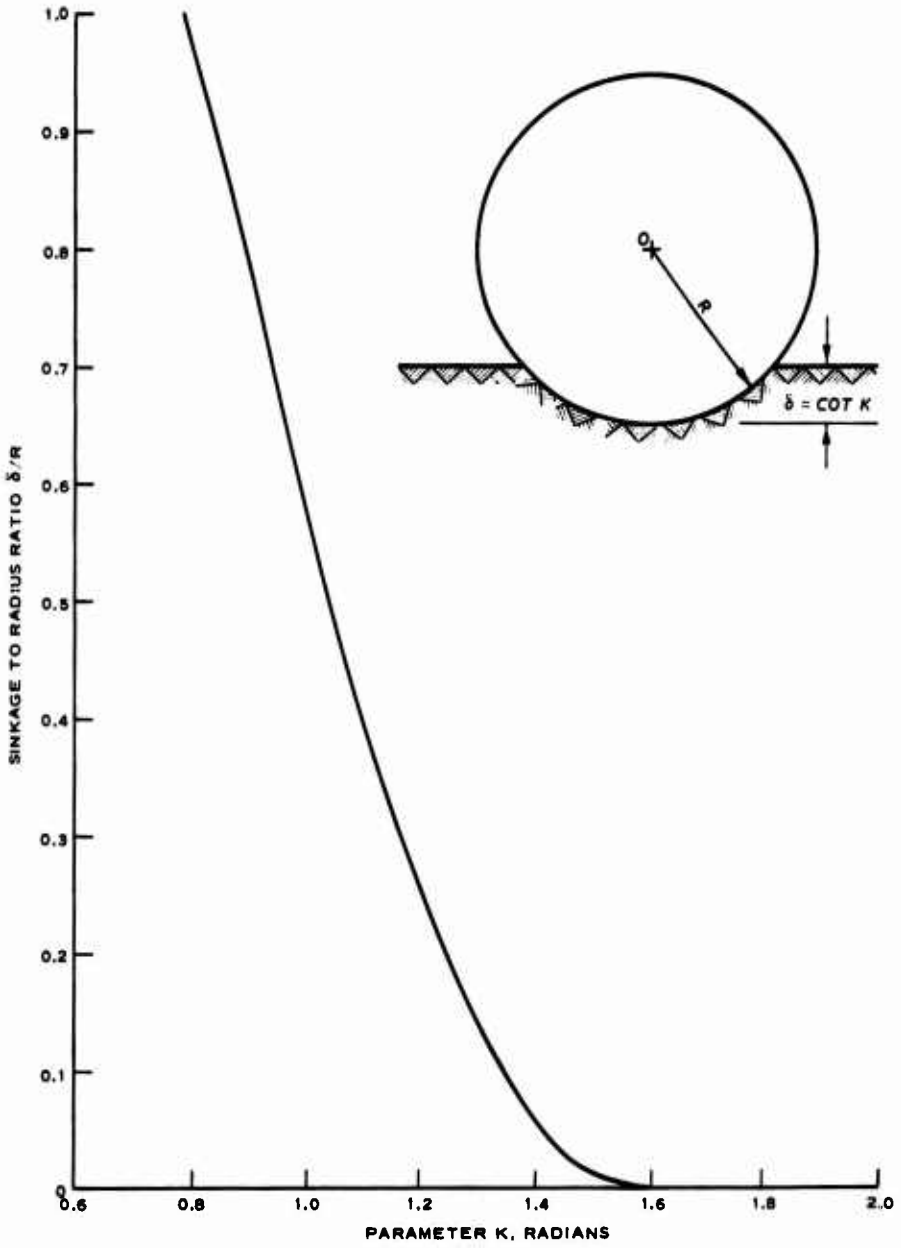

Fig. 9. Relationship between δ , R , and K

or

$$x + iy = 1 + i(0) \tag{59}$$

46. By equating the real part to be equal to the real part and the imaginary part to be equal to the imaginary part on both sides of equation 51, it follows that $x = 1$, and $y = 0$. The calculated values of x and y represent exactly the real and imaginary parts of point c on the z plane. In a similar manner, the rest of the points can be checked; therefore $z = \tanh w$ is truly the correct transformation function.

Transformation of the infinite
strip onto the semi-infinite plane

47. Since the transformation of the original region R_1 was mapped onto the infinite strip R_2 in the w plane, the problem now is to map the region bounded by the infinite strip onto the upper half of another plane, such as t plane ($t = r + is$). Theoretically, the boundary of the infinite strip shown in fig. 10 can be considered as a polygon with its vertices at infinity; thus, the Schwarz-Cristoffel equation can be applied. The Schwarz-Cristoffel transformation will map the region R_2 conformally onto the region R_3, which forms the entire upper half of the t plane. Substituting the proper values of α and r of points a, c', d, and e obtained from fig. 10 into equation 39 yields

$$w = M\int \frac{dt}{(t^2 - 1)} + N = \frac{M}{2} \ln\left(\frac{t - 1}{t + 1}\right) + N \tag{60}$$

where

M and N = complex constants

48. To determine the value of N, consider the condition corresponding to point a (i.e., $t = \infty$ for $z = \pi i/2$) and substitute in equation 60 to obtain $N = \pi i/2$. Also, at point d, $t = 0$ for $z = i[(\pi/2) - K]$, which after substituting in equation 60 yields a value of $M = -2K/\pi$. Once the values of M and N are known, equation 60 can be written as:

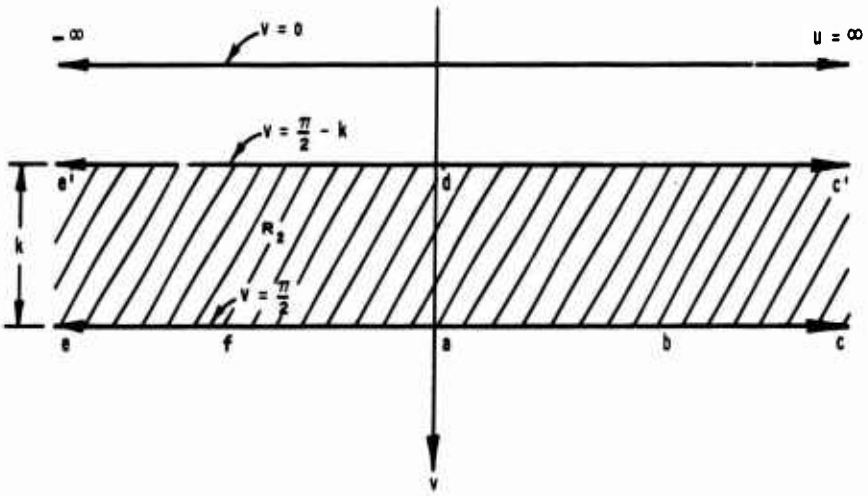

a. w PLANE

$$w = -\frac{k}{\pi} \ln\left(\frac{t-1}{t+1}\right) + \frac{\pi i}{2}$$

$$t = \frac{1 + e^{\frac{\pi}{k}\left(\frac{\pi i}{2} - w\right)}}{1 - e^{\frac{\pi}{k}\left(\frac{\pi i}{2} - w\right)}}$$

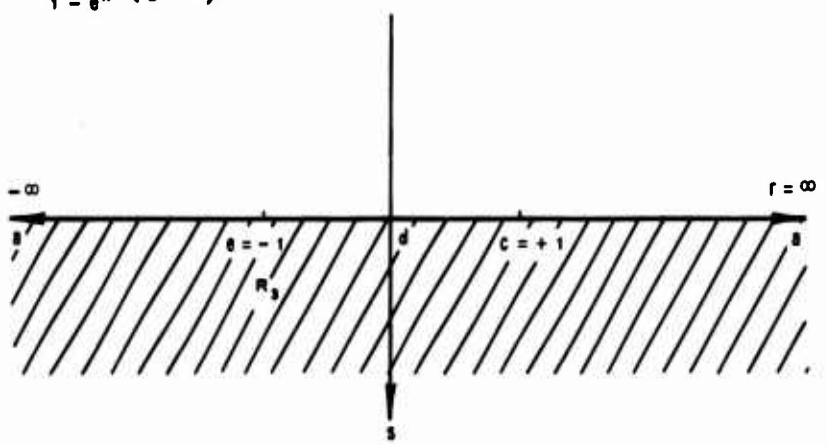

b. t PLANE

Fig. 10. Transformation of infinite strip on the upper half plane

$$w = -\frac{K}{\pi} \ln\left(\frac{t-1}{t+1}\right) + \frac{\pi i}{2} \tag{61}$$

It is possible to eliminate the auxiliary plane w by simply combining equations 61 and 55; thus

$$z = \tanh\left[-\frac{K}{\pi} \ln\left(\frac{t-1}{t+1}\right) + \frac{\pi i}{2}\right] \tag{62}$$

Geometrically, equation 62 means that the boundary of the z plane with its circular indentation will be mapped on the r axis of the t plane and each point within the region under consideration, R_1, will be mapped on a corresponding point in the upper half of the t plane.

49. Because of computer software limitations, equation 62 may be better written in the following form:

$$z = \frac{e^{2[-(K/\pi)\ln(t-1/t+1)+\pi i/2]} - 1}{e^{2[-(K/\pi)\ln(t-1/t+1)+\pi i/2]} + 1} = f(t) \tag{63}$$

Boundary Conditions

Boundary conditions in the z plane

50. In order to simplify the discussion, it is more convenient to present the boundary condition equations in general form first and then modify them to accommodate the specific problem of this study. Therefore, let the normal and shear stresses acting on the x axis of the z plane be defined as N and T; thus, the condition of equilibrium requires that N and T be equal to σ_y and τ_{xy}, respectively. In more general form, N, T, σ_y, and τ_{xy} can be combined into one equation as follows:

$$N + iT = \sigma_y + i\tau_{xy} = \frac{\sigma_x + \sigma_y}{2} + \frac{\sigma_y - \sigma_x + 2i\tau_{xy}}{2} \tag{64}$$

51. The value of $\sigma_y + i\tau_{xy}$ can be obtained easily by adding equations 38a and 38b. Then

$$\sigma_y + i\tau_{xy} = \phi(z) + \overline{\phi(z)} + \bar{z}\phi'(z) + \psi(z) = N + iT \qquad (65)$$

Denoting the boundary of the circular segment by L (see fig. 2), then equation 66 can be written as

$$[N + iT]_L = \left\{2\mathrm{Re}\left[\phi(z)\right] + \bar{z}\phi'(z) + \psi(z)\right\}_L \qquad (66)$$

Boundary conditions in the t plane

52. In a manner similar to that used in the z plane, it is possible to show that the equilibrium condition at the boundary of the t plane can be expressed as

$$N + iT = \sigma_r + i\sigma_s = \frac{\sigma_s + \sigma_r}{2} + \frac{\sigma_s - \sigma_r + z\tau_{rs}}{2} \qquad (67)$$

Also, by adding equations 53a and 53c, the values of N and T can be expressed in terms of functions of t. Then

$$N + iT = \phi(t) + \overline{\phi(t)} + \overline{f(t)}\,\frac{\phi'(t)}{\overline{f'(t)}} + \frac{f'(t)}{\overline{f'(t)}}\,\psi(t) \qquad (68)$$

53. Since the boundary of the region under consideration in the z plane (see figs. 2, 8, and 10) corresponds only to the real axis of the t plane, i.e., $s = 0$ and $t = r$, along the boundary of the t plane, equation 68 can be written as follows:

$$N + iT = \phi(r) + \overline{\phi(r)} + \overline{f(r)}\,\frac{\phi'(r)}{\overline{f'(r)}} + \frac{f'(r)}{\overline{f'(r)}}\,\psi(r) \qquad (69)$$

whose conjugate can be obtained by replacing i with -i. Then

$$N - iT = \overline{\phi(r)} + \phi(r) + f(r)\,\frac{\overline{\phi'(r)}}{\overline{f'(r)}} + \frac{\overline{f'(r)}}{\overline{f'(r)}}\,\overline{\psi(r)} \qquad (70)$$

54. The values of $f(r)$, $\overline{f(r)}$, $f'(r)$, and $\overline{f'(r)}$ can be obtained readily from equation 63; however, the values of functions $\phi(r)$ and $\psi(r)$ still need to be determined. These functions can be determined through use of the Cauchy integral.[10]

Cauchy Integral Formula

Formula

55. In the following section, a brief discussion of the Cauchy integral formula and some of its properties relevant to this study is presented. However, more detailed study on this subject can be found in any standard textbook dealing with analytic functions of complex variables.[10,15,16] Letting $H(t)$ be some analytic function anywhere within the boundary C of a simply connected region R and letting t_o be any point within the region, then the Cauchy integral can be written as

$$\frac{1}{2\pi i} \oint_C \frac{H(t)}{t - t_o} dt \tag{71}$$

where the integral is considered positive when counterclockwise around C.

56. The Cauchy integral theorems state that if $H(t)$ is a known function on the boundary of a simple closed curve C, then the value of the function and all its derivatives can be found at any point, such as t_o, inside the region R; then

$$H(t_o) = \oint_C \frac{H(t)}{t - t_o} dt \tag{72}$$

As a result of equation 72, the following properties of Cauchy integral are in order:[16]

a. If the function $H(t_o)$ is harmonic and continuous inside the region and $H(t_o)_{t=\infty} = 0$, then $1/2\pi i \oint [H(t)/t - t_o]dt$ is equal to $H(t_o)$ inside the region and to zero outside the region. This property is usually referred to as Poisson's integral formula for half-space.[10]

b. If the function $H(t_o)$ is harmonic and continuous outside the region and $H(t_o)_{t=\infty} = 0$, then $1/2\pi i \oint [H(t)/t - t_o]dt$ is equal to zero inside the region and $-H(t_o)$ outside the region.

Application for
determining stresses

57. Referring to equations 69 and 70, it can be stated that the functions $\Phi(r)$, $f(r)\left[\Phi'(r)/\overline{f'(r)}\right]$, and $\left[f'(r)/\overline{f'(r)}\right]\psi(r)$ are the boundary values of the harmonic functions in the lower half of the t plane $\Phi(t)$, $\left[f(t)/\overline{f'(t)}\right]\Phi'(t)$, and $\left[f'(t)/\overline{f'(t)}\right]\psi(t)$, respectively. Also, the functions $\overline{\Phi(r)}$, $f(r)\left[\overline{\Phi'(r)}/f'(r)\right]$, and $\overline{\psi(r)}\left[\overline{f'(r)}/f'(r)\right]$ are the boundary values of the harmonic functions in the upper half of the t plane $\overline{\Phi(t)}$, $f(t)\left[\overline{\Phi(t)}/f'(t)\right]$ and $\overline{\psi(t)}\left[\overline{f'(t)}/f'(t)\right]$, respectively. Since all these functions of t vanish at infinity, then the Cauchy integral can be applied.

58. Starting with equation 70, then

$$\frac{1}{2\pi i}\int_{-\infty}^{\infty}\frac{\overline{\Phi(r)}}{r-t}\,dr+\frac{1}{2\pi i}\int_{-\infty}^{\infty}\frac{\Phi(r)}{r-t}\,dr+\frac{1}{2\pi i}\int_{-\infty}^{\infty}\frac{f(r)\overline{\Phi'(r)}}{f'(r)(r-t)}\,dr$$

$$+\frac{1}{2\pi i}\int_{-\infty}^{\infty}\frac{\overline{f'(r)}\overline{\psi(r)}}{f'(r)(r-t)}\,dr=\frac{1}{2\pi i}\int_{-\infty}^{\infty}\frac{(N-iT)}{r-t}\,dr \qquad (73)$$

Since t is a point in the lower half of the t plane, then the first, third, and fourth integrals, according to the Cauchy integral, must be equal to zero, and the second integral is equal to $\Phi(t)$; thus, equation 73 can be reduced to

$$\Phi(t)=\frac{1}{2\pi i}\int_{-\infty}^{\infty}\frac{(N-iT)}{r-t}\,dr \qquad (74a)$$

However, the values of N and T are nonzero only at the interval $-1\leq r\leq 1$; therefore, equation 74 can be further reduced to

$$\Phi(t)=\frac{1}{2\pi i}\int_{-1}^{+1}\frac{(N-iT)}{r-t}\,dr \qquad (74b)$$

which, after integration, becomes

$$\Phi(t)=\frac{N-iT}{2\pi i}\ln\left(\frac{t-1}{t+1}\right) \qquad (74c)$$

from which $\phi'(t)$ can be obtained by simply differentiating with respect to t ; then

$$\phi'(t) = \frac{N - iT}{\pi i}\left(\frac{1}{t^2 - 1}\right) \tag{75}$$

59. In a similar manner, the value of $\psi(r)$ was obtained by operating on equation 69; thus

$$\frac{1}{2\pi i}\int_{-1}^{+1} \frac{N + iT}{r - t}\,dr = \frac{1}{2\pi i}\int_{-\infty}^{\infty} \frac{\phi(r)}{r - t}\,dr + \frac{1}{2\pi i}\int_{-\infty}^{\infty} \frac{\overline{\phi(r)}}{r - t}\,dr$$

$$+ \frac{1}{2\pi i}\int_{-\infty}^{\infty} \frac{f(r)}{f'(r)}\,\frac{\phi'(r)}{(r - t)}\,dr + \frac{1}{2\pi i}\int_{-\infty}^{\infty} \frac{f'(r)}{f'(r)}\,\frac{\psi(r)}{(r - t)}\,dr \tag{76}$$

Since the functions $f(r)$ and $f'(r)$ are defined inside the region, then $\overline{f(r)}$ and $\overline{f'(r)}$ are not analytic inside the region under consideration. Thus, the Cauchy integral cannot be applied on the last two terms of equation 76. Therefore, let the functions $G(t)$ and $G'(t)$ be two analytic functions inside the region so that at the boundary they are equal to $\overline{f(r)}$ and $\overline{f'(r)}$, respectively. Replacing $\overline{f(r)}$ with $G(r)$ and $\overline{f'(r)}$ with $G'(r)$ in equation 76 yields

$$\frac{1}{2\pi i}\int_{-1}^{+1} \frac{N + iT}{r - t}\,dr = \frac{1}{2\pi i}\int_{-\infty}^{\infty} \frac{\phi(r)}{r - t}\,dr + \frac{1}{2\pi i}\int_{-\infty}^{\infty} \frac{\overline{\phi(r)}}{r - t}\,dr$$

$$+ \frac{1}{2\pi i}\int_{-\infty}^{\infty} \frac{G(r)}{G'(r)}\,\frac{\phi'(r)}{(r - t)}\,dr + \frac{1}{2\pi i}\int_{-\infty}^{\infty} \frac{f'(r)}{G'(r)}\,\frac{\psi(r)}{(r - t)}\,dr \tag{77}$$

60. According to the Cauchy integral theorem, the third term involving $\overline{\phi(r)}$ is equal to zero; thus, equation 77 after integration is reduced to

$$\frac{N + iT}{2\pi i}\ln\frac{t - 1}{t + 1} = \phi(t) + \frac{G(t)}{G'(t)}\,\phi'(t) + \frac{f'(t)}{G'(t)}\,\psi(t) \tag{78}$$

For convenience, the value of $\phi(t)$ obtained through equation 74 can be substituted in equation 78, and after rearranging terms, the value of the function $\psi(t)$ can be expressed as follows:

$$\psi(t) = \frac{G'(t)\,\frac{T}{\pi}\ln\left(\frac{t-1}{t+1}\right) - G(t)\phi'(t)}{f'(t)} \tag{79}$$

where $\phi'(t)$ and $f'(t)$ are known, but $G(t)$ and $G'(t)$ are yet to be determined.

Determination of the Function G(t)

61. In the previous section, it was assumed that the functions $\overline{f(t)}$ and $G(t)$ are equal at the boundary of the region under consideration. Inside this region only $G(t)$ is defined, while $\overline{f(t)}$ can be determined outside the region. The graphical relationship between $f(t)$, $\overline{f(t)}$, and $G(t)$ is represented in fig. 11.

62. In order to determine the value of function $G(t)$, it is necessary to transform the region under consideration into another region with simple geometry such as a semi-infinite plane. This kind of transformation cannot be performed directly; thus, an indirect but simple approach may be employed by first transferring the region onto the w plane and then transferring the new region in the w plane to the upper half of the t plane.

63. Let the region in $G(t)$ be defined in the z plane and designated by R_4; this region can then be mapped point by point on an infinite strip of width equal to $K_1 + (\pi/2)$ in the w plane as shown in fig. 12. The mapping of region R_4 onto R_5 can be performed easily using the same transformation function described in equation 55 with the exception that the quantity K is replaced by K_1. The quantities K and K_1 can be expressed by the following equation

$$K_1 = \frac{\pi}{2} - K \tag{80}$$

64. The second step is to transform the infinite region R_5, in

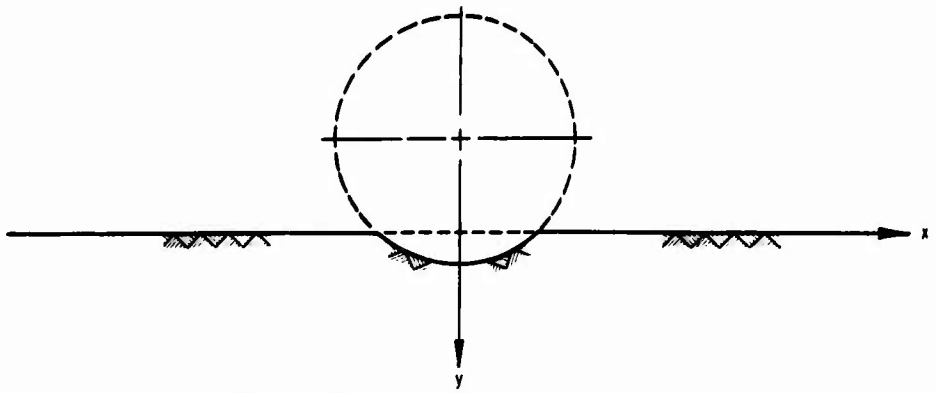

a. REGION DESCRIBED BY THE FUNCTION $z = f(t)$

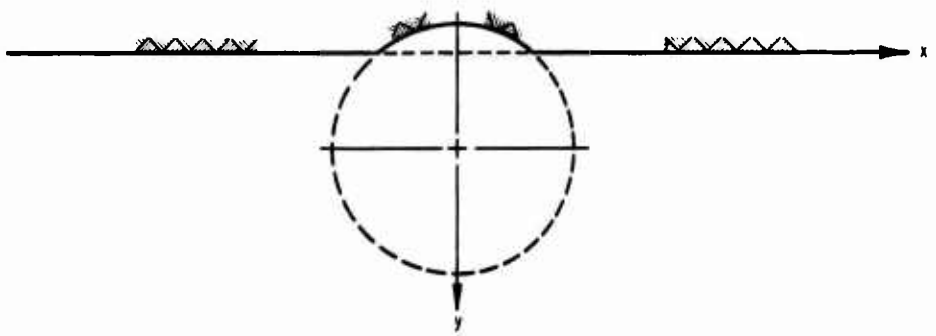

b. REGION DESCRIBED BY THE FUNCTION $z = \overline{f(t)}$

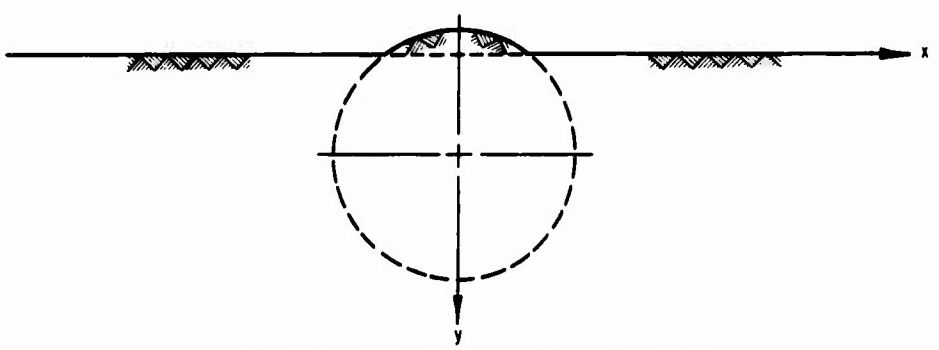

c. REGION DESCRIBED BY THE FUNCTION $z = G(t)$

Fig. 11. Graphical representation of $f(t)$, $\overline{f(t)}$, and $G(t)$

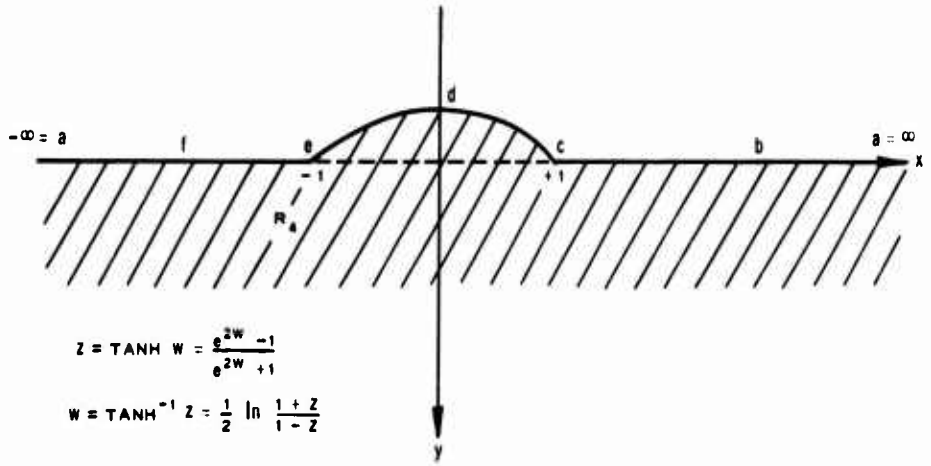

a. z PLANE

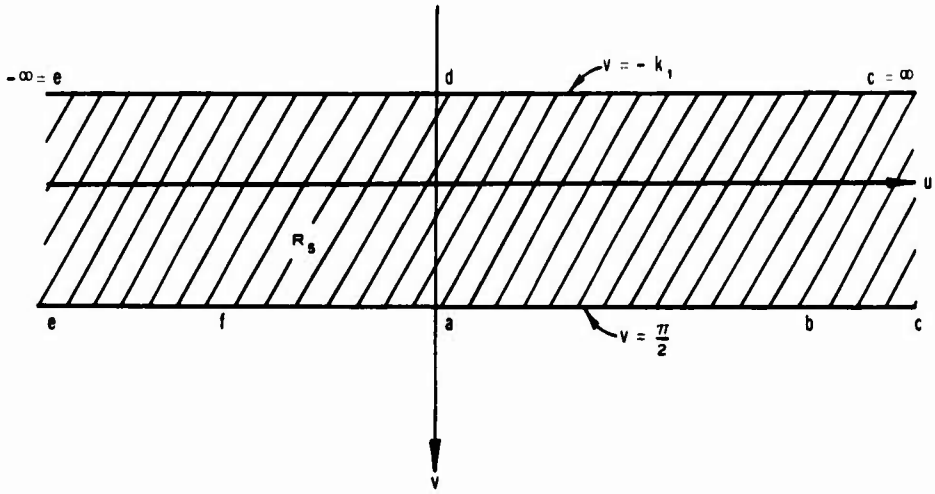

b. w PLANE

Fig. 12. Transformation of half plane with circular segment onto infinite strip

the w plane, onto a semi-infinite region. This can be accomplished by applying the Schwarz-Christoffel transformation to map conformally the infinite strip R_5, in the w plane, onto the upper half of the t plane, as shown in fig. 13. The procedure used is exactly the same as that discussed earlier in Part III, which in the final analysis yields the following transformation function;

$$w = \left(-\frac{K_1}{\pi} - \frac{1}{2}\right)\ln\left(\frac{t-1}{t+1}\right) + \frac{\pi i}{2} \tag{81}$$

65. The w plane can be eliminated completely by simply substituting equation 81 into equation 55; then

$$z = \tanh\left[\left(-\frac{K_1}{\pi} - \frac{1}{2}\right)\ln\left(\frac{t-1}{t+1}\right) + \frac{\pi i}{2}\right] \tag{82}$$

Although equation 82 describes the geometry of the region under consideration, it does not map the entire boundary point by point. However, if a new complex function is introduced so that its imaginary part is equal to the imaginary part of w while its real part is equal to the real part of w multiplied by $K/(\pi - K)$, then the region R_4 in the z plane will be mapped point by point on the t plane. The new function w_1 can be written as follows:

$$w_1 = \left(\frac{K}{\pi - K}\right)\mathrm{Re}(w) + i\,\mathrm{Im}(w) \tag{83}$$

where Im is the imaginary part of the function. If the function w_1 is substituted into equation 55, the value of $G(t)$ can be obtained as follows:

$$z = \tanh w_1 = G(t) \tag{84}$$

66. From equation 84, the function $G'(t)$ can be obtained. Knowing the values of functions $G(t)$ and $G'(t)$, the function $\psi(t)$ (equation 79) can be evaluated. Finally, the stresses σ_x, σ_y, and τ_{xy} can be presented in the following equations:

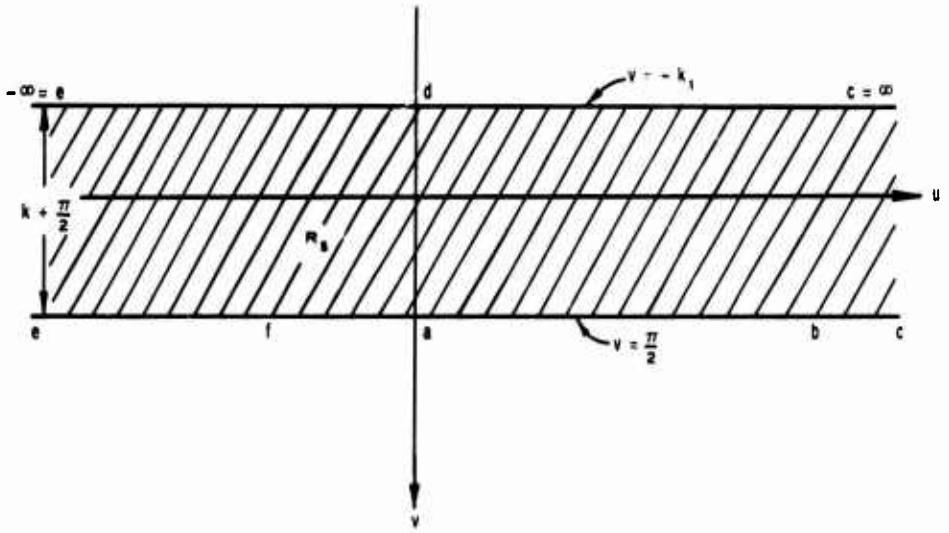

a. w PLANE

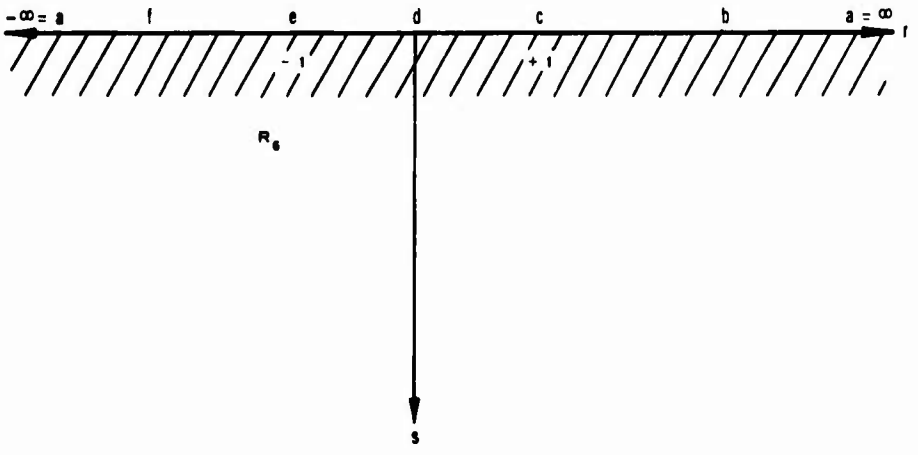

b. t PLANE

Fig. 13. Transformation of infinite strip with width of $K_1 + (\pi/2)$ onto the upper half of the t plane

$$\sigma_y = 2\mathrm{Re}\left[\phi(t)\right] + \mathrm{Re}\left[\overline{f(t)}\,\frac{\phi'(t)}{f'(t)} + \psi(t)\right] \tag{85}$$

$$\sigma_x = 2\mathrm{Re}\left[\phi(t)\right] - \mathrm{Re}\left[\overline{f(t)}\,\frac{\phi'(t)}{f'(t)} + \psi(t)\right] \tag{86}$$

$$\tau_{xy} = \mathrm{Im}\left[\overline{f(t)}\,\frac{\phi'(t)}{f'(t)} + \psi(t)\right] \tag{87}$$

Equations 85, 86, and 87 provide the solution to the problem.

Reduction of Data

67. The computation of σ_x, σ_y, and τ_{xy} was programmed on the WES GE-400 computer.

Illustrative Examples

68. Two examples are presented to illustrate the use of the theoretical solution. In the first example, a hypothetical wheel of radius R is partially buried in soil, as shown in fig. 14, so that the effective contact length and the sinkage were assumed to be 2 and 0.25 units, respectively. The wheel was also assumed to exert only uniform radial stress along the contact surface between the soil and the wheel. A computer program was prepared to calculate the stresses σ_y, σ_x, τ_{xy}, and τ_{max} at any point within the vicinity of the wheel. For illustration only, the stresses along a plane 1.2 units below the soil surface are presented in fig. 14 in the form of stress distribution diagrams in the interest of generality. In the second example, the same hypothetical wheel was used except that the wheel exerted only uniform shear stress along the contact surface between the wheel and the soil. The stress distribution diagrams for σ_y, σ_x, τ_{xy}, and τ_{max} are presented in fig. 15.

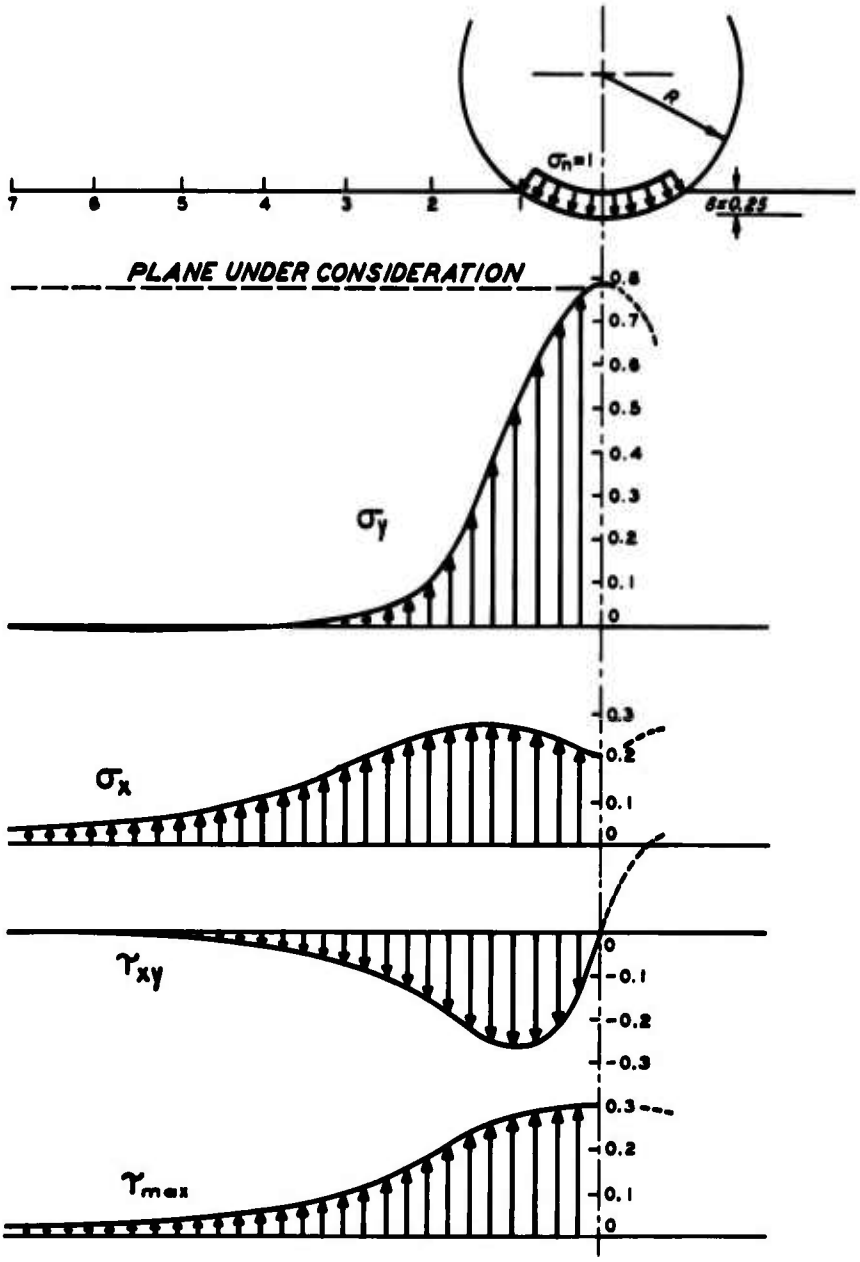

Fig. 14. Stress distribution diagrams for σ_y, σ_x, τ_{xy}, and τ_{max} due to a uniform radial stress of 1 unit

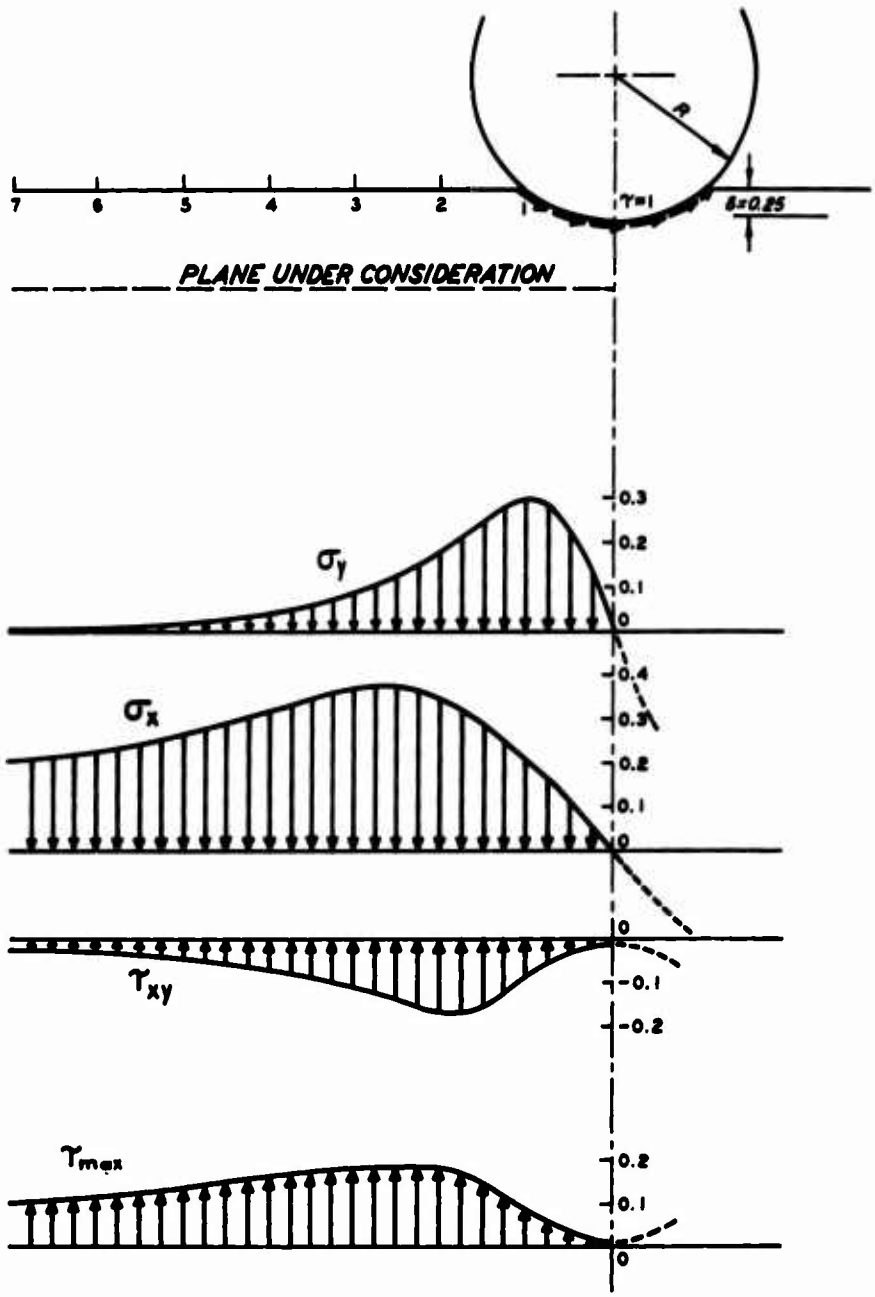

Fig. 15. Stress distribution diagrams for σ_y, σ_x, τ_{xy}, and τ_{max} due to a uniform tangential stress of 1 unit

PART IV: LABORATORY EXPERIMENTS

69. In previous parts of this report, a set of analytical equations was developed to calculate σ_x, σ_y, and τ_{xy} at any point within the soil medium in the vicinity of the wheel. These stresses were expressed in terms of the radial stress N and the tangential stress T that might be generated on the contact surface between the soil and the wheel of a moving vehicle. However, since the radial and tangential stresses are greatly influenced by the physical properties of both wheel and soil, the study of the stress distribution cannot be considered complete unless it is associated with soil strength characteristics along a potential failure surface within the framework of the soil-wheel system.

70. The knowledge of the physical properties of soils is essential not only to estimate the relationship between the normal and shear stresses that a soil can sustain, but also to check the capacity of the soil to support the vehicle under consideration. It might be worthwhile to mention that vehicle traction involves the topsoil, which does not exceed a few inches in depth, while the sinkage problem involves the yielding of deeper layers.

71. In the study reported herein, a plastic clay was tested under controlled conditions to simulate field conditions as closely as possible. The data obtained from the experimental tests were then applied in the theoretical solution. Because the objective of the laboratory tests was to simulate field soil-wheel interaction, the drainage conditions and the speed at which the soil beneath the wheel is deformed were also considered.

Testing Equipment and Material

Equipment

72. The entire testing program was performed using the WES 1947 low-capacity annular shear apparatus. This apparatus is described in detail in reference 17. The test specimen is 4.50 in. in outside

diameter and 2.50 in. in inside diameter, giving a cross-sectional area of 11 sq in. (71 sq cm). Since the laboratory testing program of this study was intended to simulate field conditions as closely as possible, it was desirable to shear the soil specimens under constant-volume conditions at a rate of strain higher than that commonly used in soil testing.

73. Because of these requirements, the torsion shear machine was modified and adapted to conduct torsion shear at constant volume under wide ranges of axial stresses and rates of shear deformation. The major modifications that were introduced were the constant-volume loading system and the automatic recording system. Descriptions of the constant-volume loading system and the automatic recording system are presented in Appendix A.

Material

74. CH soil (Vicksburg buckshot clay) was used in this testing program. Index properties of this material are as follows:

Liquid limit	56
Plastic limit	22
Plasticity index	34
Activity	0.88
Specific gravity	2.68

The contents of one carton (80-85 lb) were thoroughly mixed on a flat surface and then split into 5-lb (mass) portions, which were stored in plastic bags until needed for tests.

Sample Preparation

75. The soil moisture-density condition used in the testing was determined using the Modified Berkeley Pneumatic Tamper.[18] Small batches of the soil were mixed at different water contents ranging from 21 to 28 percent. The material was mixed by adding water slowly to the dry material while spreading with a spatula to break down any large lumps (this material was not forced through a screen). The soils were stored in airtight glass jars and allowed to cure for 10 days. After

curing, the material was compacted in a standard triaxial mold using the tamper set at 11 lb (force) per tamp, with 30 tamps per layer on each of eight layers. The moisture-density curve developed for these compacting conditions showed an optimum water of 25.6 percent and a maximum dry density of 95 pcf (fig. 16). It was decided to prepare specimens for the shear tests at the optimum water content and maximum dry density. Enough material for 35 shear tests was mixed at the proper water content in a manner very similar to that used in preparing material for the compaction test.

76. For the annular shear tests on soil alone, the quantity of material required to produce a compacted specimen 3/4 in. thick with a dry density of 95 pcf was determined. The soil was placed in the annular shear assembly and compacted in two layers, the first layer being 1/4 in. thick. After compaction of the first layer, the top surface of the soil specimen was scarified, then the second layer, 1/2 in. thick, was compacted.

77. The pneumatic tamper was used with a 3/8-in.-diam Teflon tamping foot shaped to fit a segment of the annular ring (fig. 17). The tamping force needed to produce the desired specimen thickness was calibrated by using a number of tamping forces and successively correcting the forces until the desired thickness was reached. Three coverages were used in compacting each layer. In tests to determine the shearing resistance of soil against rubber and soil against steel, one-half of the volume of a full soil specimen was used, and the material was compacted in a single layer with three coverages of the tamper. This procedure used to prepare and compact the soil ensured an adequate supply of identical specimens for the testing program, and it is believed that, within the limits of experimental variation, the specimens tested possessed identical initial properties.

Test Program

78. Torsion shear tests were performed on four types of specimens in this study, as follows:

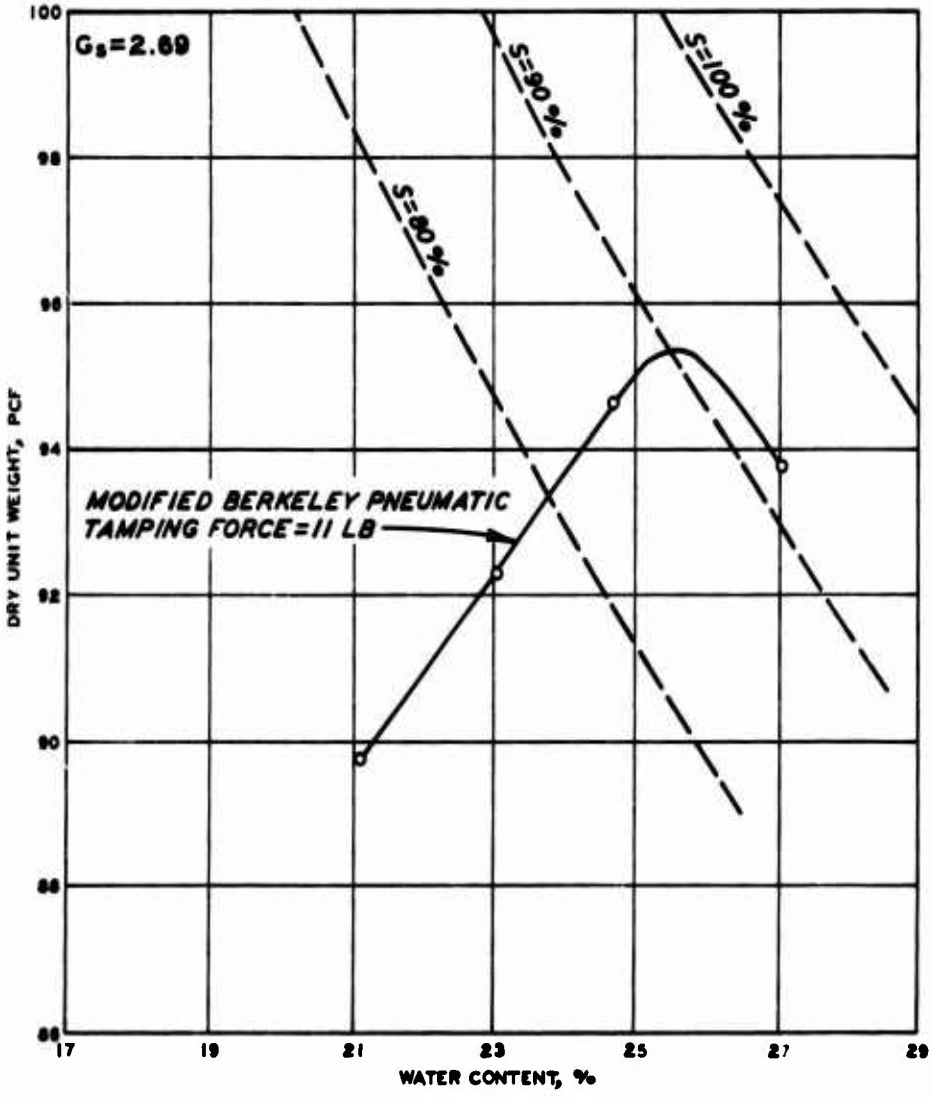

Fig. 16. Moisture-density relationship for CH soil

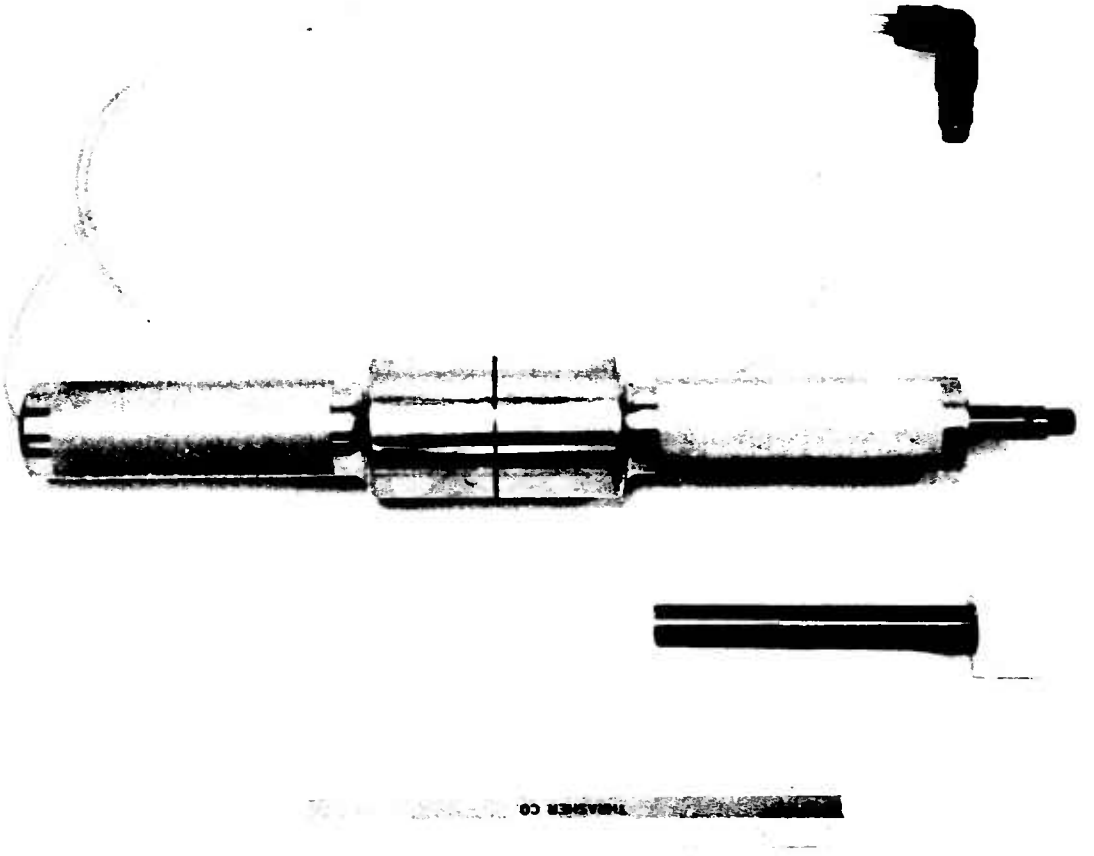

Fig. 17. Modified Berkeley pneumatic tamper

a. Homogeneous. The purpose of this test was to evaluate the shear strength of the soil itself.

b. Rubber on soil. In this type of test, a smooth rubber was molded in the form of a hollow cylinder to occupy the lower half of the torsion shear box, while the upper half was filled with compacted soil. The purpose of this test was to evaluate the shear stress developing between tire rubber and soil under different radial stresses. The molding of the rubber ring is described in Appendix B.

c. Steel on soil. This test was similar to that described in subparagraph b, with the exception that the molded rubber was replaced by polished stainless steel.

d. Nonhomogeneous soil. In this test, the lower part of the torsion shear box was filled with soil compacted at a water content of 16 percent, the surface of the compacted soil was smoothed, and then the upper part of the box was filled with the soil compacted at a water content of 26 percent. The densities of the upper and lower layers after compaction were about 95 and 89 pcf, respectively. The purpose of this preliminary test was to initiate a study of the effect of differences in water content at the shear plane on soil resistance.

79. The initial normal stresses used in each type of test were 5, 15, and 30 psi, and the rates of shear deformation were 0.002, 0.2, and 2 in./min. All tests were conducted under constant-volume conditions.

PART V: PRESENTATION AND DISCUSSION OF TEST DATA

80. A summary of pertinent information on tests performed at the time of this reporting is presented in table 1, and the shear and normal stresses for each type of test are presented graphically.

Homogeneous Soil Specimens

Test results

81. The CH materials compacted in the annular shear box at an average water content of 26 percent and dry density of 95 pcf, grouped under three rates of shear deformation, are presented in figs. 18-20. The upper curves in each figure represent the variation of the shear stress τ with respect to the elapsed time during the test, and the lower curves represent the variation of the normal stress σ' during shear for the same test. The elapsed time and the rate of shear deformation in each test were used to obtain data on the amount of shear displacement that took place along the shear plane.

82. Tests for which results are shown in fig. 18 were conducted at initial normal stresses σ_i of 5, 15, and 30 psi and sheared at a rate of shear deformation equal to 0.002 in./min. The same initial normal stresses were repeated in tests whose results are given in figs. 19 and 20, but the rates of shear deformation used were 0.2 and 2.0 in./min, respectively. The shear stress, fig. 18, increased almost linearly at the beginning of the test until the shear deformation was about 0.06 to 0.1 in., being lower for tests with lower initial normal stress. Then the shear stress decreased gradually until the average deformation was about 0.2 in. Beyond that point, the shear stress stayed constant as the soil behaved as a plastic material. The pattern of normal stress, on the other hand, was quite different from that of shear stress. While the tests conducted under σ_i of 5 psi showed an increase in the normal stress during shear, indicating the tendency of the material to dilate, the other two tests showed a decrease in normal stress with increasing deformation, suggesting a compressional tendency

Table 1

Summary of Experimental Results

Initial Normal Stress, psi	Rate of Shear Deformation in./min	Stress at Failure, psi Normal	Shear
Homogeneous Soil			
5	0.002	7.97	6.36
5	0.2	9.82	10.32
5	2.0	15.00	13.57
15	0.002	8.18	8.56
15	0.2	16.18	12.30
15	2.0	19.27	15.97
30	0.002	12.27	12.24
30	0.2	18.88	14.70
30	2.0	22.73	17.25
Smooth Rubber on Soil			
5	0.002	4.09	2.40
5	0.2	5.18	4.64
5	2.0	5.00	4.91
15	0.002	13.09	4.18
15	0.2	15.00	6.50
15	2.0	14.91	9.09
30	0.002	23.64	5.65
30	0.2	29.82	9.05
30	2.0	29.45	11.79
Polished Stainless Steel on Soil			
5	0.002	4.73	1.61
5	0.2	4.55	1.98
5	2.0	5.00	2.00
15	0.002	14.00	2.11
15	0.2	14.73	2.91
15	2.0	15.00	3.76
30	0.002	28.46	4.60
30	0.2	29.82	5.83
30	2.0	29.55	5.75
Nonhomogeneous Soil			
5	0.002	4.73	6.08
5	0.2	10.00	10.80
5	2.0	7.45	8.20
15	0.002	10.00	13.57
15	0.2	15.45	13.57
15	2.0	13.45	13.01
30	0.002	15.45	14.28
30	0.2	18.18	16.54
30	2.0	30.00	18.38
Wet Smooth Rubber on Soil			
5	2.0	4.91	1.95
15	2.0	14.54	3.11
30	2.0	29.82	5.29
Wet Polished Steel on Soil			
5	2.0	5.00	2.54
15	2.0	14.55	2.97
30	2.0	30.00	2.54

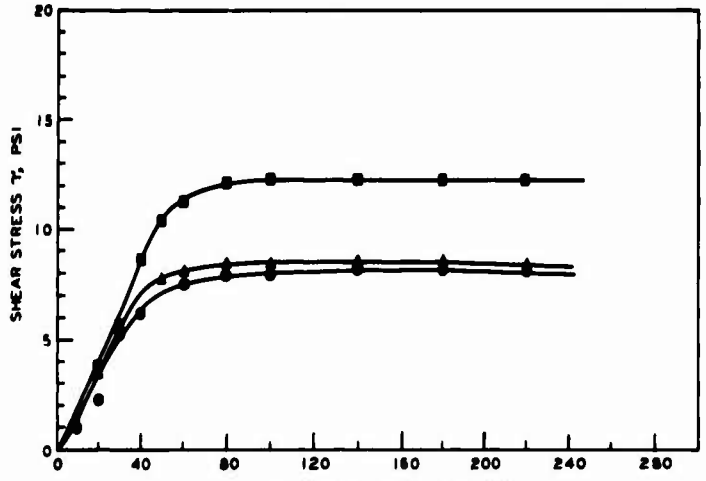

a. SHEAR STRESS

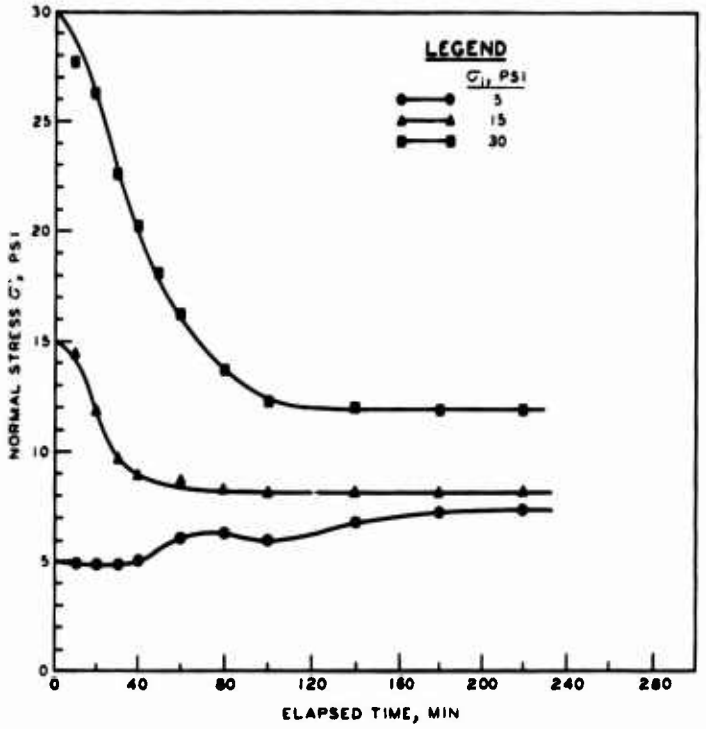

b. NORMAL STRESS

Fig. 18. Variation of shear and normal stresses for a homogeneous soil specimen sheared at a rate of deformation equal to 0.002 in./min

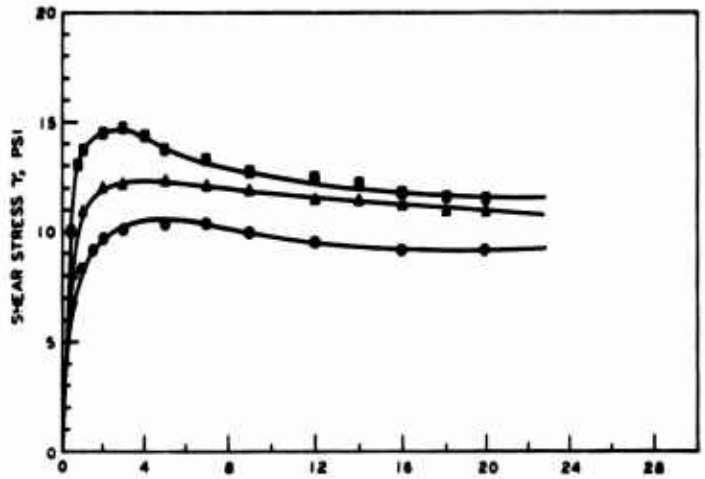

a. SHEAR STRESS

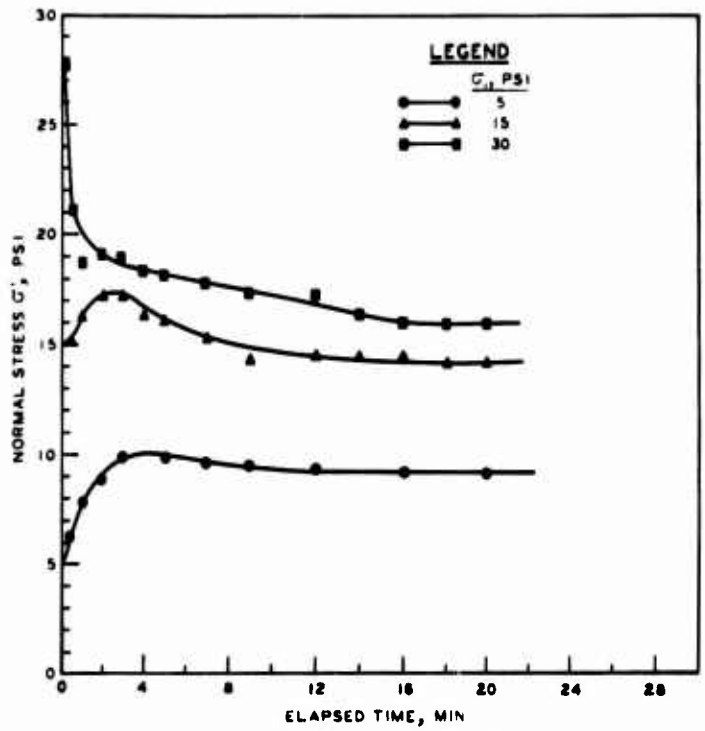

b. NORMAL STRESS

Fig. 19. Variation of shear and normal stresses for a homogeneous soil specimen sheared at a rate of deformation equal to 0.2 in./min

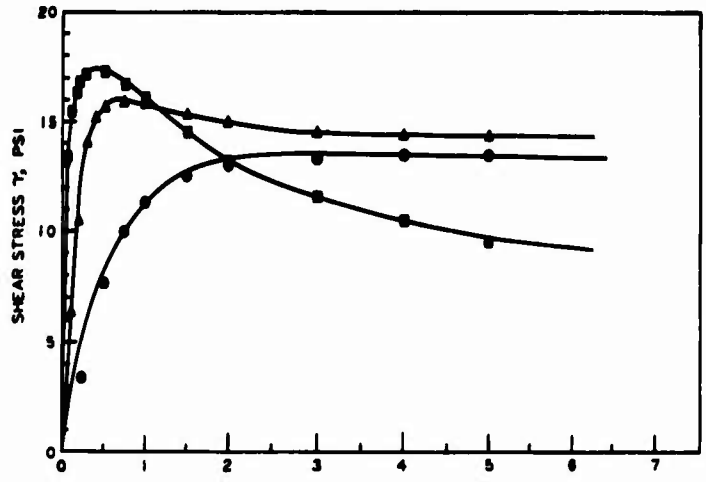

a. SHEAR STRESS

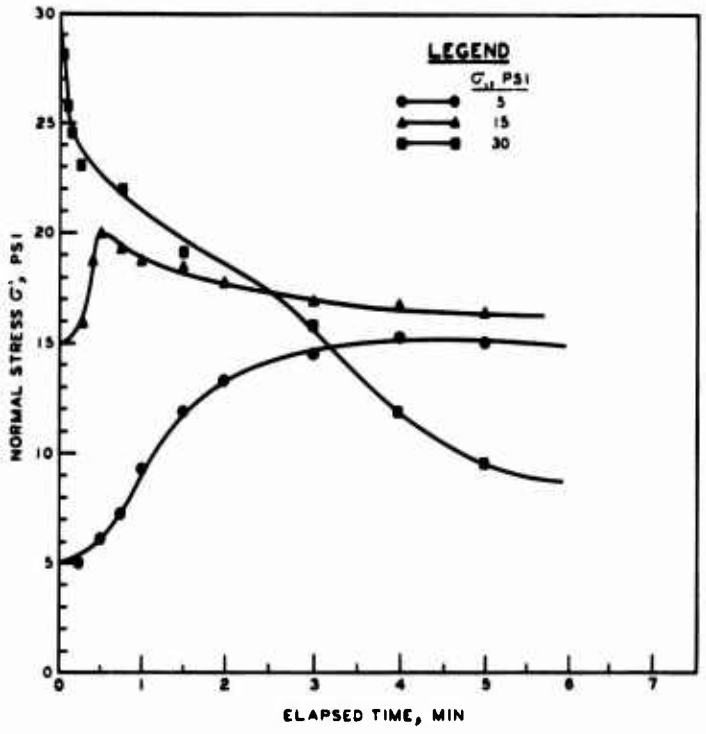

b. NORMAL STRESS

Fig. 20. Variation of shear and normal stresses for a homogeneous soil specimen sheared at a rate of deformation equal to 2.0 in./min

during shear. Consequently, it might be expected that negative pore pressure developed, causing an increase in strength for specimens tested at the lower initial normal stresses, while at higher initial normal stress, it might be expected that a positive pore pressure developed, causing a decrease in soil strength during shear.

83. Because of the nature of the apparatus used in this study, it was not possible to saturate the specimen. It is likely that the presence of air voids in the compacted specimen made any changes in pore pressure of little consequence. Therefore, assuming no development of pore pressures from the beginning of the test up to the failure point,* total stresses would be effective stresses. Beyond failure, however, the shear stresses are somewhat affected by the maximum rate of flow,[19] and the stress-displacement curve can be used only as an approximate curve.

84. The stress versus elapsed time curves in fig. 19 are slightly different from those presented in fig. 18 because the shear deformation was increased from 0.002 to 0.2 in./min. As shown in fig. 19, shear stress also increased linearly until the shear deformation was about 0.1 in.; then it started to curve rapidly until it reached the peak and started to decrease gradually until the shear deformation was about 3 in. Beyond that point, the shear stress showed no significant change. The curves also show that the shear deformations at failure occurred at about 0.6 to 0.8 in., being lowest for tests conducted at initial normal stress of 30 psi, and were much higher than those shown in fig. 18. Thus, increasing the rate of shear deformation not only increases the peak shear stress but also the shear deformation at failure. Increasing the rate of shear deformation increases the tendency of the soil specimen to dilate, which is reflected by the great increase in the normal stress for specimens sheared at initial normal stresses of 5 and 15 psi. However, the test conducted at an initial normal stress of 30 psi indicated a tendency toward compression during shear.

---

* The state of failure is defined by the point of maximum shear stress in this study.

85. The general variations of shear and normal stresses with respect to the elapsed time for specimens shown in fig. 20 are similar to those presented in fig. 19, although the peak stresses are slightly higher, reflecting the effect of increasing the rate of shear deformation. In fig. 20, the shear and normal stresses for specimens sheared at an initial normal stress of 30 psi showed a continuous decline beyond the failure point simply because the soil started to extrude from the shear box and the assumption of constant volume was not valid in that particular test. The same thing happened when the test was repeated.

Soil strength parameters

86. It has been recognized that the shear strength is equal to the cohesion c for purely cohesive soil and is equal to $\sigma \tan \phi$ for purely frictional soil, where σ is the applied normal stress on the failure plane and ϕ is the angle of internal friction. However, most soils possess the properties of both cohesion and friction; for these materials, the shear strength can be expressed as follows:

$$\tau = c + \sigma \tan \phi \tag{88}$$

The tests described so far in this report to simulate in situ conditions were of relatively short duration and can be considered unconsolidated-undrained (i.e., Q tests) for all practical purposes. These tests were conducted to serve one purpose: to obtain a relationship between the shear and normal stresses that may occur in the vicinity of a wheel moving on a soil. The strength may also be determined directly by triaxial compression tests, and results can be correlated with cone index, which is commonly used in trafficability studies. However, the following discussion is limited to compacted soil tested with annular shear apparatus and sheared at a constant rate of shear deformation under constant volume.

87. The relationship between the shear stress τ and the normal stress σ for the CH material shown in fig. 21 suggests that the peak shear stress increases with increasing initial normal stress as well as the rate of shear deformation. The best-fit line for the experimental

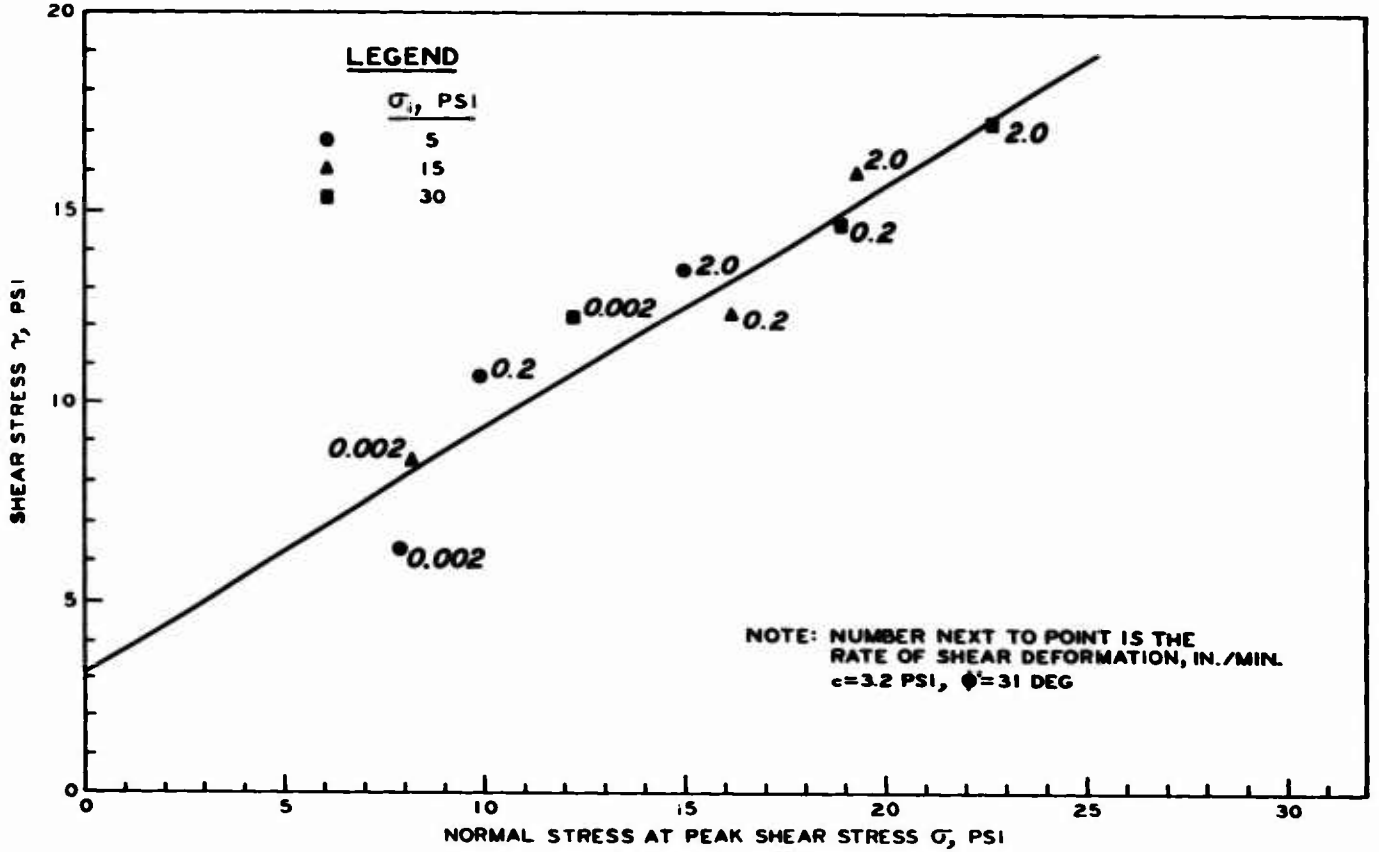

Fig. 21. Relationships between the shear and normal stresses at failure for homogeneous soil specimens

results, as obtained by the method of least squares, yields a cohesion intercept equal to 3.25 psi and ϕ equal to 31 deg. By substituting the values of c and ϕ in equation 88, the linear relationship between τ and σ can be expressed as follows:

$$\tau = 3.25 + 0.62\sigma \tag{89}$$

where σ is measured in pounds per square inch. The values of c and ϕ obtained in this study were compared with those obtained on the same material by other investigators as shown in the tabulation below:

Type of Test	Initial Water Content, %	Dry Density pcf	Cohesion c', psi	Friction Angle ϕ', deg	Rate of Strain in./min
Q annular shear	26.0	95.0	3.25	31	0.002 to 2.0
S direct shear[20]	24.0	98.0	2.80	21	--
R triaxial[20]	24.5	93.1	4.17	23	0.03 to 0.6
R triaxial[21]	24.5	92.3	1.10	29	0.0036

88. The data presented in the table indicate that the value c' obtained in this study is within the range of those found by other investigators; however, the value of ϕ was slightly higher than the values obtained by direct shear or triaxial compression tests. This, of course, was expected because the average rate of shear strain under which the tests in this study were conducted was much higher than the rates used in other studies. The difference may be attributed to the nonuniform strain distribution associated with the annular shear test and also to the slight change in pore pressure during the tests. Some caution must be applied in using the data obtained in this study to predict the strength of the CH material as accepted by standard procedures. However, these data provide a more realistic picture of the relationship between τ and σ in soil under the action of a moving wheel than the same data obtained from other tests.

Effect of rate of shear deformation on peak strength

89. Plastic material similar to viscous material exhibits a

resistance to shear strain that varies with the speed at which the shearing strain is applied. For perfectly viscous fluid (i.e., Newtonian), the applied stress is directly proportional to the rate of shear strain $\dot{\varepsilon}$ and can be expressed as follows:

$$\sigma = \eta\dot{\varepsilon} \tag{90}$$

where

η = the viscosity

$\dot{\varepsilon} = d\varepsilon/dt$

Since clay soil is a three-phase system, its deformation characteristics are greatly affected by environmental conditions. At high water content, clay behaves as a viscous fluid similar to that of Newtonian material; as water content is gradually reduced, the flow properties of clay are also reduced and its plastic properties begin to disappear. As the water content decreases further, the clay soil becomes harder, and its properties take on properties of solids similar to those of Hookean material where time has no effect on strength. Under most natural conditions, clay soils are quite different from Hookean material since their strengths depend on the rate of strain and they also differ from Newtonian material because their viscosity is not constant. According to Hvorslev,[19] the coefficient of viscosity also depends upon the maximum velocity gradient and upon the time elapsed after the maximum velocity has been attained.

90. The relationship between the shear stress τ and the initial normal stress σ_i, as shown in fig. 22, suggests that the strength of the CH material increases with increasing σ_i for all three rates of strain used. The effect of the rate of shear deformation on the strength of the soil is demonstrated in fig. 23, which clearly shows that there is a substantial increase in the strength of the compacted CH material as a result of increasing the rate of strain from 0.002 to 2.0 in./min. The increase in strength with respect to $\dot{\varepsilon}$ is the most significant for specimens tested at an initial normal stress of 5 psi and the least significant for those tested at 30 psi. Such an increase

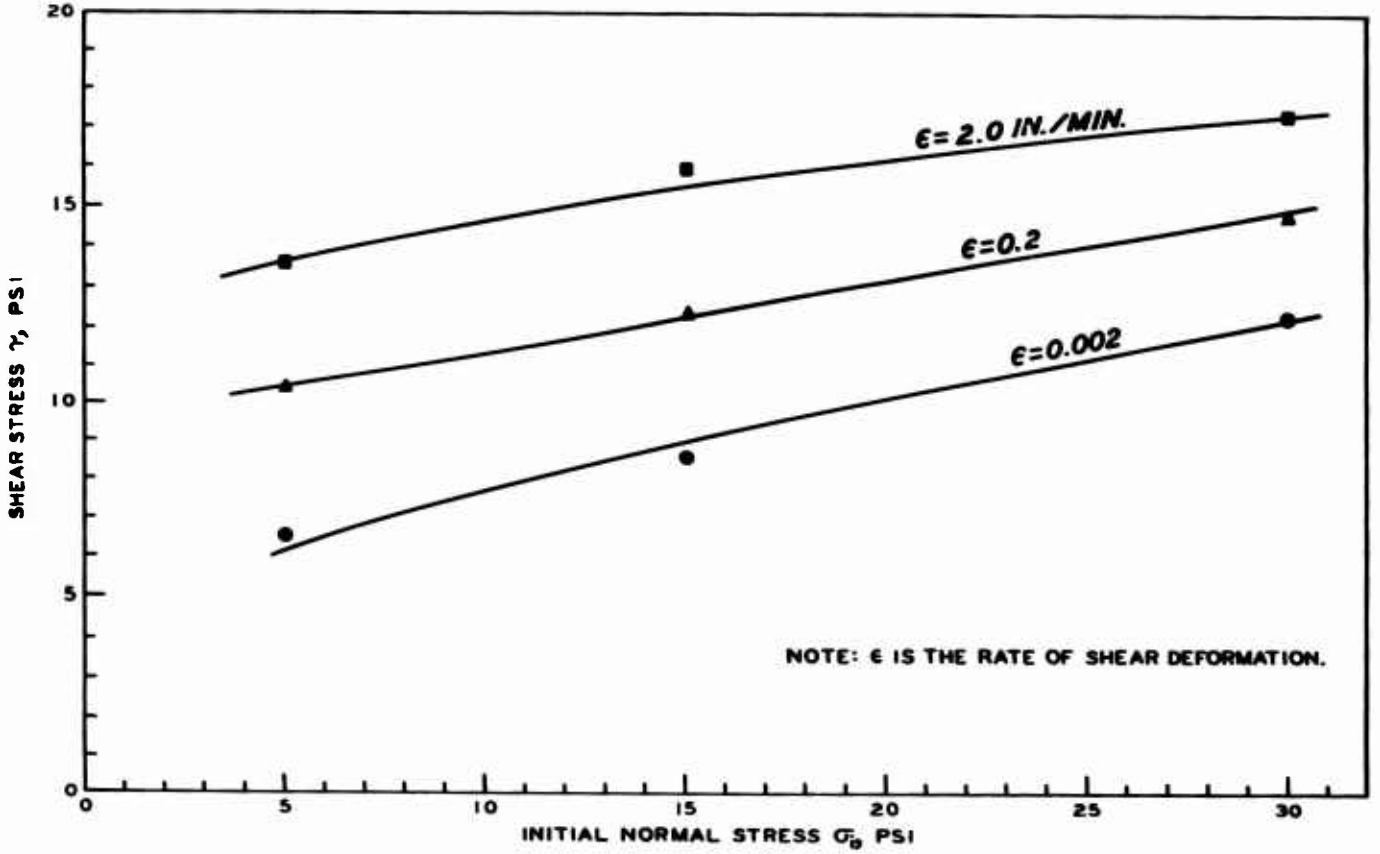

Fig. 22. Relationship between the shear stress and initial normal stress for homogeneous soil specimen

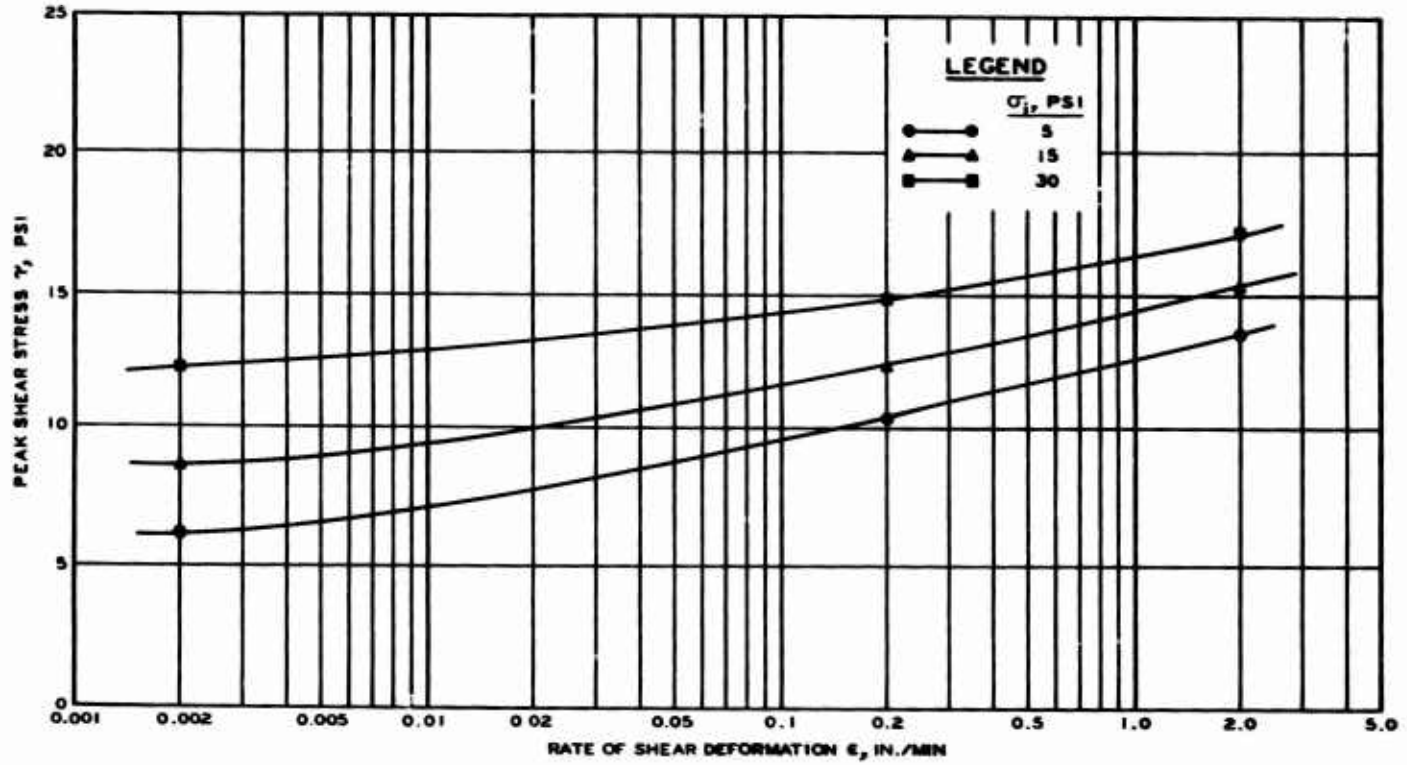

Fig. 23. Relationship between peak shear stress and rate of shear deformation for homogeneous soil specimens

in strength is mostly due to the viscous properties of clay as explained previously.

91. The increase in the strength of soil as a result of increasing the rate of shear deformation has been reported previously by Taylor[22] (on Boston blue clay) and also by Donaghe (on CH material).[21] In both investigations, triaxial compression apparatus was used; however, the trend of the results was similar to that presented in fig. 22. As a result of his experimental study, Taylor proposed the following expression:

$$\tau = (\sigma + p_i)\left[\tan \phi' + f\left(\frac{d\epsilon}{dt}\right)\right] \qquad (91)$$

where

p_i = the intrinsic pressure equal to $c/\tan \phi$

$f(d\epsilon/dt)$ = a function of $\dot{\epsilon}$

Smooth Rubber on Soil

Test results

92. In this series of tests, the CH material was compacted on smooth tire rubber that filled the lower part of the annular shear box. The compaction effort was similar to that used in the previous series of tests. The initial normal stresses and rates of shear deformation used in this series were exactly the same as those for the homogeneous soil specimens. Results of the constant-volume tests of soil shear on rubber in the annular shear apparatus are presented in figs. 24-26.

93. Fig. 24 shows the variation of shear and normal stresses during the tests of three specimens tested at a rate of shear deformation of 0.002 in./min and under initial normal stresses of 5, 15, and 30 psi. The shear stress for each test increased almost linearly with respect to time until failure. Beyond the peak point, the shear stress dropped slightly, then stayed about constant till the end of the test. The normal stress, on the other hand, decreased for all tests with increasing shear deformation from the beginning of the test until slightly

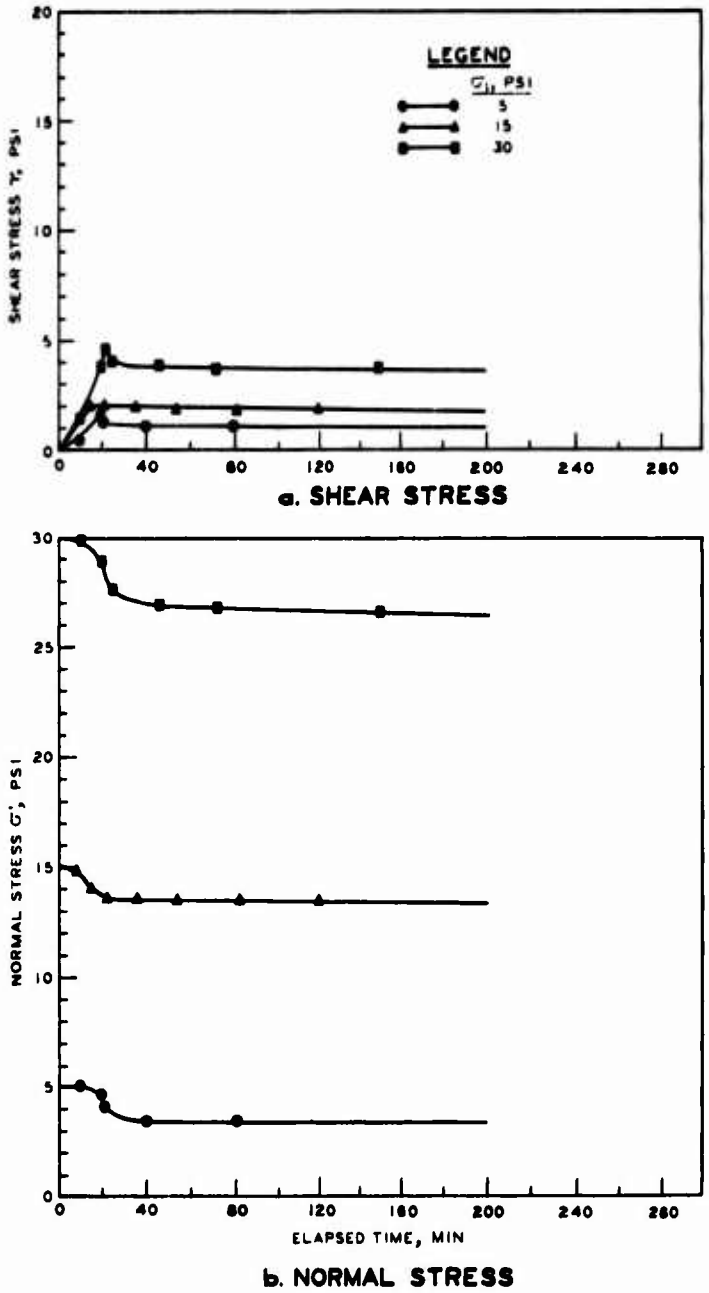

Fig. 24. Variation of τ and σ for rubber on soil sheared at a rate of 0.002 in./min

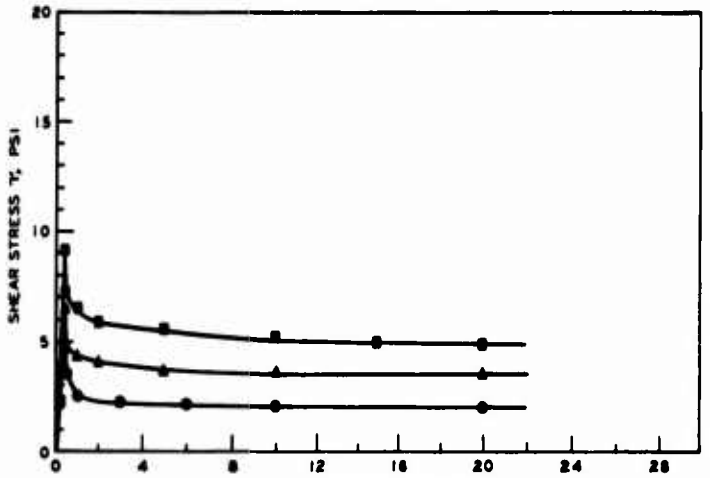

a. SHEAR STRESS

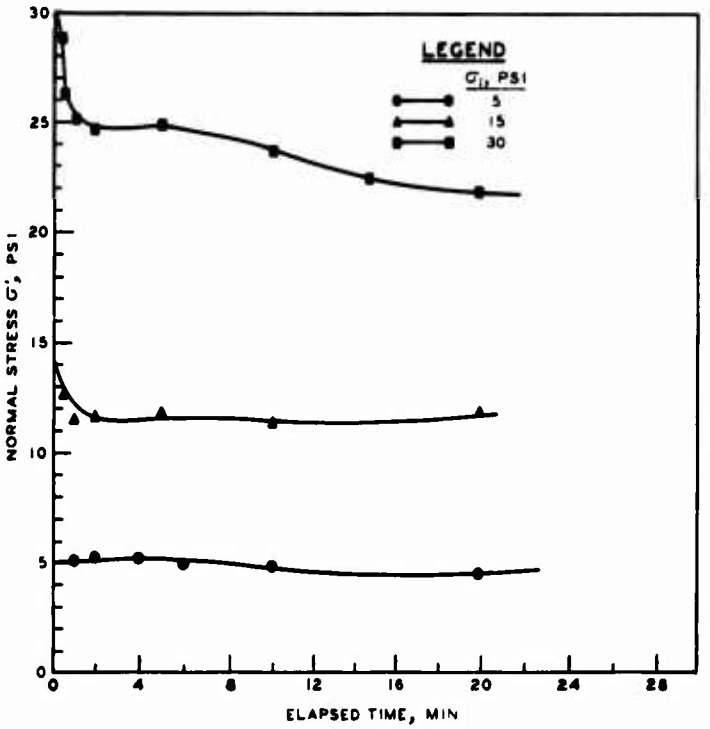

b. NORMAL STRESS

Fig. 25. Variation of τ and σ for rubber on soil sheared at a rate of 0.2 in./min

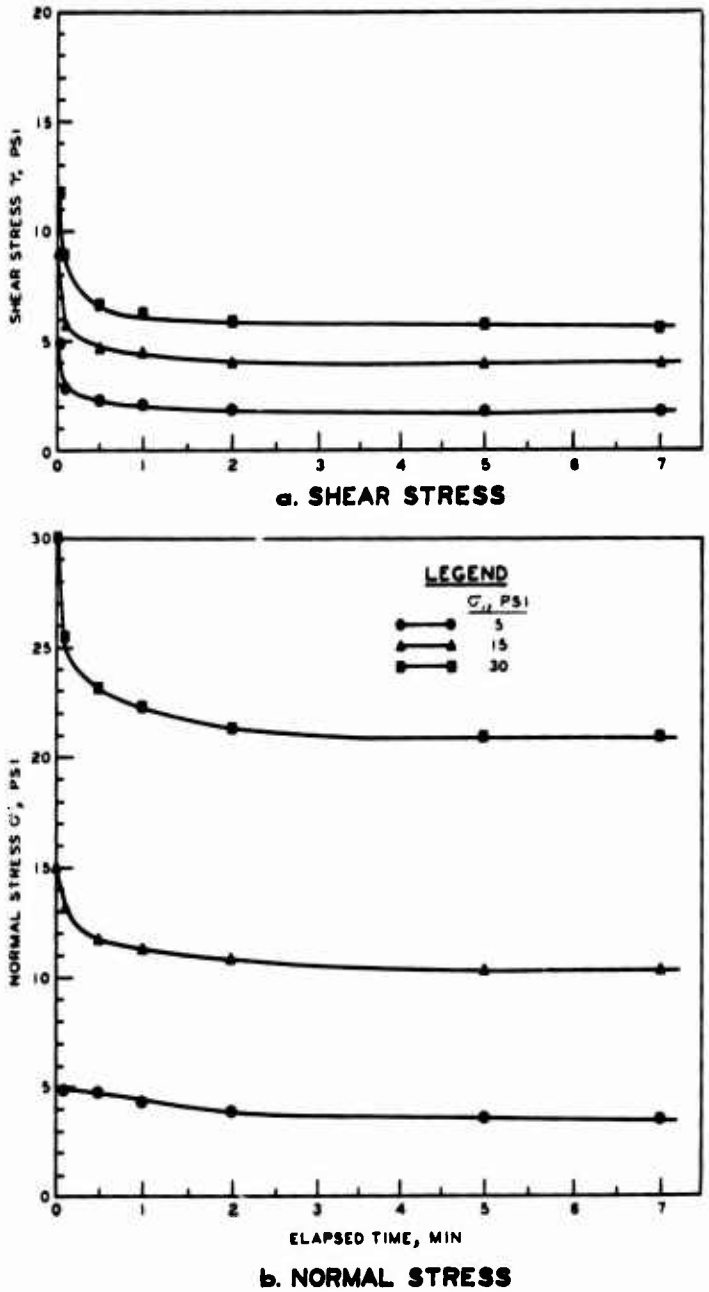

Fig. 26. Variation of τ and σ for rubber on soil sheared at a rate of 2.0 in./min

after the peak point; then it leveled off at about the same time that the shear stress stayed constant. It is apparent that all three specimens, even those tested at an initial normal stress of 5 psi, showed a tendency to compress or consolidate during shear.

94. Visual examination of specimens after tests showed that all the movement occurred at the plane of contact between the rubber and the soil, which was characterized by a shiny polished surface where the soil specimen moved as an intact block over the rubber. Figs. 25 and 26 are graphs similar to those presented in fig. 24, with the exception that rates of shear deformation used were 0.2 and 2.0 in./min, respectively. A comparison of figs. 24, 25, and 26 shows that the failure point became more pronounced with increasing rate of shear deformation, and also that the shear strength increased with increasing speed of the test. However, the normal stress during shear did not seem significantly affected by the speed of the test.

Strength parameters

95. Since the shear plane occurs between the soil and the rubber, the concept of failure based on Mohr-Coulomb criteria as described by equation 88 is not valid. However, it might be possible to express the shear stress occurring at the plane of contact between the soil and rubber by the adhesion a and surface friction angle δ in a manner similar to that of Mohr-Coulomb equation for homogeneous material. Then

$$\tau = a + \sigma \tan \delta \qquad (92)$$

96. The relationship between the shear and normal stresses at failure for rubber on soil is presented in fig. 27. The figure shows that the shear stress increases with increasing initial normal stress as well as with increasing rate of shear deformation. Both adhesion and friction increased with increasing rate of shear strain. The average value of adhesion increased from about 1.6 to 3.1 psi, and the angle δ increased from 12 to 19 deg when the rate of strain was increased from 0.002 to 2.0 in./min. Therefore, it is not possible to correlate the shear strength with the normal stress at failure in a manner similar to

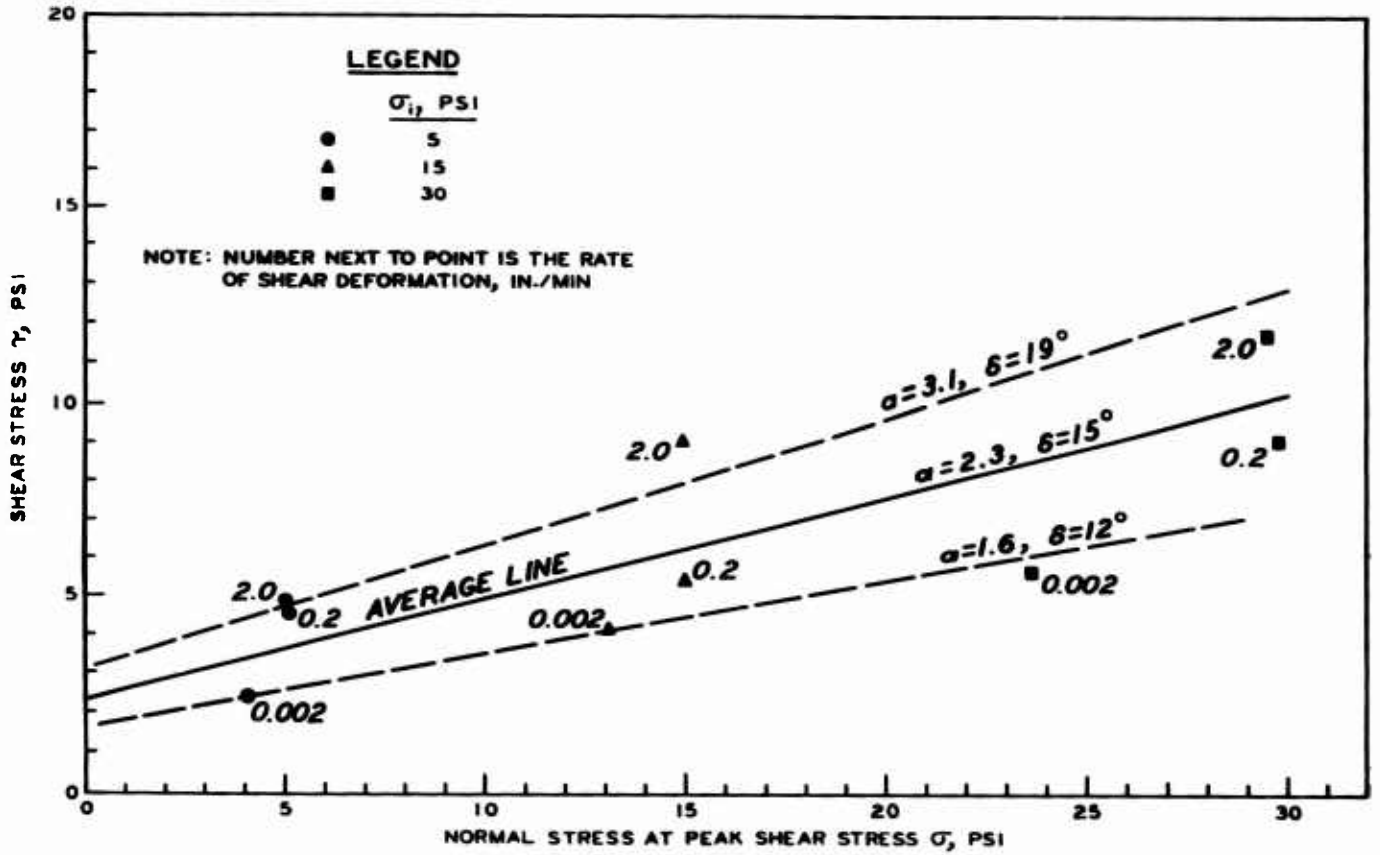

Fig. 27. Relationship between shear and normal stresses at failure for rubber on soil

that described by equation 92. However, if the best-fit line is considered in expressing the relationship between τ and σ at the interface between soil and rubber, then the following relationship can be introduced:

$$\tau = 2.3 + 0.265\sigma \qquad (93)$$

Effect of rate of shear deformation on strength at interface of soil and rubber

97. The relationship between the maximum shear stress developed at the interface of the rubber and the CH material and the rate of shear deformation $\dot{\varepsilon}$ is depicted in fig. 28. There is a striking resemblance between this figure and fig. 23, both showing that the shear stress increased with increasing rate of shear deformation. Both figures show that the curve for each set of tests is concave upward, giving the impression that the shear stress at failure increases indefinitely with respect to the increase of the rate of strain. However, it is also possible that the curve might change course and follow another direction with increasing rates of strain beyond those used in this test program. This point needs further study.

Effect of wetness on the shear stress at the interface of soil and rubber

98. Three tests were conducted in a manner similar to that used in previous tests with the exception that the rubber surface was covered with a film of water, using wet paper toweling prior to preparing the specimen, and all specimens were sheared at a rate of deformation of 2.0 in./min.

99. The values of the shear and normal stresses at failure of the wetted rubber surface are presented in fig. 29; on the same figure results of comparable tests with a dry rubber surface are also shown. Fig. 29 clearly shows that wetting the rubber surface reduced the shear resistance to about 50 percent of what it was before wetting, even though the normal stress was not appreciably affected. This may explain

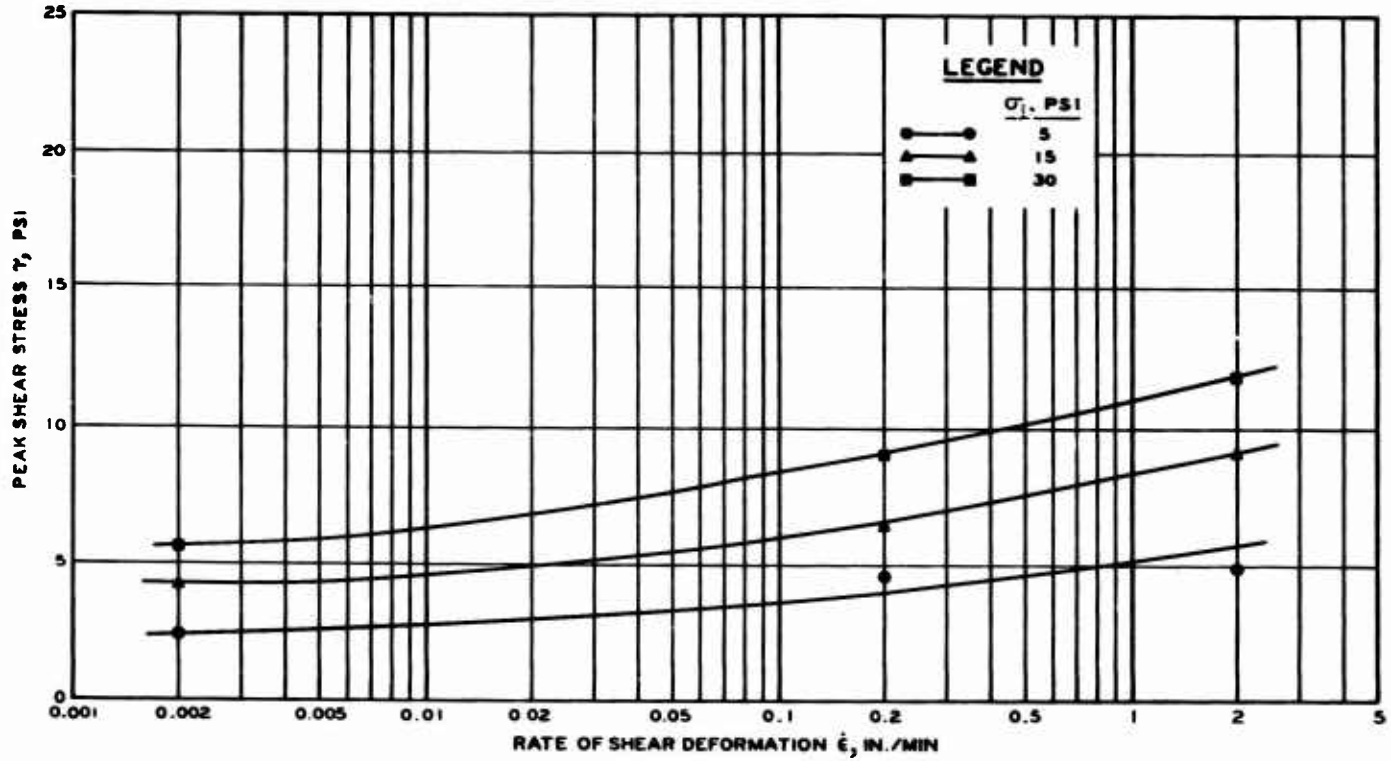

Fig. 28. Relationship between the shear stress τ and the rate of shear deformation at interface of soil and rubber

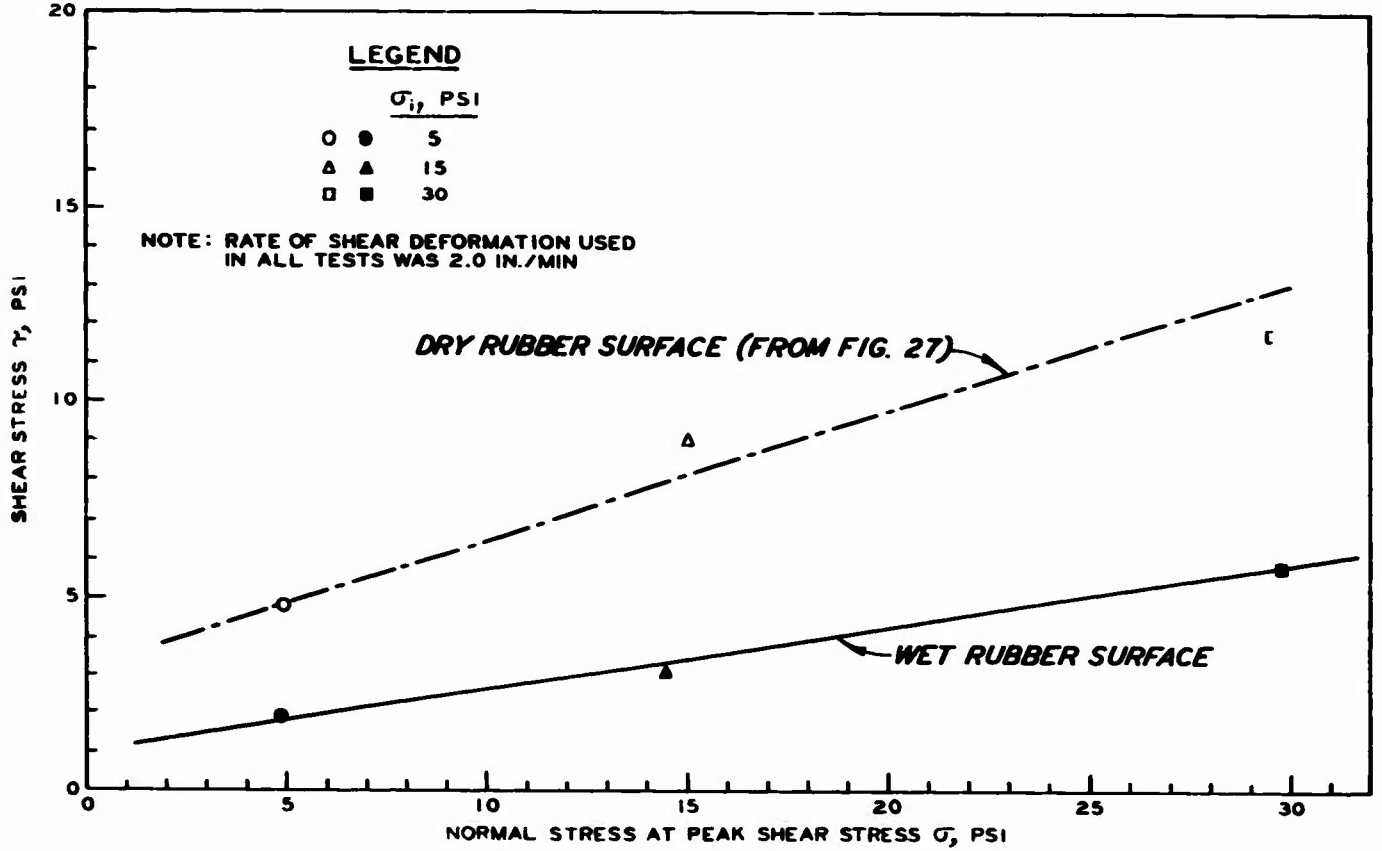

Fig. 29. Effect of degree of wetness on the peak shear stress at the interface of soil and rubber

why vehicles with pneumatic tires become immobilized, even after rain of short duration.

Steel on Soil

Test results

100. In this test series, the CH material obtained from the same batch used in previous tests was compacted on a smooth and polished stainless steel that filled the lower part of the annular shear box. The test was conducted under the same conditions that were imposed during the rubber on soil series.

101. Plots of the shear and normal stresses versus elapsed time with test data grouped under each of the three rates of shear deformation used in the test program are shown in figs. 30-32. The variations in shear and normal stresses with respect to time of these three groups greatly resemble those presented in figs. 24-26 for the rubber on soil series. The average deformation to failure was about the same for both test series, while the peak shear stress was slightly lower for steel on soil than for rubber on soil.

Strength parameters

102. The relationship between the shear and normal stresses at failure for soil specimens sheared on the polished stainless steel is shown in fig. 33. The figure shows that the peak shear stress increased with increasing initial normal stress and also with the speed at which the test was conducted. However, the spread of the results is much less than that observed for the rubber on soil series shown in fig. 27. Also, the strength of soil sheared on polished steel was about half the strength of soil sheared on rubber under comparable testing conditions. Therefore, it may be concluded that the traction forces associated with a pneumatic tire are larger than those associated with a rigid wheel.

103. The best-fit line of the failure points shown in fig. 33 indicates an adhesion intercept of 1.1 psi and an angle of surface friction equal to 9.5 deg. Based on the experimental values of a and δ obtained, the linear relationship between the shear and normal stress at

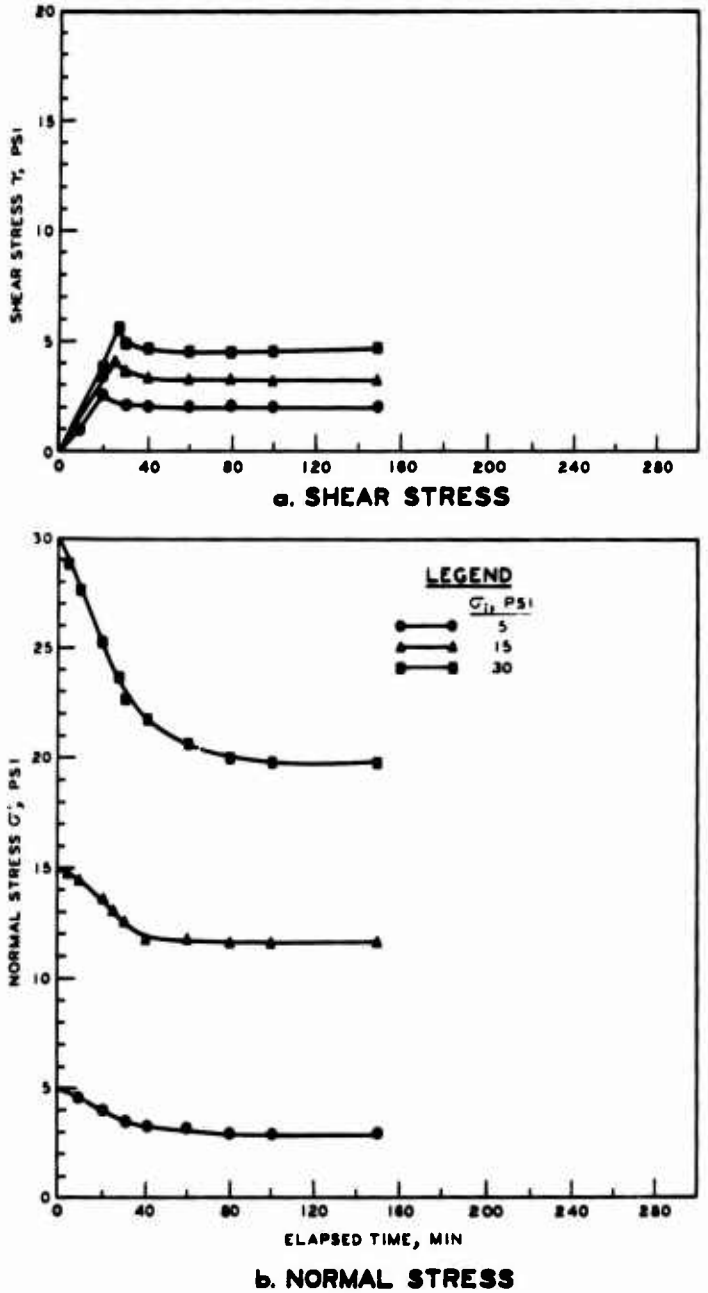

Fig. 30. Variation of τ and σ with time for soil sheared against polished steel at rate of shear deformation of 0.002 in./min

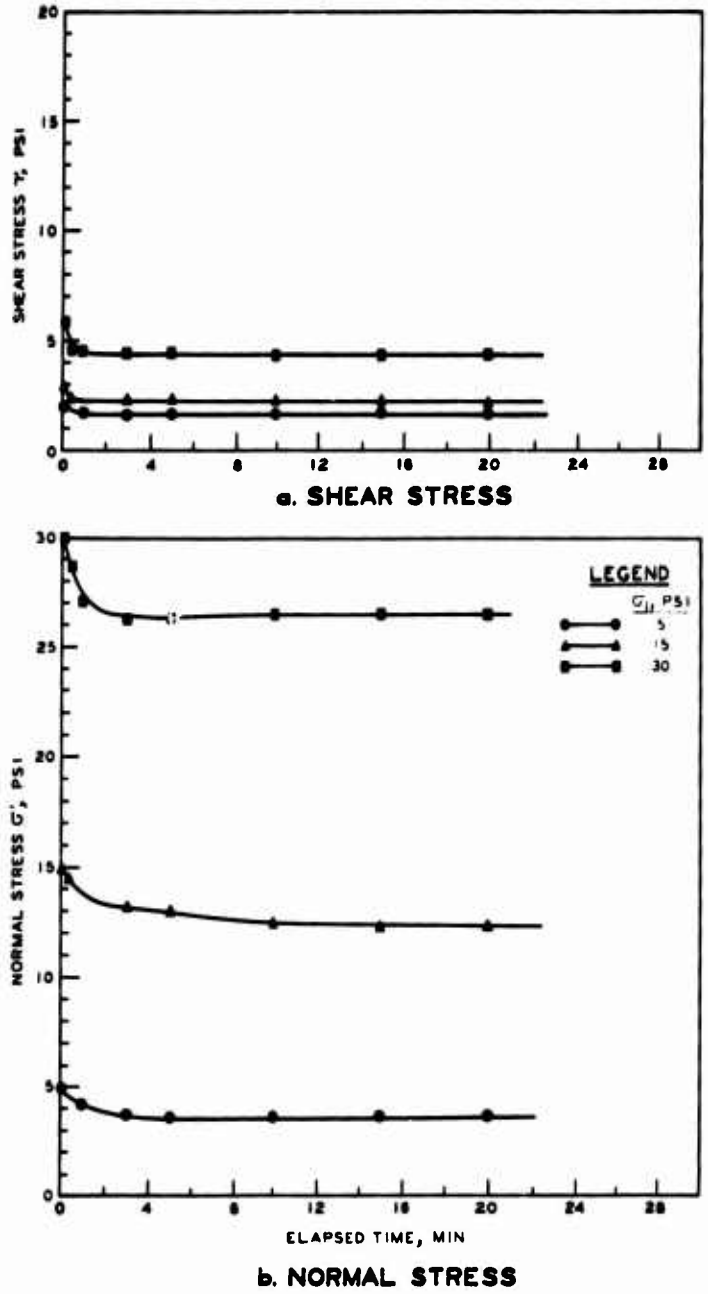

Fig. 31. Variation of τ and σ with time for soil on polished steel at rate of shear deformation of 0.2 in./min

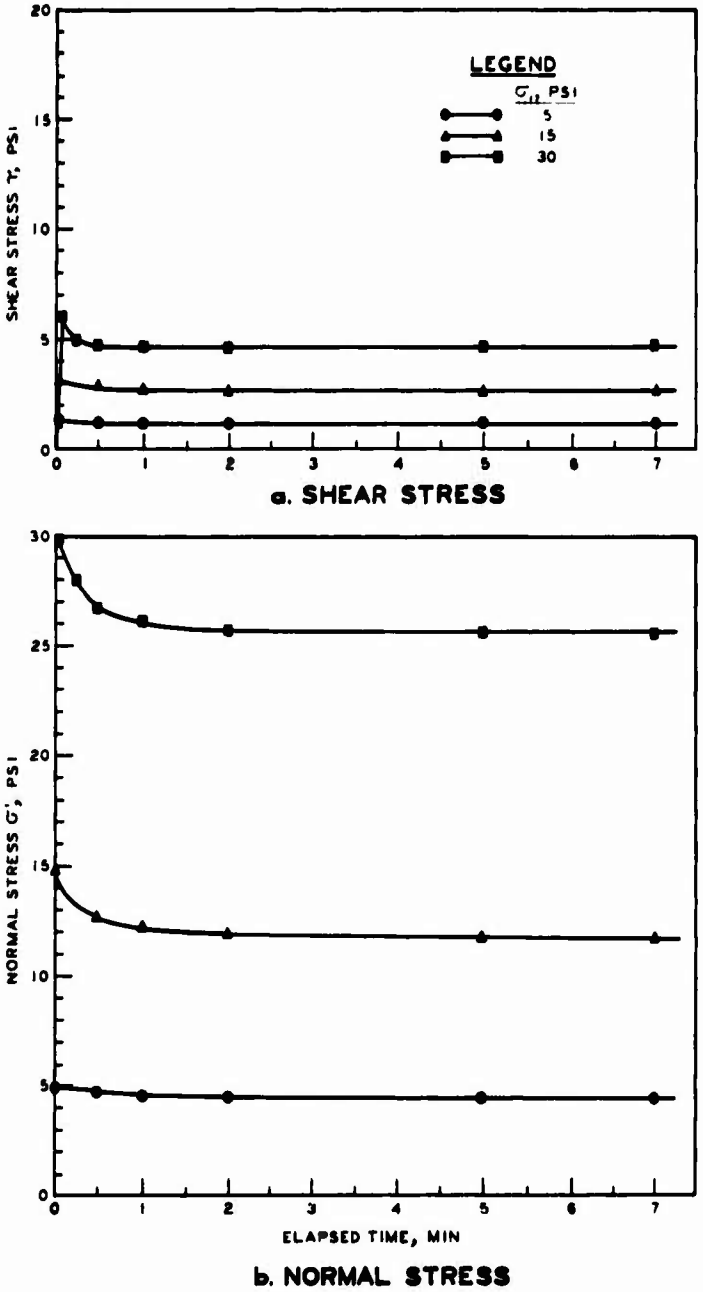

Fig. 32. Variation of τ and σ with time for soil on polished steel at rate of shear deformation of 2.0 in./min

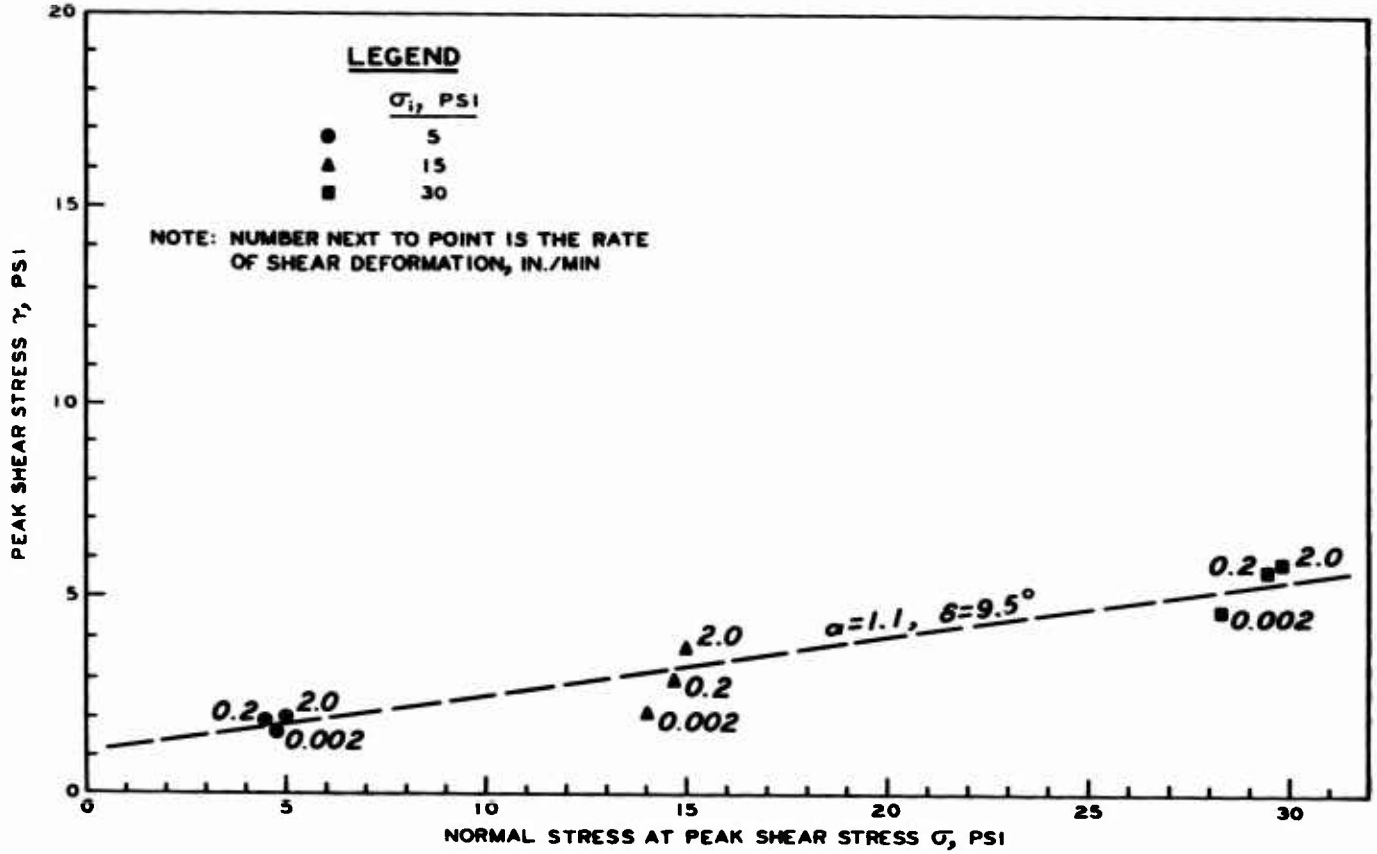

Fig. 33. Relationship between normal and shear stresses at failure at interface of soil and steel

the contact surface between soil and polished steel can be expressed as follows:

$$\tau = 1.1 + 0.15\sigma \qquad (94)$$

Effect of rate of shear deformation on strength at interface of soil and steel

104. The relationships between the maximum shear stress that developed at the interface of the soil and the polished steel and the rate of shear deformation are shown in fig. 34. Once again the peak shear stress showed an increase with increasing rate of shear deformation. However, the rate of the increase was much lower than that observed at the interface of the soil and rubber or in the homogeneous soil.

Effect of wetness on the shear stress at interface of soil and steel

105. Three tests were conducted in which the surface of the polished stainless steel in contact with soil was covered with a film of water in a manner similar to that used in the rubber on soil series. The tests were also conducted at initial normal stresses of 5, 15, and 30 psi, and all were sheared undrained at a rate of shear deformation equal to 2.0 in./min.

106. The relationship between the shear and normal stresses for specimens tested with a wet steel surface and those with a dry steel surface is shown in fig. 35. The figure clearly shows that the water film decreased the peak shear stress to about 65 percent of that with a dry steel surface. Thus, the degree of wetness would appreciably reduce the traction characteristics of a rigid wheel.

Nonhomogeneous Soil Specimens

Test results

107. The CH material in this test series was compacted in two layers of equal thickness but with two different degrees of wetness.

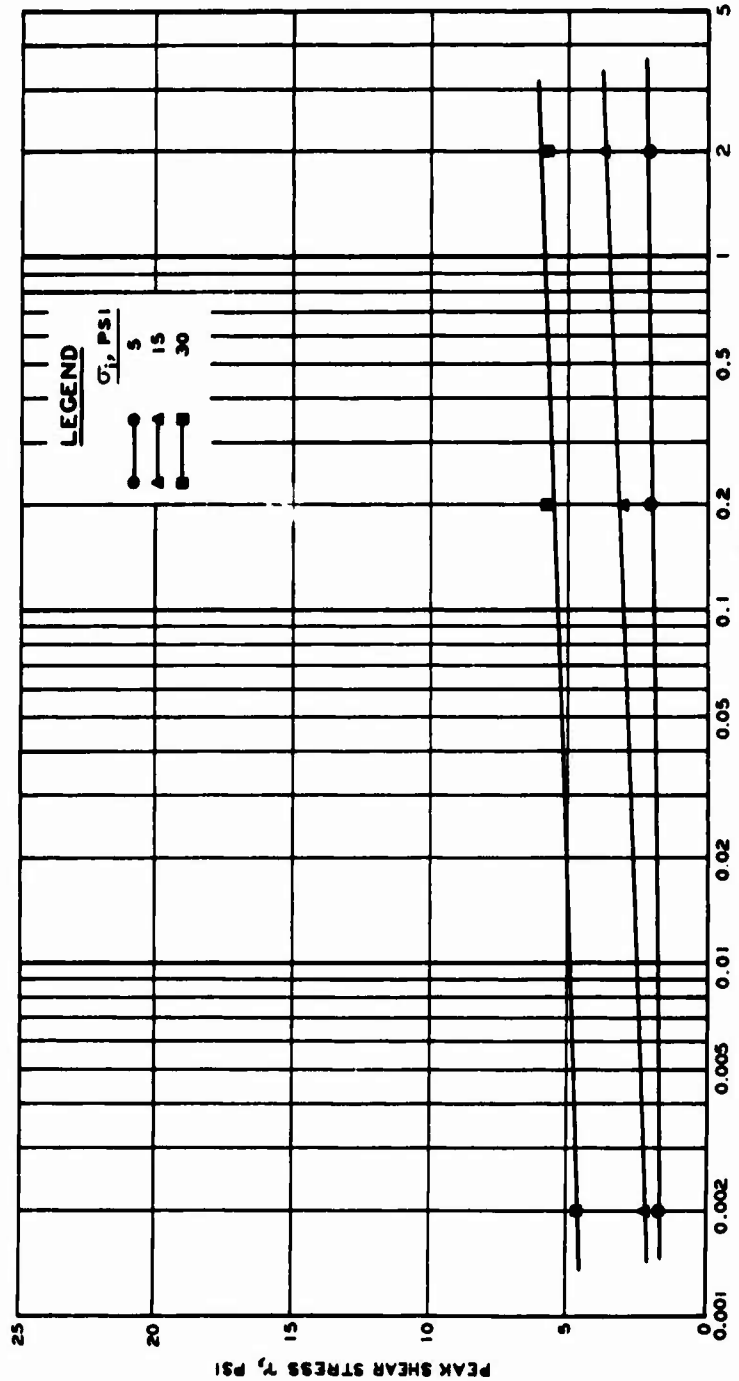

Fig. 34. Relationship between the peak shear stress τ and rate of deformation at interface of soil and steel

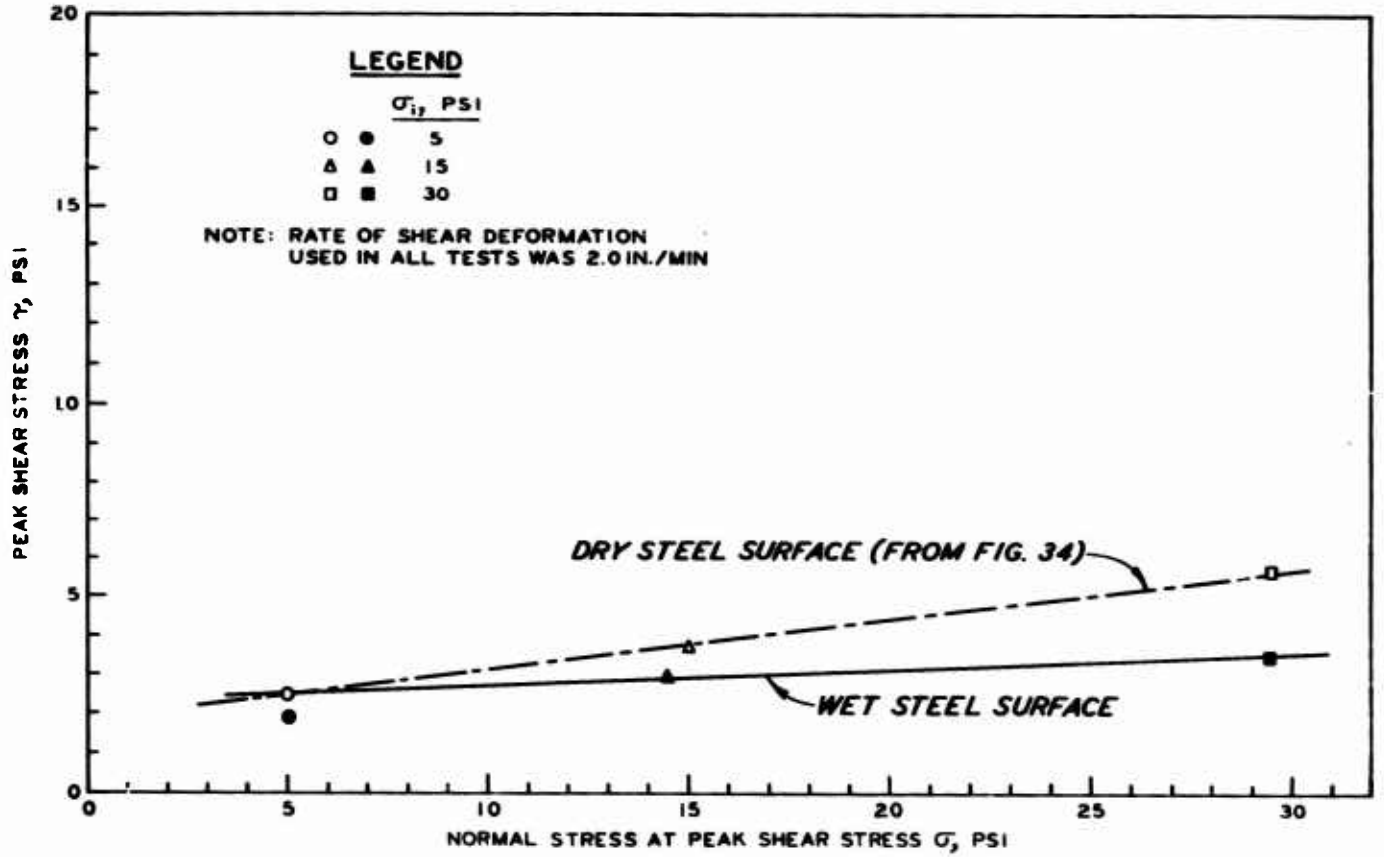

Fig. 35. Effect of degree of wetness on the peak shear stress developed at interface of soil and steel

The water contents of the upper and lower layers were 26 and 16 percent, respectively, and both layers were compacted with the same compaction effort used in the homogeneous soil series. Other testing conditions such as the initial normal stresses and the rates of shear deformation used in this test were kept the same as those used in previous test series.

108. It was expected that the stress versus deformation curves for the nonhomogeneous specimens would be comparable to those of the homogeneous specimens on the assumption that the portion of the soil specimen with the lower water content would have the major effect on the strength and deformation characteristics of the nonhomogeneous specimens. However, the results showed that although the shape of the curves (not shown) resembled very much those presented in figs. 18-20, the peak strengths of the nonhomogeneous soil specimens were much higher than those determined by comparable tests of the homogeneous soil specimens.

Soil strength parameters

109. The relationship between the shear and normal stresses at failure, shown in fig. 36, suggested a cohesion intercept of 2.5 psi and an angle of internal friction of 37 deg. It is apparent that the value of $\emptyset'$ based on the best-fit line is about 6 deg higher than that for the homogeneous soil, while the cohesion intercept is about 0.7 psi lower. This difference may be attributed to the slight migration of water from the upper layer to the drier lower layer, making the overall water content at the failure plane of the nonhomogeneous specimen lower than 26 percent, which caused the nonhomogeneous soil specimen to behave in a less plastic manner than the homogeneous specimens.

110. Because of funding limitations, it was not possible to test nonhomogeneous specimens of which both halves were quite wet of optimum, with one half very much wetter.

Relationship Between the Analytical and Experimental Investigations

111. In Part III of this report, it is shown that the state of stress at any point within a soil under a uniformly loaded circular

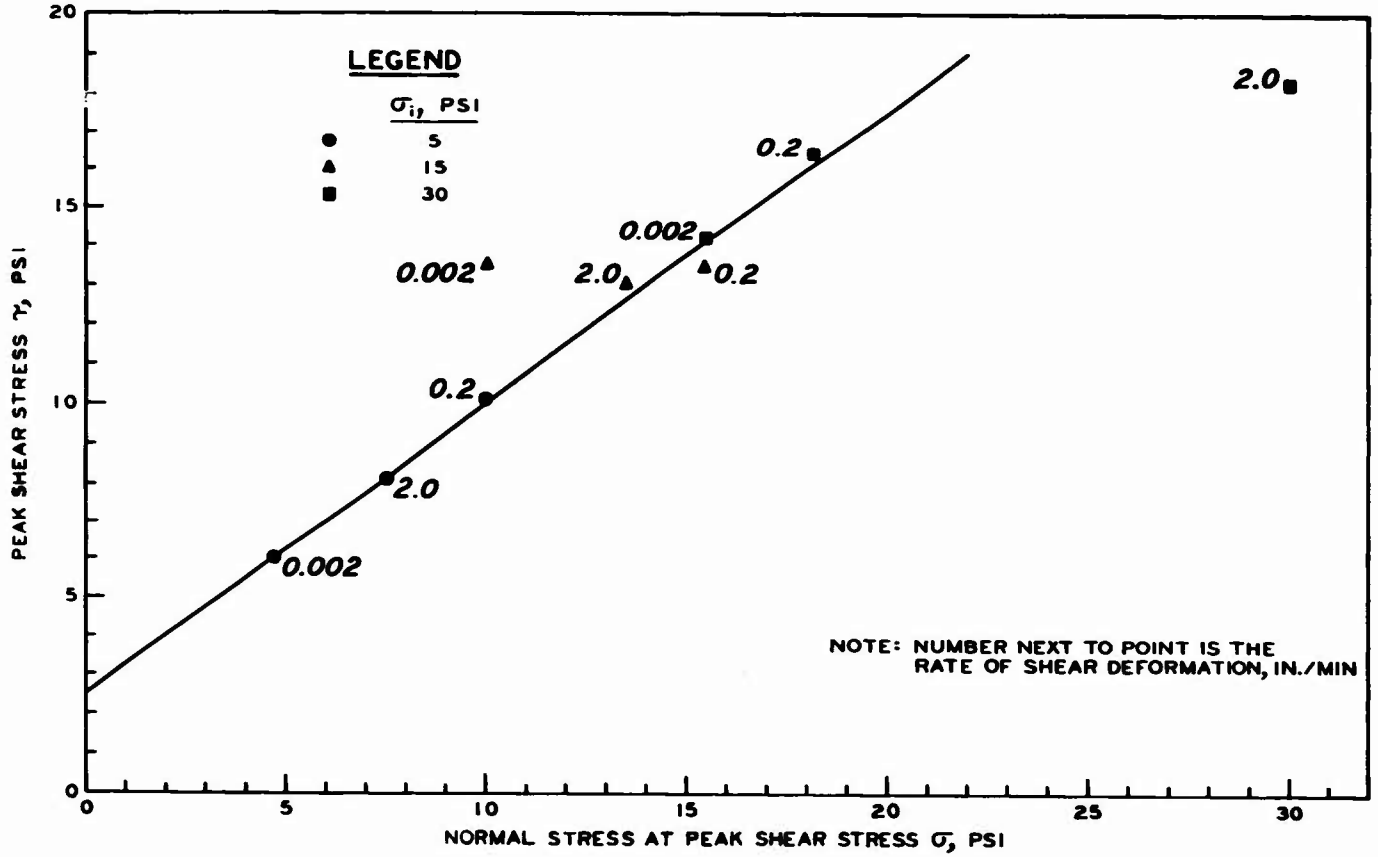

Fig. 36. Relationship between the shear and normal stresses at failure for nonhomogeneous soil specimens

segment can be expressed as follows:

$$\sigma_y = 2\mathrm{Re}\left[\phi(t)\right] + \mathrm{Re}\left[\overline{f(t)}\,\frac{\phi'(t)}{f'(t)} + \psi(t)\right] \qquad (85\text{ bis})$$

$$\sigma_x = 2\mathrm{Re}\left[\phi(t)\right] - \mathrm{Re}\left[\overline{f(t)}\,\frac{\phi'(t)}{f'(t)} + \psi(t)\right] \qquad (86\text{ bis})$$

$$\tau_{xy} = \mathrm{Im}\left[\overline{f(t)}\,\frac{\phi'(t)}{f'(t)} + \psi(t)\right] \qquad (87\text{ bis})$$

where $\phi(t)$, $f(t)$, and $\psi(t)$ are analytic functions that depend on the geometrical configuration, boundary condition, and applied stresses. The function $\psi(t)$ depends on the values of $\phi(t)$ and $f(t)$, which can be expressed as follows:

$$\phi(t) = \frac{N - iT}{2\pi i}\ln\left(\frac{t-1}{t+1}\right) \qquad (74c\text{ bis})$$

$$f(t) = \tanh\left[-\frac{k}{\pi}\ln\left(\frac{t-1}{t+1}\right) + \frac{\pi i}{2}\right] = x + iy \qquad (95)$$

It is quite obvious that the function $f(t)$ depends only on the geometrical shape of the medium (i.e., soil-wheel system), while $\phi(t)$ depends on the applied radial and tangential stresses N^* and T,* respectively.

112. In Part IV of this report, it is shown that the value of shear stress τ, which is equivalent to T, can be linearly related to the applied normal stress; such a linear relationship is greatly influenced by the type of wheel and soil properties. Therefore, if the type of wheel used, the properties of the soil, and the applied normal stresses are known, it is possible to estimate the value of the corresponding shear stress. If the normal and shear stresses at the soil-wheel interface and also the geometry and boundary conditions of the soil-wheel systems are known, it is possible to evaluate the functions

---

* The values of N and T in the analytical solution are equivalent to σ and τ, respectively.

$\phi(t)$, $f(t)$, and $\psi(t)$. Once these functions are known, equations 85-87 can be used to evaluate the state of stress at any point beneath the wheel. The procedure outlined is illustrated by the following example.*

113. Consider a 51-in.-diam rubber-rimmed wheel imbedded 3 in. in soil with properties similar to the CH material used in this study (see fig. 37a). Assuming that the wheel is in a state of impending motion while exerting a uniform radial stress of 25 psi on the underlying soil, it is desired to evaluate the state of stress at point A 1.2 ft below the soil surface and 2.3 ft to the left of the center line of the wheel.

114. The first step is to estimate the maximum shear stress that can be developed along the interface of the soil and the wheel, using equation 93 ($\tau = 2.3 + 0.265\sigma$). Then:

$$\tau = 2.3 + (0.265 \times 25) \quad \text{or } 8.925 \text{ psi}$$

115. The second step is to idealize the wheel so that the analytical solution can be applied directly. This can be done by introducing such a scale factor that the projection of the contact surface L from the center line of the wheel is equal to unity, as shown in fig. 37b.

116. The third step is to evaluate the value of K using either equation 54 or fig. 9. Then

$$\frac{\delta}{L} = \cot K = 0.25$$

$$K = 1.32587 \text{ radians}$$

Once the values of K , σ , and τ are known, it is possible to evaluate the stresses directly using the computer program in Appendix A to get the values of σ_x , σ_y , and τ_{xy} for the point under consideration. For this problem, the computer program yielded the following stresses at point A: $\sigma_x = -2.646$ psi; $\sigma_y = -0.165$ psi; and $\tau_{xy} = 1.811$ psi.

---

* The example is presented to illustrate the method of solution proposed in this report and is not necessarily the solution of a practical problem.

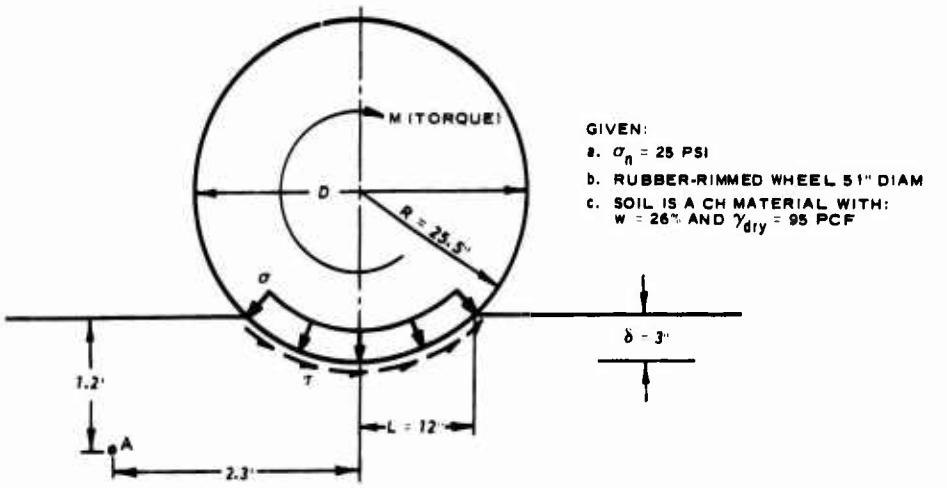

a. ACTUAL WHEEL

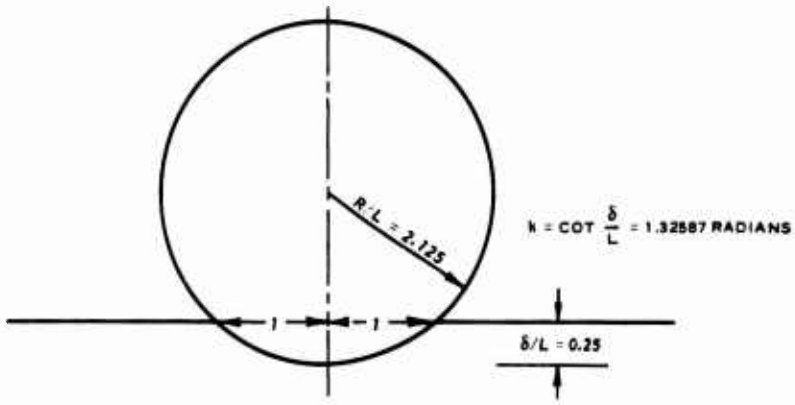

b. IDEALIZED WHEEL

Fig. 37. Rigid wheel in a state of impending motion

117. Because of the similarity between the ideal wheel presented in fig. 37b and that shown in figs. 14 and 15, diagrams presented in figs. 14 and 15 can be used to evaluate the state of stress at point A. This can be done simply by measuring the ordinates of respective stress diagrams and multiplying them by 25 for evaluating stresses resulting from the normal stress alone and by 8.925 for evaluating stresses resulting from shear stress alone. The resulting stresses can be added together by applying the principle of superposition as shown below:

a. Stresses at point A due to normal stress alone

$$\sigma_x = -0.239 \times 25 = -5.975 \text{ psi}$$

$$\sigma_y = -0.0565 \times 25 = -1.413 \text{ psi}$$

$$\tau_{xy} = 0.124 \times 25 = 3.100 \text{ psi}$$

b. Stresses at point A due to shear stress alone

$$\sigma_x = 0.372 \times 8.925 = 3.320 \text{ psi}$$

$$\sigma_y = 0.1402 \times 8.925 = 1.251 \text{ psi}$$

$$\tau_{xy} = -0.144 \times 8.925 = -1.285 \text{ psi}$$

By adding the stresses in a and b, the following results are obtained:

$$\sigma_x = -5.975 + 3.320 = -2.655 \text{ psi}$$

$$\sigma_y = -1.413 + 1.251 = -0.162 \text{ psi}$$

$$\tau_{xy} = 3.100 - 1.285 = 1.815 \text{ psi}$$

These values agree closely with those yielded by the computer program and presented in paragraph 116.

PART VI: CONCLUSIONS AND RECOMMENDATIONS

Conclusions

118. The following conclusions are believed warranted by the findings of this study:

a. The state of stress and the orientation of stresses at any point within a region beneath a wheel can be obtained analytically in terms of the radial and tangential stresses generated by the wheel. For plane strain cases, the normal and shear stresses beneath the wheel are independent of the properties of the supporting medium.

b. The soil-wheel interaction problem can be solved by a rational approach using the instantaneous stresses in providing design criteria regarding trafficability problems.

c. The experimental study demonstrates that much pertinent information regarding immobilization due to inadequate traction can be obtained through relatively simple laboratory tests.

d. Based on limited experimental tests, it was found that the traction forces on any potential failure plane increased with increasing rate of shear deformation and increasing normal stresses acting on that plane. However, these traction forces decreased sharply with increasing wetness of the potential failure surface.

e. The maximum shear stress at the interface of soil and smooth rubber is higher than that at the interface of soil and polished stainless steel. Stresses at both these interfaces are lower than the strength of the soil alone.

f. The relationship between the shear and normal stresses obtained through the experimental tests can be combined with the analytical solution to provide rational solutions in the field of terramechanics.

Recommendations

119. It is known that the study of relationship between soils and wheels of moving vehicles could take various approaches depending on the type of vehicle and the performance desired. With regard to further

development of the findings of this study, the following recommendations are made:

a. Extend the theoretical solution to include cases in which the radial and tangential stresses between the soil and the wheel vary along the surface of contact. The variation of these stresses could be assumed to be sinusoidal, parabolic, or other geometric distributions that more realistically simulate field conditions.

b. Present the analytical solution of wheels with different sizes and sinkage in the form of influence charts and tables, thus eliminating the need for tedious calculation or individual computer runs.

c. Extend the present solution to develop expressions for the evaluation of strains and displacement within soil in the vicinity of the wheel.

d. Follow the same procedures in evaluating stresses, but assume the soil to be a linear viscoelastic material.

e. Extend the scope of the experimental study on the plastic clay used in this study and also study other soils, particularly with respect to loss of traction due to slipperiness.

f. Verify, if possible, the findings of this study using true model testing.

g. Adapt the analytical solution for the study of stresses around circular cavities at or near the soil surface.

120. Other recommendations that are related to the vehicle traction problem but are not directly related to the findings presented in this study are:

a. Study the plastic equilibrium of soil in the vicinity of a wheel under the influence of forces generated by a moving vehicle. This problem could be treated by either considering the distribution of normal stresses along the rupture surface (i.e., stability problem) or by assuming that every point in the rupture zone is in a state of limiting equilibrium (i.e., limiting equilibrium problem). In either case, use must be made of an appropriate failure criterion such as Mohr, Tresca, Von Mises, or others.

b. Apply the procedure outlined in subparagraph a to solve the problem of a grouser analytically or experimentally or both, taking into consideration the effect of size and shape of the grouser and of the distance between two adjacent grousers on the performance of a vehicle.

c. Develop as an ultimate goal a prediction equation that can relate the energy or force input by the vehicle to the energies or forces lost by traction, friction, and slippage; soil compaction; and soil flow and other actual measurements or reasonable estimates of these quantities.

REFERENCES

1. Thompson, A. B., "Stresses Under Moving Vehicles; A Pilot Study of WES Earth Pressure Cell Action in Comparatively Soft Soil," Miscellaneous Paper No. 4-230, Report 1, Jul 1957, U. S. Army Engineer Waterways Experiment Station, CE, Vicksburg, Miss.

2. Meyerhof, G. G., "The Bearing Capacity of Soils Under Vehicle Loads," Proceedings, First International Conference on Mechanics of Soil-Vehicle System, Torino-Saint Vincent, Italy, 1961, pp 81-86.

3. Freitag, D. R. and Green, A. J., "Distribution of Stresses on an Unyielding Surface Beneath a Pneumatic Tire," Miscellaneous Paper No. 4-469, Feb 1962, U. S. Army Engineer Waterways Experiment Station, CE, Vicksburg, Miss.

4. Green, A. J., Jr., and Murphy, N. R., Jr., "Stresses Under Moving Vehicles; Distribution of Stresses Beneath a Towed Pneumatic Tire in Air-Dry Sand," Technical Report No. 3-545, Report 5, Jul 1965, U. S. Army Engineer Waterways Experiment Station, CE, Vicksburg, Miss.

5. Todhunter, I., A History of the Theory of Elasticity and of the Strength of Materials, Vol II, Dover, New York, 1960, p 237.

6. Egorov, K. E., "Concerning the Question of Calculation for Base Under Foundation with Footing in the Form of a Ring," Mekhanika Gruntov, Sb Tr., No. 34, Gosstroiizdot, Moscow, 1958.

7. Ahlvin, R. G., "Investigations of Pressures and Deflections for Flexible Pavements; Homogeneous Sand Test Section," Technical Memorandum No. 3-323, Report 4, Dec 1954, U. S. Army Engineer Waterways Experiment Station, CE, Vicksburg, Miss.

8. Green, J. E. and Knight, S. J., "Preliminary Study of Stresses Under Off-Road Vehicles," Miscellaneous Paper No. 4-362, Oct 1959, U. S. Army Engineer Waterways Experiment Station, CE, Vicksburg, Miss.

9. Timoshenko, S. and Goodier, J. N., Theory of Elasticity, 2d ed., McGraw-Hill, New York, 1951.

10. Spiegel, M. R., Theory and Problems of Complex Variables, McGraw-Hill, New York, 1964.

11. Muskhelishvili, N. I., Some Basic Problems of Mathematical Theory of Elasticity, Translated from the Russian by J. R. M. Mardik, P. Noordhoff, Ltd., Groningen, Netherlands, 1963.

12. Baladi, G. Y., Distribution of Stresses and Displacement Within and Under Long Elastic and Viscoelastic Embankments, Ph. D. Dissertation, Purdue University, Lafayette, Ind., 1968.

13. Harr, M. E., Groundwater and Seepage, McGraw-Hill, New York, 1962, p 69.

14. Kober, H., Dictionary of Conformal Representations, 2d ed., Dover, New York, 1957.

15. Churchill, R. V., Complex Variables and Applications, 2d ed., McGraw-Hill, New York, 1960.

16. Wylie, C. R., Advanced Engineering Mathematics, 3d ed., McGraw-Hill, New York, 1966.

17. U. S. Army Engineer Waterways Experiment Station, CE, "Soil Mechanics Testing Facilities at the Waterways Experiment Station," Brochure, Oct 1970, Vicksburg, Miss.

18. MacIver, B. N. and Donaghe, R. T., "Evaluation of Soil Mechanics Laboratory Equipment; Modified Berkeley Pneumatic Tamper for Compacting Test Specimens of Cohesive Soils," Miscellaneous Paper No. 3-478, Report 12, Jun 1971, U. S. Army Engineer Waterways Experiment Station, CE, Vicksburg, Miss.

19. Hvorslev, M. J., "Physical Properties of Remolded Cohesive Soils," Translation No. 69-5, Jun 1969, U. S. Army Engineer Waterways Experiment Station, CE, Vicksburg, Miss.

20. Strohm, W. E., Jr., "Preliminary Analysis of Results of Division Laboratory Tests on Standard Soil Samples," Miscellaneous Paper No. 3-813, Apr 1966, U. S. Army Engineer Waterways Experiment Station, CE, Vicksburg, Miss.

21. Donaghe, R. T., "Effects of Strain Rate in Consolidated-Undrained Triaxial Compression Test of Cohesive Soils; Vicksburg Buckshot Clay (CH)," Miscellaneous Paper S-70-8, Report 2, May 1971, U. S. Army Engineer Waterways Experiment Station, CE, Vicksburg, Miss.

22. Taylor, D. W., Fundamentals of Soil Mechanics, Wiley, New York, 1949, p 378.

23. Hvorslev, M. J. and Kaufman, R. I., "Torsion Shear Apparatus and Testing Procedures," Bulletin No. 38, May 1952, U. S. Army Engineer Waterways Experiment Station, CE, Vicksburg, Miss.

APPENDIX A: ANNULAR TORSION SHEAR APPARATUS

1. The test apparatus used in this program was an annular shear device designed and built by the U. S. Army Engineer Waterways Experiment Station (WES) in 1947. The device is described in detail in reference 23.* The annular shear test was employed in this investigation because any desired amount of displacement may be obtained with an annular test specimen, and shear strengths at large displacements were of interest. The 1947 version of the annular shear apparatus had to be modified so that data could be recorded electronically; this modification was necessary since the rapid rates of displacement used would not permit manual observation.

Shear Assembly

2. The unmodified device employed a load frame to measure the torque from which the shear stress was computed. A section through the unmodified shear apparatus is shown in fig. A1. The soil specimen is confined by inner and outer rings that are divided into an upper and lower pair. The upper inner ring is guided by a special ball bearing, permitting both rotation and vertical movement. The lower ring fits snugly over a rib in the rotating base, which is supported and guided by bearings on the stationary base. The rotating base can be rotated by hand or motor through the self-locking worm gear that holds the base stationary when the drive shaft is not rotated.

3. For this testing program, the shear apparatus was modified by replacing the upper and lower dentated porous plates with nonporous plates having blades 0.034 in. thick and 1/8 in. high and spaced at 30-deg intervals around the annulus. The bladed plates are shown in fig. A2; the top bladed plate is shown attached to the torque wheel. The device was modified in this manner because for soil on soil tests,

---

* Reference numbers refer to like-numbered items in the list of references at the end of the main text.

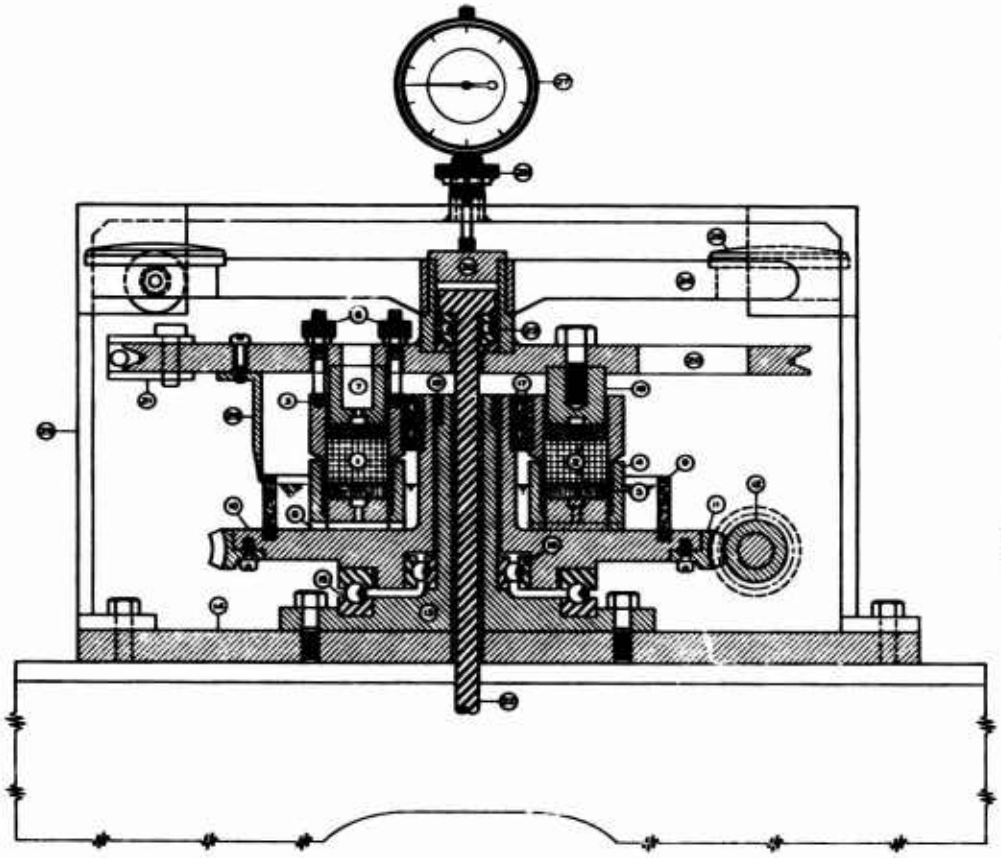

LEGEND

1 RING TEST SPECIMEN
2 DENTATED POROUS PLATES
3 UPPER CONFINING RINGS
4 LOWER CONFINING RINGS
5 TRANSFER RINGS
6 RING ELEVATOR SCREWS
7 UPPER WATER OUTLET
8 LOWER WATER OUTLET
9 PLEXIGLAS CYLINDER
10 ROTATING BASE
11 BASE GEAR
12 WORM GEAR
13 PINION WITH FLANGE
14 FIXED BASE PLATE
15 BASE THRUST BEARING
16 BASE GUIDE BEARING
17 RING GUIDE BEARING
18 OILITE PINION BEARING
19 RING PISTON
20 TORQUE WHEEL
21 WIRE ROPE CLAMP
22 LOADING ROD

Fig. A1. WES annular shear apparatus

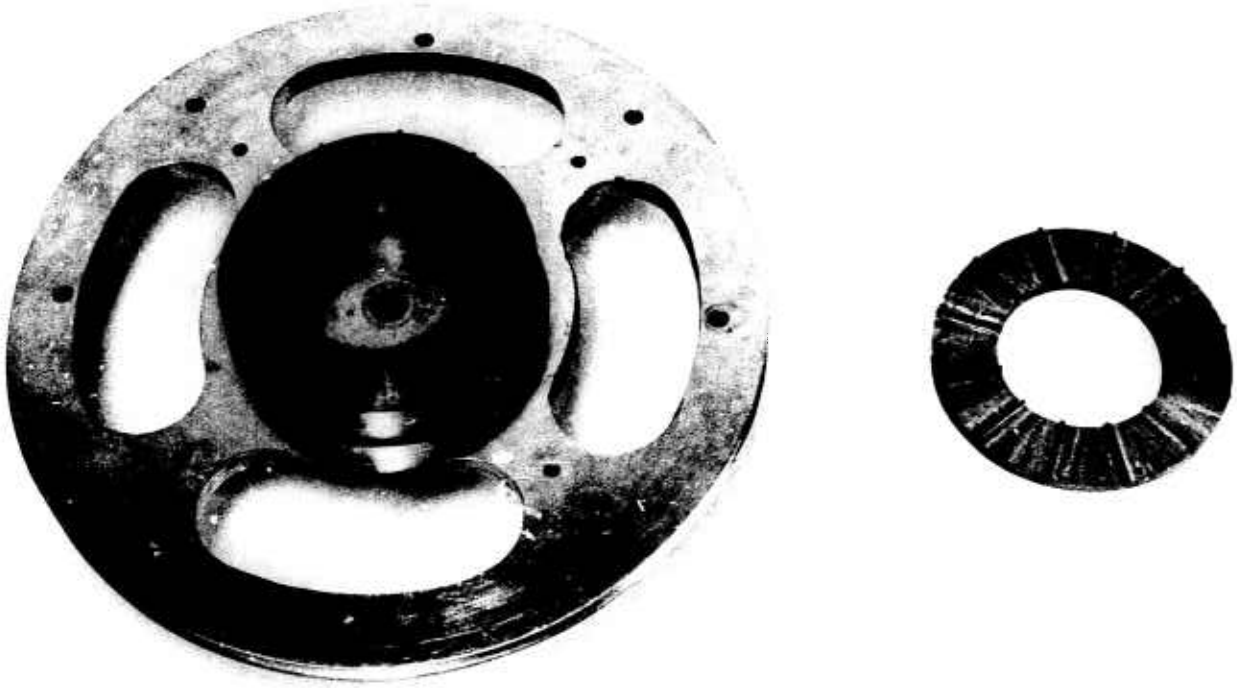

Fig. A2. Nonporous bladed plates

the dentated porous plates could not provide sufficient frictional resistance against the top and bottom surfaces of the soil specimen to prevent slippage. It was not necessary that the bladed plates be porous since undrained tests were performed. The zones of disturbance at the top and bottom of the soil specimen were not thought to influence the test results since the blades were thin and short (1/8 in. high) and the soil specimen was 3/4 in. thick.

Torque Loading System

4. As the rotary base rotates, a torque is produced by pulling on two flexible wire cables that are attached to the torque wheel. The cables pass over horizontal and vertical guide sheaves and connect to the balance beam, which reacts on the frame of the device through a knife edge. The vertical guide sheaves are attached to the yoke of the load frame, which deflects as the torque load increases. All guide sheaves can be raised or lowered so that they are in a horizontal plane with the torque wheel at the start of a test. The torque loading system is shown in fig. A3.

5. For this testing program, the very rapid rates of displacement required that test data be recorded electronically. To accomplish this, a linear variable differential transformer (LVDT) was mounted on the load frame to measure its deflection. This modification can be seen in fig. A4. From the deflection of the load frame, the shear stress in the soil can be computed.

Normal Loading System

6. Details of the unmodified normal loading system are shown in fig. A5. The unmodified system consisted of a hanger and counterbalanced double lever to which dead weights were added. The load was transmitted to the torque wheel and annular piston by a loading rod. A turnbuckle on this rod permitted adjustment of the levers to a horizontal position.

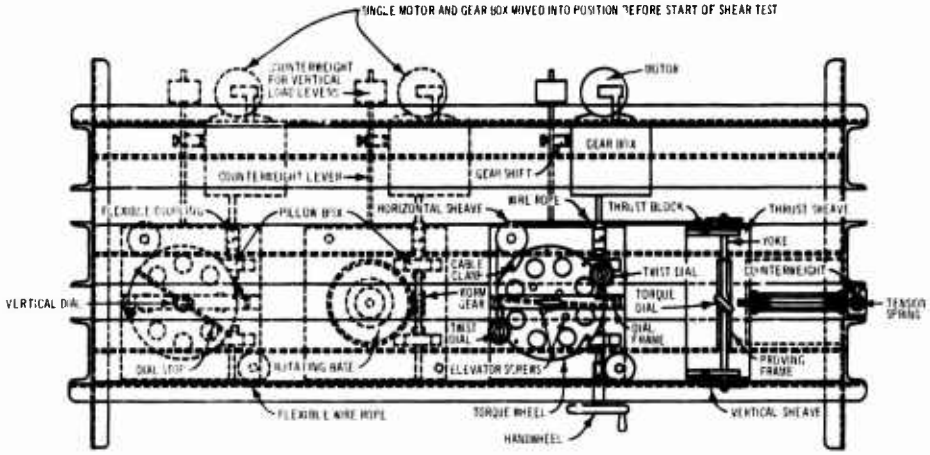

PLAN

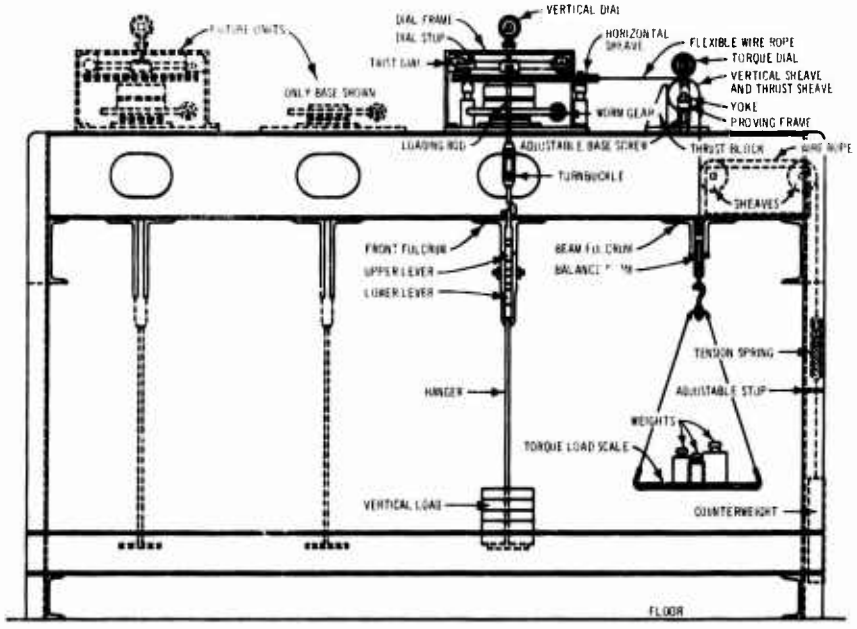

ELEVATION

SCALE

5 0 5 10 15 IN

Fig. A3. Unmodified torque loading system

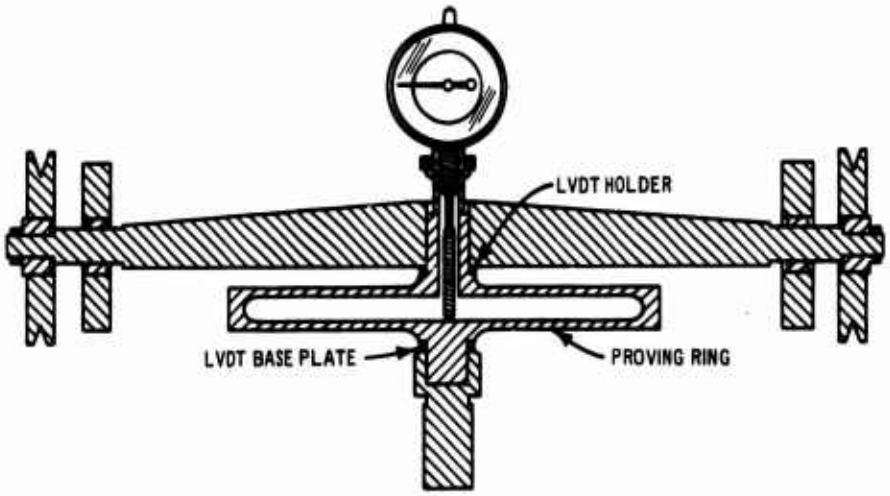

LONGITUDINAL SECTION

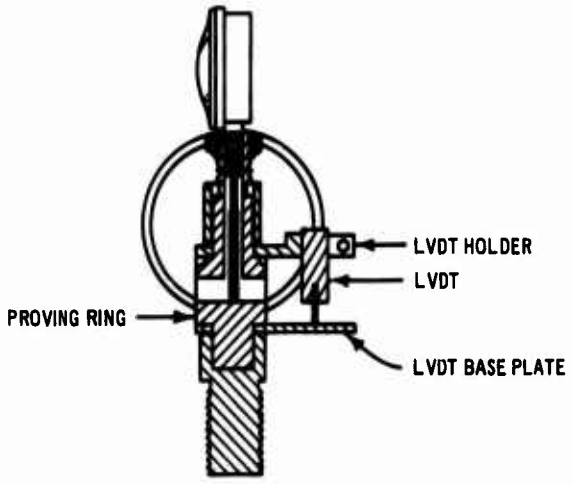

LATERAL SECTION

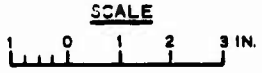

Fig. A4. Revised torsional loading system

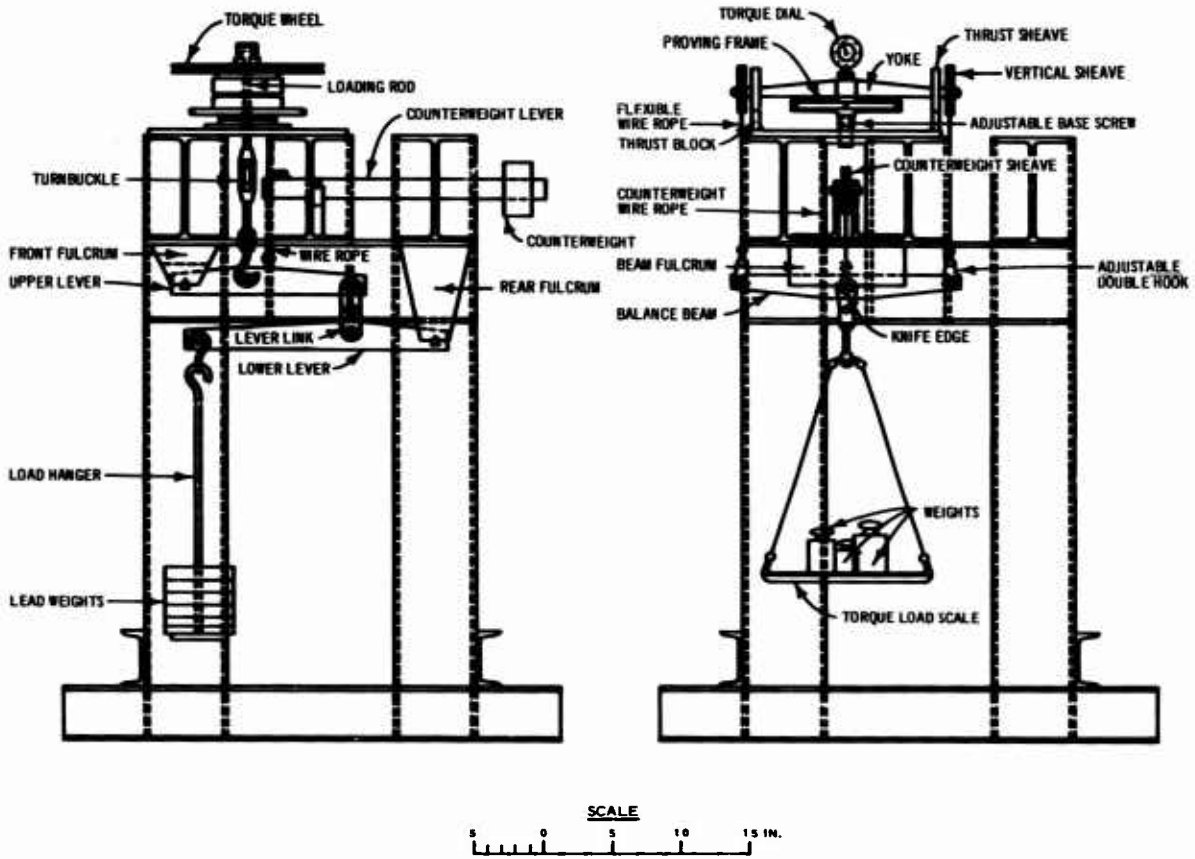

Fig. A5. Details of unmodified normal loading system

7. In this testing program, soil specimens were sheared under constant volume; i.e., during shear, the normal stress was continuously varied to counteract any tendency of the soil specimen to expand or contract. Operating in this manner ensured that no drainage would occur, and hence a measure of undrained shearing resistance was obtained. The mechanisms of the constant-volume test in a direct shear box are discussed in detail in reference 23. The basic principles of the constant-volume direct shear test also apply to the constant-volume annular shear test.

8. In order to record and control the normal load, the lever system was replaced by a 1000-lb electronic load cell, which was held at the lower end by a rod and bearing that was fastened to the frame of the device and which at the upper end was connected to the loading rod by a turnbuckle. The rod and bearing provided alignment for the load cell, and the turnbuckle provided any necessary load adjustment. The modified normal loading system is shown in figs. A6 and A7.

Volume Control

9. The volume of the annular shear test specimen was controlled by controlling the thickness of the specimen. A 0.001-in. Ames dial indicator was used to control the thickness during shear within a range of $\pm$0.0001 in. The vertical thickness dial is held rigidly in the dial frame, which clamps to the frame of the device. The dial stem rests on the top cap, which is held in the torque plate that is rigidly clamped to the annular piston. The annular piston rests on the test specimen. With this assembly, any tendency for vertical expansion or contraction of the soil can be detected with the dial indicator, and the normal stress can be adjusted to counteract this tendency for movement.

10. The signals from the electronic load cell and the LVDT were amplified and recorded on a strip chart recorder. The composite testing apparatus is shown in fig. A8.

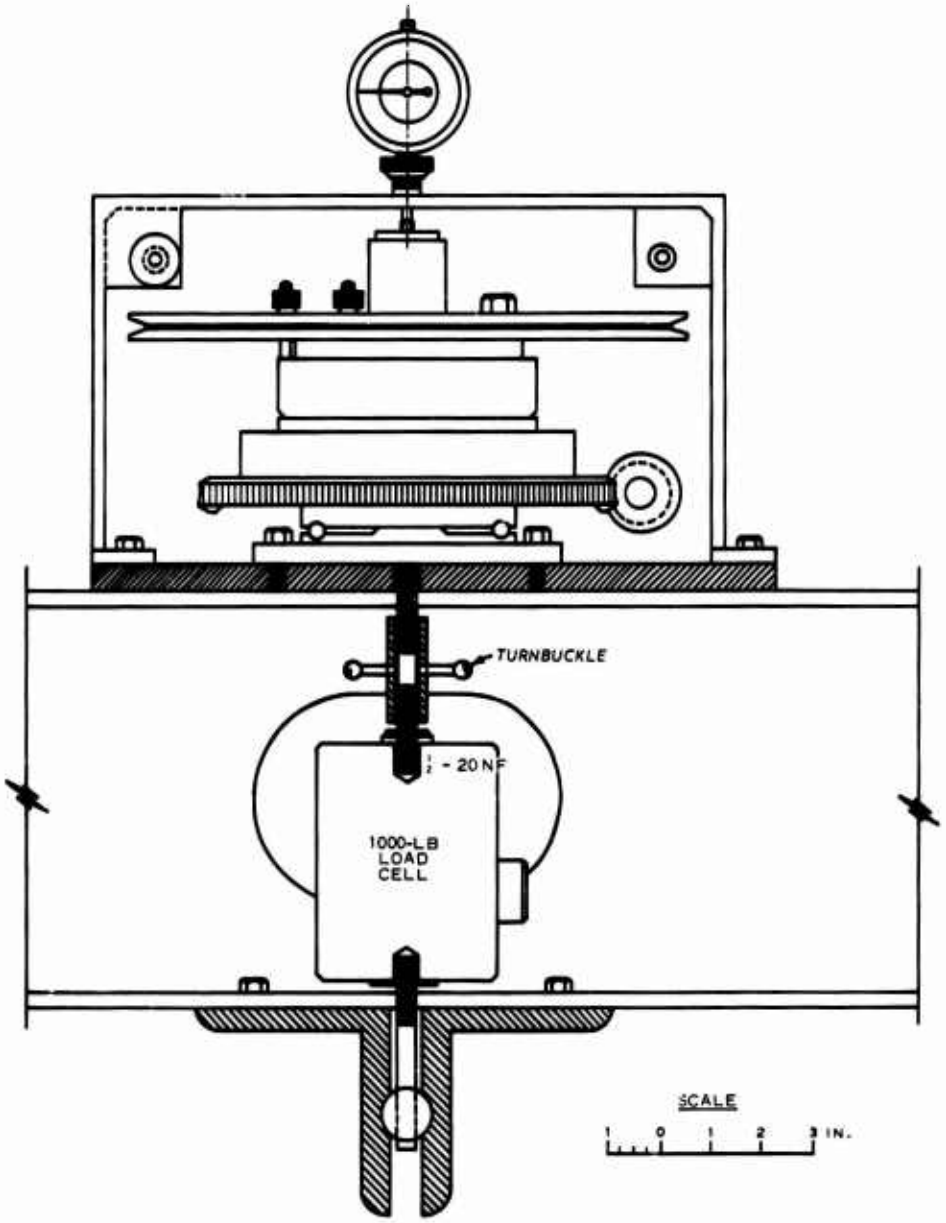

Fig. A6. Side view of modified normal loading system

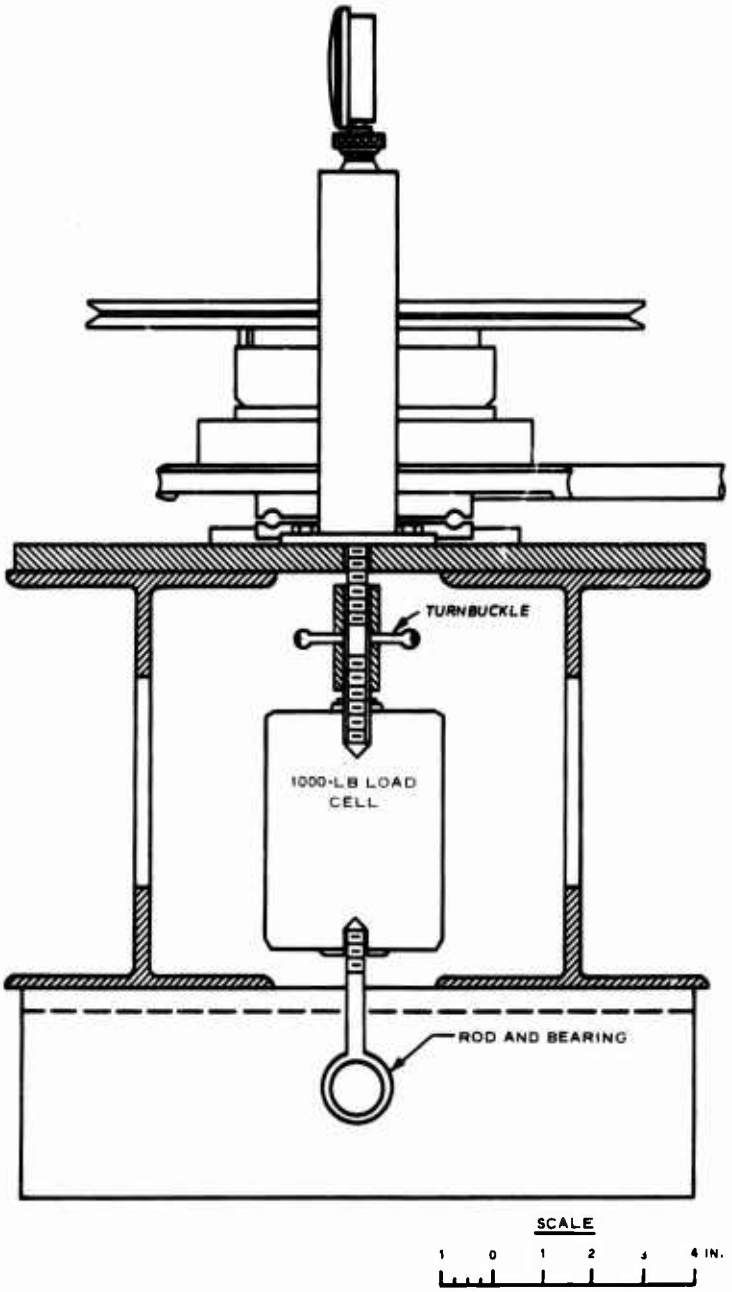

Fig. A7. End view of modified normal loading system

Fig. A8. Modified annular shear apparatus

APPENDIX B: PREPARATION OF RUBBER ANNULUS

1. In order to obtain a realistic measure of the resistance at the interface of soil and rubber for the wheel-soil interaction study, a rubber annulus was fabricated in order that annular torsion tests could be performed.

2. The rubber used to mold the annulus was of the type used commercially for retreading truck tires. The annulus used in this testing program was prepared using a procedure that simulated the commercial retreading operation as closely as possible.

3. A mold that would allow the forming of the annulus in its final dimensions was constructed; it can be seen schematically in fig. B1. A photograph of the mold is presented in fig. B2. A quantity of uncured rubber available commercially from the General Tire and Rubber Company was obtained and cut into an annular geometry, 1/2 in. thick, which would fit into the mold. The rubber was bonded to the cleated stainless steel plate (fig. B3). The rigid plate ensured that the rubber annulus would keep its geometric shape and provided a means of mechanical linkage to the shear apparatus.

4. The steel plate was put into the bottom of the mold, the annulus of uncured rubber was put in on top of the plate, and a smooth steel ring was put on top of the uncured rubber. The mold was then completely assembled and a torque applied to the top nut of the assembly to give a pressure on the rubber of 160 psi. The assembly was then placed in an oven at 149 C (or about 300 F) and allowed to cure at this temperature for a period of 45 min. The assembly was then allowed to cool, and the cured rubber annulus and its steel linkage plate forced from the mold. The final product is shown in fig. B4.

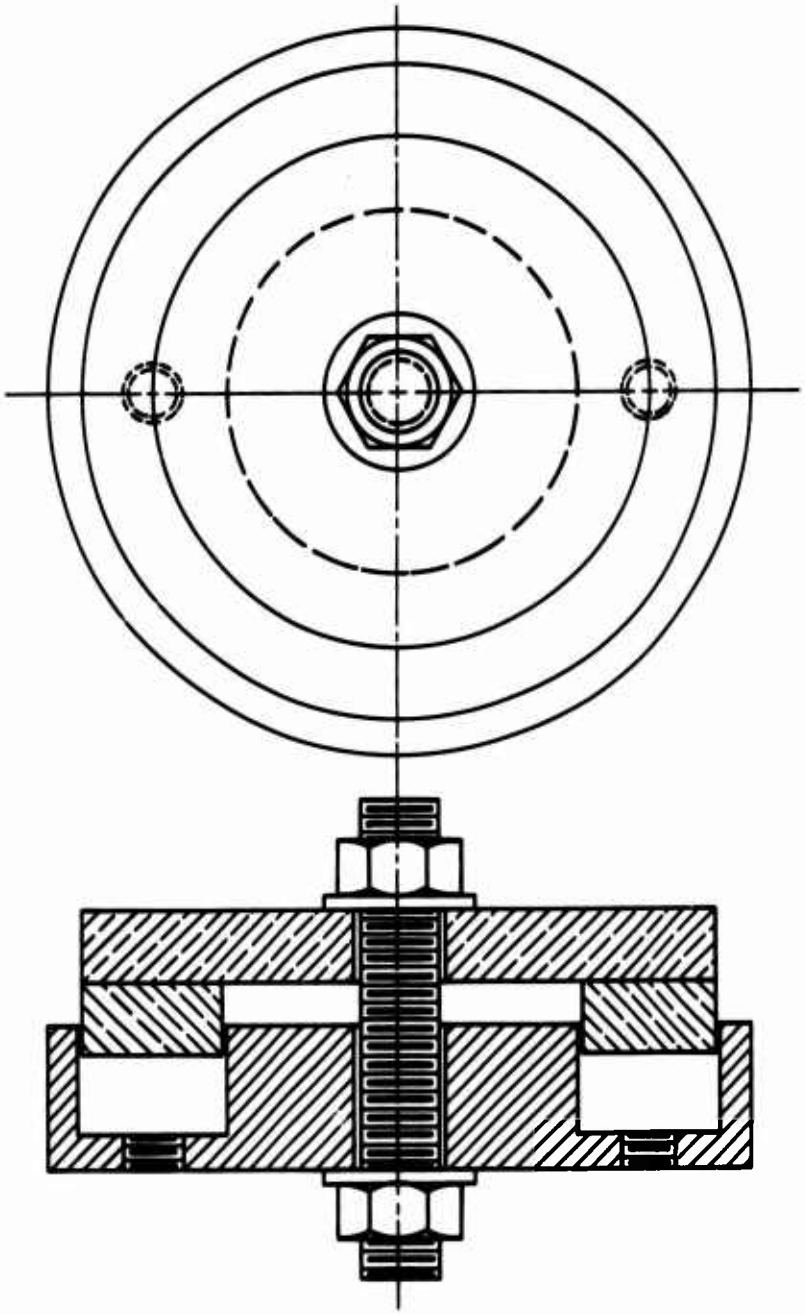

Fig. B1. Schematic of annular rubber mold

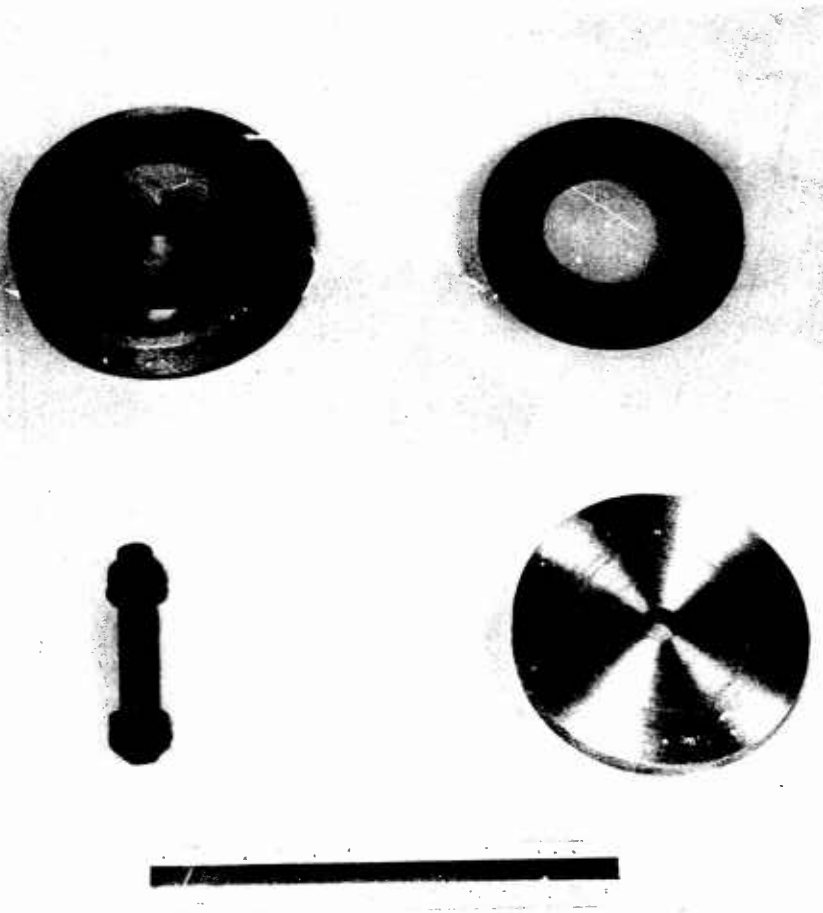

Fig. B2. Component parts of annular mold

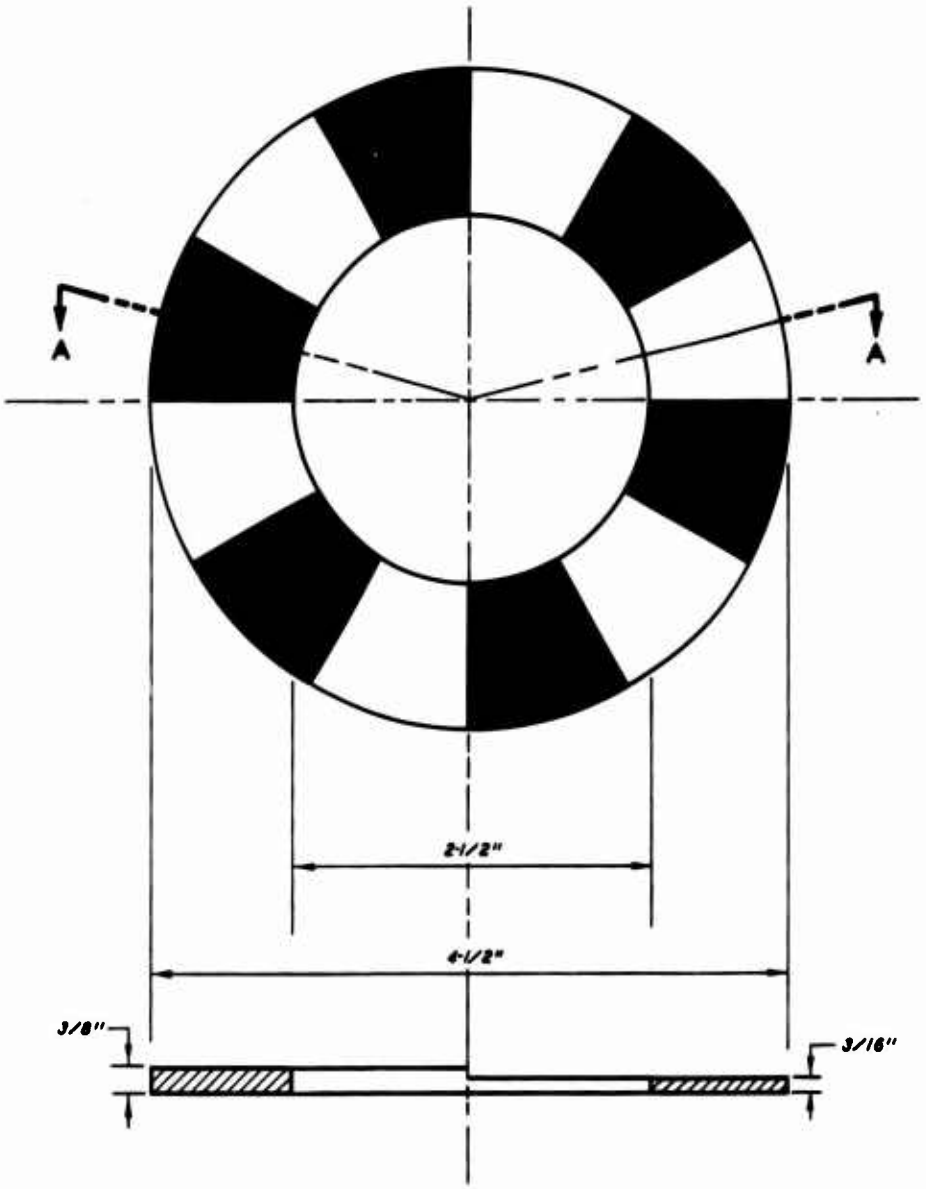

SECTION A-A

Fig. B3. Clcated stainless steel plate

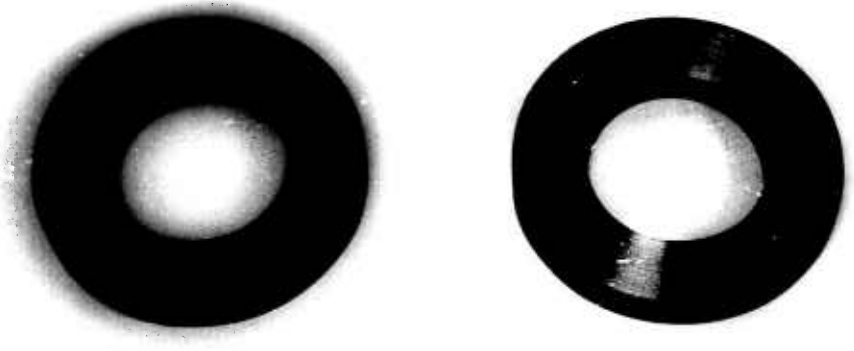

Fig. B4. Finished rubber annulus shown with steel annulus